Subcellular localization and characterisation of MAPKs, and cytoskeleton adaptation to stress in *Arabidopsis* roots

Dissertation

zur

Erlangung der Doktorgrades (Dr. rer. nat.)

der

Mathematisch-Naturwissenschaftlichen Fakultät

der

Rheinischen Friedrich-Wilhelms-Universität Bonn

vorgelegt von

Jens Müller

aus

Leverkusen

Bonn 2009

Angefertigt mit Genehmigung der Mathematisch-Naturwissenschaftlichen Fakultät der Rheinischen Friedrich-Wilhelms-Universität Bonn

1. Referent: PD Dr. Jozef Samaj
2. Referent: Prof. Dr. Diedrik Menzel

Tag der mündlichen Prüfung: 16.11.2009
Erscheinungsjahr: 2009

Diese Dissertation ist auf dem Hochschulschriftenserver der ULB Bonn http://hss.ulb.uni-bonn.de/diss_online elektronisch publiziert

TABLE OF CONTENTS

1. INTRODUCTION

1.1 General background

The constantly changing environment is one of the most important challenges for each individual organism. The ability to undergo adaptation determines as to how successful an organism can cope with environmental stresses and pathogen attack. Eventually, the ability to adapt decides on the survival and propagation of a species. In contrast to animals, plants are sessile organisms, unable to move away from unfavorable changes in the environment but rather react by metabolic adaptation involving rapid sensing mechanisms followed by the appropriate responses ranging from the cellular to the systemic level.

On the cellular level, stress response starts with the perception of an extracellular stimulus and is followed by signal transduction through the cell. Each signalling event causes the formation of a specific pattern of enzymatic activities and gene expression. One general mechanism that allows propagation of a signal is the transient phosphorylation and dephosphorylation of proteins that are organized in cascade like manner. Protein phosphotransferases, also called protein kinases are found in all organisms and are highly conserved among all organisms. It is estimated that about 30% of all proteins of eukaryotic cells are phosphorylated by protein kinases.

Due to the decoding of several genomes, the high complexity of signalling mechanisms in plants appeared obvious. While the human genome encodes 518 protein kinases, *Arabidopsis* encodes 1019 and rice even 1429 protein kinases which represent around 5% of the plant proteins (Wang *et al.* 2003; Dardick *et al.* 2007). Around 10% of these protein kinases are part of so called mitogen activated protein kinase (MAPK) modules. MAPK modules consist of variable multi-protein complexes, whose members are phosphorylating each other in a cascade like manner, thereby transducing signals throughout the cell (MAPK group 2002).

Subunit composition of a MAPK complex, and the duration and intensity of its signalling activity are precisely regulated and give rise to a highly specific cellular response. Regulation of signalling intervenes on several levels including the assembly and composition of a given MAPK module (for review see Colcombet and Hirt 2008), deactivation of single or multiple elements of a cascade by dephosphorylating enzymes (Meskiene *et al.* 1998 and 2003; Ulm *et al.* 2002; Luan 2003; Naoi and Hashimoto 2004), and last but not least, by its

specific spatial organization (see also the following chapters). It is well known from animal cells, that MAPK modules are spatially associated with different cellular domains such as endosomal organelles (for example Howe *et al.* 2001, Teiss *et al.* 2002 and 2006, Taub *et al.* 2007) and cytoskeleton (reviewed by Pullikuth and Catling 2007). Additionally, MAPK members undergo shuttling between the cytosol and the nucleus, where they activate a multitude of transcription factors (TFs) and others target proteins (reviewed by Turjanski *et al.* 2007). However, little is known about the subcellular organization of MAPK modules in plants.

The cytoskeleton also seems to be a key player in the transduction of signals from the outside and between cells in terms of development and plant responses to the environment (for example Dhonukshe *et al.* 2003; Šamaj *et al.* 2006; Yang *et al.* 2008; Wasteneys and Ambrose 2009). Moreover, there appear to be mutual interactions between the cytoskeleton and MAPK modules (Nishihama *et al.* 2002; Limmongkon *et al.* 2004; Naoi and Hashimoto 2004; Šamaj *et al.* 2002 and 2004a; Smertenko *et al.* 2006).

1.2 Mitogen activated protein kinases (MAPKs)

Mitogen activated protein kinases (MAPKs) are evolutionarily conserved serine/threonine kinases, which play an essential role in signal transduction involved in the regulation of cell growth, differentiation, and stress response. Like in animals and yeast, plant MAPKs are part of a complex network of signalling modules, which consist of a core of at least two more kinases, namely MAPK kinase (MAP2K or MAPKK or MKK) and MAPK kinase kinase (MAP3K or MAPKKK or MEKK). Such modules assemble in a cascade-like manner, generally starting with MAP3K, which activates MAP2K by phosphorylation of a S/T-X_{3-5}-S/T motif. Subsequently, the MAP2K acts as a dual-specific kinase phosphorylating MAPK both on threonine and tyrosine within a T-X-Y motif. MAPKs, in turn, are able to phosphorylate a wide range of substrates, including cytosolic and nuclear proteins (MAPK group 2002; Feilner *et al.* 2005; Nakagami *et al.* 2005; Popescu *et al.* 2009).

Mammalian MAPKs are divided into different groups, including the extracellular signal-regulated kinases (ERK), the p38 MAP kinases and the c-Jun N-terminal kinases (JNK) (for review see Junttila *et al.* 2008). Phylogenetically, all plant MAPKs belong to the mammalian ERK subgroup of MAPKs, and they are further divided into four classes (A-D) (MAPK Group 2002; Hamel *et al.* 2006).

In contrast to the yeast and human genomes, which encode 6 and 13 MAPKs, repectively (Meskiene and Hirt, 2000), higher plants possess a larger number of genes coding for MAPK-related kinases. At least 20 putative MAPKs, 10 putative MAP2Ks and 80 putative MAP3Ks have been identified in the *Arabidopsis thaliana* genome (MAPK group 2002 and TAIR; http://www.arabidopsis.org) allowing a multitude of different combinations with diverse molecular composition of MAPK cascades.

Exceeding the role of MAPKs in animals and yeast, a big number of stimuli triggers MAPK-mediated phosphorylation of downstream substrates in plants (Feilner *et al.* 2005; Nakagami *et al.* 2005; Popescu *et al.* 2009). Depending on the incipient signal, one single MAPK is able to target various proteins. Recently, Popescu *et al.* (2009) identified about 570 potential substrates for 10 out of 20 *Arabidopsis* MAPKs using microarray analysis. The authors reported about a pronounced area of overlap with respect to their targets between different kinases. Several studies demonstrated such versatility of MAPKs in the recent years. For example, MPK6, one of the best characterized MAPKs in *Arabidopsis*, is supposed to be a part of at least six different modules, which are maintaining correct patterning of stomata (Wang *et al.* 2007) and are involved in responses to the bacterial elicitor flagellin (Asai *et al.* 2002) as well as to the phytohormones ethylene (Yoo *et al.* 2008) and jasmonic acid (Takahashi *et al.* 2007), to oxidative stress (Kovtun *et al.* 2000), to cold and salt (Teige *et al.* 2004).

So far, a number of studies suggest that the composition of a particular cascade also determines the process that is finally affected by the respective downstream MAPK in the module. Moreover, one stimulus might initiate multiple modules, and each of them can activate a specific subset of MAPKs. Thus, the perception of the bacterial elicitor flagellin causes not only the activation of *Arabidopsis* MPK6 and MPK3 via MEKK1 (MAP3K) and MKK4/MKK5 (MAP2Ks) (Asai *et al.* 2002) but also leads to the activation of *Arabidopsis* MPK4 by MEKK1 (MAP3K) and MKK1/MKK2 (MAP2Ks) (Suarez-Rodriguez *et al.* 2007).

The specificity is, however, not only provided by the module-composition, but it seems to be heavily dependent on a variety of regulatory elements. Among these, dual-specific phosphatases, so called MKPs (MAPK phosphatases), were described as specific negative regulators of MAPKs in animals, yeast and plants (Luan 2003). While mammalian cells encode ten MKPs (for review see Owens and Keyse 2007), the *Arabidopsis* genome encodes only five (Kerk *et al.* 2002), namely AtMKP1, AtMKP2, DsPTP1, PHS1 and IBR5 (for references see Lee *et al.* 2009). Additionally, a multitude of single protein tyrosine phosphatases (PTPs) and protein serine/threonine phosphatases (PSPs) are known to regulate

MAPK activity in animals (reviewed by Junttila *et al.* 2008). These phosphatases have also been described in plants (Meskiene *et al.* 1998 and 2003). Recently, Schweighöfer *et al.* (2007) reported that AP2C1, a member of the *Arabidopsis* Ser/Thr phosphatase type 2C (PP2C) family, negatively regulates MPK4 and MPK6. The PP2C family comprises 76 putative members in *Arabidopsis thaliana,* which can serve in spatio-temporal regulation of MAPK signalling-activity in plant cells.

In animals and yeast, scaffold proteins turn out to be the main organizers of MAPK modules. With their multiple binding-domains they are able to accomplish correct assembly of specific MAPK modules (reviewed by Dhanasekaran *et al*. 2007). Further, scaffold proteins seem to regulate MAPK signalling by recruiting regulatory proteins such as phosphatases that either regulate the scaffold itself (Ory *et al.* 2003) or a specific MAPK within the module (Willoughby *et al.* 2003). Until now, only one scaffold protein has been identified in plants, namely OMTK1 (oxidative stress activated MAPK triple kinase 1) representing a MAP3K from *Medicago sativa.* This kinase is involved in the response to oxidative, stress and it was shown to be part of a protein complex with *Medicago* MAPK 3 (MMK3) (Nakagami *et al.* 2004). Interestingly, MEKK1, the closest *Arabidopsis* homolog of OMTK1 has also been described as a putative scaffold for *Arabidopsis* MPK4 (Nakagami *et al.* 2006).

One of the most important functions of scaffold proteins is their ability to determine the specific subcellular location of MAPK modules within a cell (Dhanasekaran *et al.* 2007). In animal cells some MAPKs dissociate from their scaffold upon complex activation and become relocated from the cytoplasm to the nucleus (reviewed by Turjanski *et al.* 2007). Further, Faure *et al.* (1999) showed that an activated MAPK from rat liver cells localizes to the plasma membrane (PM) and to endosomes following the binding of epidermal growth factor (EGF) to its receptor (EGFR), which in turn gave rise to endocytosis of the receptor-ligand complex. Several previous studies have demonstrated that EGF binding to its receptor activates a MAPK pathway through a distinct sequence of events leading to mitosis (reviewed by van der Geer *et al.* 1994).

Howe *et al.* (2001) provided evidence for the so called “signalling endosome hypothesis”. In analogy to the previous studies these authors showed, that the complex of nerve growth factor (NGF) and it´s receptor (NGFR) in neuronal cells is sequestered into clathrin coated vesicles (CCVs) and subsequently migrates from the axon back to the cell body. They also demonstrated that signalling of the MAPK-module, activated in this way, originates from these vesicles. Further studies confirmed the localization of MAPK modules

to endosomes and thus underlined the fundamental role of scaffold proteins. In mammalian cells, it has been shown that the scaffold protein MP1 (MEK1-partner) mediates late endosomal localization of the MAPK complex Raf/MEK/ERK via binding to the small adaptor protein p14 (Teis *et al.* 2002). Assembly and activation of this module is known to be regulated by the small G-protein Ras, which itself is activated after binding of EGF to EGFR (van der Geer *et al.* 1994). Because the PM-resident p14/MP1 complex is not able to activate the MAPK complex, it is likely that endocytosis itself is essential for proper signalling (Teis *et al.* 2002). A strong mutual interaction between endosomal trafficking and MAPK signalling has been demonstrated in a study providing evidence that late endosomes and lysosomes are displaced to the cell periphery in homozygous $p14^{-/-}$ and $mek1^{-/-}$ knockout lines of mouse embryo fibroblasts (Teis *et al.* 2006). Another study showed that artificial mislocalization of late endosomes caused prolonged EGFR activity and sustained ERK signalling (Taub *et al.* 2007). Most recently, p18 a novel adapter protein was identified to anchor the MEK1-ERK to lipid rafts on late endosomes and it was concluded that proper function of this anchoring protein is essential for controlling endosome dynamics (Nada *et al.* 2009). A theoretical model of a typical signalling cascade mediated by a MAPK module is shown in Fig 1.

In summary, a well-regulated subcellular organization of MAPK modules seems to be essential for proper signalling within a cell. It is remarkable that there is little known about a putative subcellular organization of such modules within plant cells. Up to now, MAPKs are mostly described as shuttling between the cytosol and the nucleus and it has been shown in some cases that these MAPKs activate signal specific transcription factors there (Andreasson *et al.* 2005; Qiu *et al.* 2008). However, in most cases the targets of such MAPKs are unknown. One of the first studies, which provided evidence for such nuclear shuttling, described the pathogen induced translocation of a non-identified MAPK into the nucleus in parsley cells (Ligterink *et al.* 1997). Another example was reported by Ahlfors *et al.* (2004) who described the nuclear translocation of *Arabidopsis* MPK3 and MPK6 in ozone treated plants. Further, Coronado *et al.* (2002 and 2007) proposed that tobacco Ntf4 relocates to the nucleus in specific stages of pollen maturation.

One indication for a putative association of plant MAPKs with particular subcellular structures comes from a previous study on *Medicago sativa* roots that demonstrated that inhibition of MAPK activation by the MAPKK inhibitor UO126 results in disturbed root hair formation and tip growth accompanied by adverse effects on vesicular trafficking (Šamaj *et al.* 2002). Additionally, this study showed that SIMK (stress induced MAPK) from *Medicago*

localizes to spot-like structures within the tip of growing root hairs, and that treatment with brefeldin A (BFA), an inhibitor of secretion and membrane recycling (reviewed by Müller *et al.* 2007b), caused random relocation of these spots. Interestingly, Baluška *et al.* (2000) previously described the translocation of SIMK from the nucleus to the cell plate in dividing root cells. A similar behaviour has also been described for tobacco NPK1 (*Nicotiana* protein kinase 1), which resides in the nucleus during interphase (Ishikawa *et al.* 2002) but relocates to the phragmoplast during cytokinesis (Nishihama *et al.* 2002) (see also chapter 1.5)

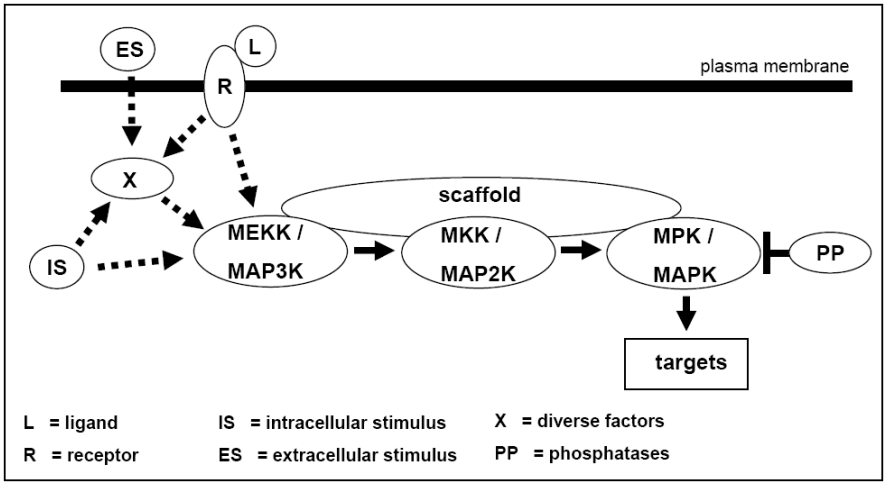

Figure 1. Model of the putative signalling cascade mediated by a MAPK module in plants. A typical MAPK-cascade starts with a stimulus that might come from the extracellular enviroment (like PAMPs), the neighbouring cells (like phytohormones) or from the cell interior (like changes in the cytoskeletal architecture) (**ES**; **E**; **IS**). Perception may start with the recognition by a PM-resident receptor (**R**) (for instance FLS2, **Robatzek *et al.* 2006)** or a receptor in the cytoplasm (**X**) as in the case of ethylene response at the endoplasmatic reticulum (**Gao *et al.* 2003**). Once the MAP3K is activated it phosphorylates a specific MAP2K at a S/T-X_{3-5}-S/T motif. MAP2K then phosphorylates a specific downstream MAPK on a T-X-Y motif. Activated MAPK phosphorylates and therefore activates or inactivates specific target proteins. Specificity of module composition might be governed by scaffold proteins that bind module components selectively. Regulation of kinase activity might be achieved by negative regulators such as protein phosphatases (**PP**). Dashed line arrows indicate postulated pathways.

1.3 MAPKs in *Arabidopsis thaliana*

Until now, most knowledge about MAPK mediated signalling in *Arabidopsis* comes from characterization of three MAPKs, namely MPK3, MPK4 and MPK6. All three were shown to assemble in multiple modules that are activated by diverse sets of abiotic and biotic stimuli as well as by developmental cues (Table 1 and Fig 2). The following chapter will summarize the most important present knowledge about these three MAPKs.

A multitude of abiotic stresses were shown to activate MAPKs in *Arabidopsis* including heat, cold, touch, wounding, osmotic shock, UV, salt as well as the application of

reactive oxygen species. However, respective compositions of MAPK modules and putative targets of the specific cascades are only barely discovered.

One complete module consisting of MEKK1, MKK2 and MPK4/MPK6 was described for cold and salt (Teige *et al.* 2004). Interestingly, this stress-induced cascade is identical to the flagellin induced cascade activating MPK4 but not MPK6 (see below). The fact that identical upstream MAP3Ks and MAP2Ks activate a specific subset of MAPKs in dependence to the respective stimulus seems to be a common phenomenon. For example, both MPK3 and MPK6 are activated by upstream MKK4 and MKK5 in three pathways comprising response to flagellin via MEKK1, response to oxidative stress via ANP1 (Kovtun *et al.* 2000) as well as via YODA during stomata development (Wang *et al.* 2007).
One common component in many cascades is H_2O_2, which seems to act as an upstream second messenger in early response reactions to several stimuli and it has been shown to activate MPK1, MPK2, MPK3, MPK4 MPK6 and MPK7 in *Arabidopsis* (reviewed by Colcombet and Hirt 2008).

Early recognition and an appropriate response to pathogen attack is one of the main challenges for plants. Generally, higher plants developed the so called innate immune response representing a very effective defence mechanism. The innate immune response comprises a first non pathogen specific answer, initiated by the recognition of PAMPs (pathogen associated molecular pattern) such as structural proteins and/or cell wall components, which are typical for a large range of pathogens. Challenged by these PAMPs, plant cells change their enzymatic activity and gene expression sometimes resulting in the hypersensitive response (HR), which is characterized by local programmed cell death (PCD) in order to prevent spreading of the pathogen. Amongst others, the HR is regulated by the activity of a specific set of phytohormones, namely jasmonic acid (JA), ethylene and salicylic acid (SA). Additionally, these phytohormones are also involved in the development of a pathogen-specific long term resistence, which is called systemic aquired resistance (SAR) (for review see Jones and Dangl 2006).

In recent years, MAPKs have been recognized as important players that are involved in both, innate immune response and the development of SAR. *Arabidopsis thaliana* FLAGELLIN SENSING 2 (FLS2), is a membrane-integral receptor-like kinase (RLK), described as PM receptor that is known to be internalized via receptor mediated endocytosis (RME) after application of the bacterial PAMP called flagellin (Robatzek *et al.* 2006). FLS is a pattern-recognition receptor (PRR) that binds bacterial flagellin and initiates the immune

response, which involves activation of the MAPKs MPK3, MPK4 and MPK6 (Asai *et al.* 2002; Suarez-Rodriguez *et al.* 2007). Due to binding of flagellin, FLS dimerizes with another PM protein called BRI1-ASSOCIATED KINASE 1 (BAK1). This complex is known to be internalized into an endocytotic organelle (Chinchilla *et al.* 2007; Heese *et al.* 2007). Flagellin was shown to trigger the activation of at least two different MAPK cascades. One of them comprises the activation of MPK3 and MPK6 via MKK4 and MKK5 (Asai *et al.* 2002). The second cascade activates MPK4 via MKK1 and MKK2, a module that is also known to trigger cold and salt tolerance (Ichimura *et al.* 1998; Teige *et al.* 2004). Both seem to share the same upstream MAP3K, namely MEKK1.

While MPK3 activates VirE1-INTERACTING PROTEIN 1 (VIP1) a transcription factor that is known to induce the expression of defense-related genes (Djamei *et al.* 2007), MPK6 phosphorylates ACC (1-amino-cyclopropane-1-carboxylic acid) SYNTHASE 6 (ACS6) an enzyme that is involved in the synthesis of the phytohormone ethylene (ET) (Liu *et al.* 2004; Joo *et al.* 2008). Interestingly, MPK6 not only seems to be involved in PAMP triggered ET synthesis but also gets activated by ET via MKK9 (Novikova *et al.* 2000; Ouaked *et al.* 2003; Yoo *et al.* 2008).

In contrast, MPK4 was proposed to act as a negative regulator of immune response because *mpk4* and *mekk1* mutants show elevated levels of SA and H_2O_2, which cause PCD induced by PAMP (Ichimura *et al.* 1998; Petersen *et al.* 2000; Suarez-Rodriguez *et al.* 2007). MPK4 is known to target the two transcription factors (TFs), WRK25 and WRK33, as well as MPK4 substrate1 (MKS1) that is known to be involved in pathogen response (Andreasson *et al.* 2005). However, it is not clear, whether these targets are indeed activated by flagellin. Although, both cascades act antagonistically, they seem to be tightly connected to each other, since it was shown that MPK3 and MPK6 activity is impaired in *mkk1* mutants (Meszaros *et al.* 2006).

Interestingly, signalling pathways activated by flagellin might represent general components of a pathogen-related response mechanism. It was shown that not only flagellin but also several other PAMPs, such as fungal chitin and harpin, activate MPK3/MPK6 or MPK4, respectively and that they trigger similar gene regulation and HR resulting in PCD (Desikan *et al.* 1999 and 2001; Miya *et al.* 2007).

A recent overview on MAPK cacades involved in plant signalling events is provided in Fig 2.

	activating stimulus
MPK3	osmotic stress; H_2O_2; O_3; ABA; ET; PAMPs
MPK4	osmotic stress; O3; PAMPs; cold; salt
MPK6	osmotic stress; H_2O_2; O_3; JA; ET; PAMPs

for references see Colcombet and Hirt (2008)

Table 1. Stimuli activating MPK3, MPK4 and MPK6. Several stimuli activate one or more of these three MAPKs. The list of stimuli was modified from Colcombet and Hirt (2008). References are listed there. ABA=abscisic acid; ET=ethylene; PAMP=pathogen associated molecular pattern; JA=jasmonic acid.

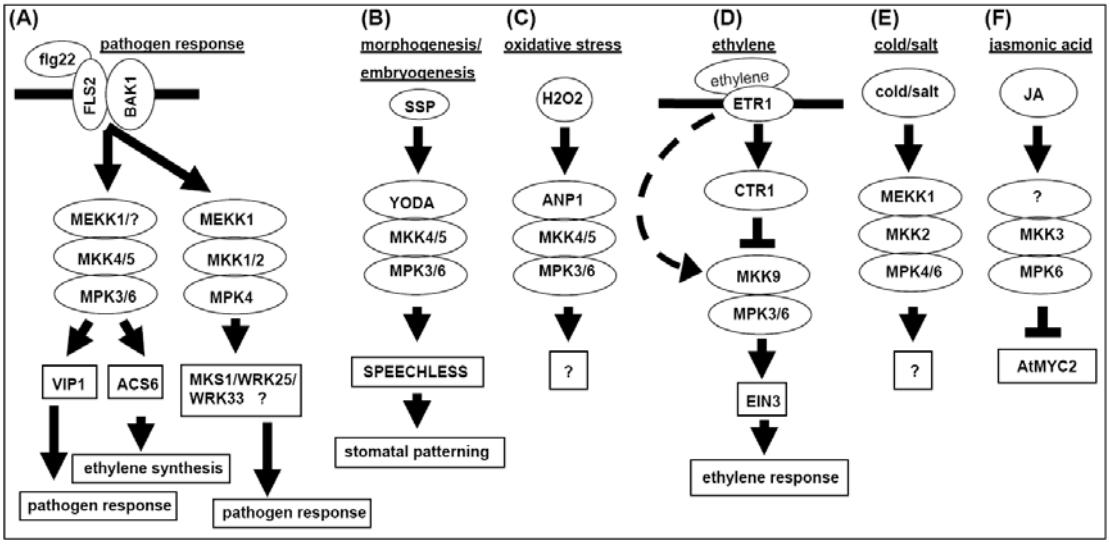

Figure 2. Composition of known MAPK cascades involving MPK3, MPK4 and/or MPK6. (A) pathogen response: Activation of MPK3 and MPK6 in a MEKK1-MKK4/MKK5-MPK3/MPK6 module and activation of MPK4 in a MEKK1-MKK1/MKK2-MPK4 module after recognition of bacterial flagellin (flg22) by the flagellin receptor FLS2. Targets of MPK3/6 are the transcription factor (TF) VIP1, which is involved in gene activation in the course of pathogen response. Another target is ACS6, which is responsible for ethylene synthesis. MPK4-targets in flagellin response patahway are not yet identified, but it was shown elsewhere that MPK4 may target TFs involved in pathogen response. **(B) morphogenesis:** activation of MPK3/6 in a YODA-MKK4/MKK5-MPK3/MPK6 module, which is involved in stomatal patterning and embryo development. SPEECHLESS, a TF that is responsible for initiation of stomata was recently reported as a target of MPK3/MPK6 (**Lampard *et al.* 2008**). SHORT SUSPENSOR (SSP) was recently proposed to induce YODA-dependent signalling in the zygote and in leaves **(Bayer *et al.* 2009) (C) oxidative stress:** activation of MPK3/6 in an ANP1-MKK4/MKK5-MPK3/MPK6 module by hydrogen peroxide as the upstream stimulus. Targets are not known. **(D) ethylene response:** Activation of MPK3/6 by upstream MKK9. MKK9 gets activated in response to recognition of ethylene by the ER resident ethylene receptor ETR1. ETR1 also activates the CTR1, which seems to have a negative effect on MPK3/6 activation. **(E) cold/salt:** Activation of MPK4/6 in a MEKK1- MKK2-MPK4/MPK6 module. Targets are unknown. **(F) jasmonic acid (JA):** Activation of MPK6 by JA might be a secondary effect, wether there is a direct activation of MPK6 by MKK3, is not clear. The pathways presented in this figure are created on the basis of the review article by **Colcombet and Hirt (2008)**. Updated elements are supplemented with references, and all other references can be found in this article.

1.4 Endocytosis in plants

The first indications for the existence of endocytosis in plants have been obtained two decades ago. For instance, electron-dense tracers have been applied to prove uptake via the plasma membrane into membrane bound intracellular structures (Tanchak and Fowke, 1987; Hillmer *et al.*, 1986 and 1988; Galway *et al.*, 1993) and clathrin coated pits associated with the plasma membrane (PM) have been identified in plant cells (Robinson and Hillmer, 1990). Nevertheless, unambiguous and conclusive evidence for the operation of endocytosis and its vital role in plant cells have been missing for a long time.

In the past years, however, a broad range of molecular markers was developed (for example Ueda *et al.*, 2004; Uemura *et al.*, 2004; Voigt *et al.* 2005; Jaillais *et al.*, 2006; Ortiz-Zapater *et al.*, 2006; Lam *et al.*, 2007a,b) and, together with vital marker-dyes such as FM1-43 and FM4-64 (Vida and Emr, 1995; Emans *et al*. 2002; Bolte *et al.*, 2004), widely used to analyse PM-recycling and endocytosis, as well as to identify and characterize corresponding endomembrane compartments. It is now firmly established that the uptake of extracellular cargo by endocytosis and recycling of diverse membrane-bound and cell-wall-associated components not only exist, but are highly organized and crucial for plants. Endocytosis is also regarded as essential for the plant development and for plant adaptation to the environment.

One of the most striking discoveries of the last years was the demonstration of receptor mediated endocytosis (RME) in plants. Although, it has long been speculated about the existence of RME (Horn *et al.*, 1990), and a set of candidate receptors have been proposed to reside in the PM and in endosomal structures (for references see Geldner and Jürgens, 2006), the clear evidence for RME was provided by Robatzek *et al.* (2006) only recently. These authors showed that the *Arabidopsis* LRR (leucine rich repeat) receptor FLS2 (Flagellin sensitive 2) resides at the PM and gets internalized into endosomal compartments upon specific binding of its ligand flg22, a small flagellin peptide, which is known to elicit basal defence responses (Gomez-Gomez *et al.*, 2001; Gommez-Gommez and Boller, 2002) (see also chapter 1.3). There are more candidates possibly involved in induced endo- and exocytotic events mediating plant immune-responses (Robatzek, 2007) and future work will show if RME is, like in animals, a key regulator in the plant´s specific recognition of putative pathogens.

1.4.1 Identification of endosomal compartments – markers and reporters

One straight forward approach to analyse the organization of the endosomal system within plants is to identify the intracellular compartments, which are involved in this trafficking route. A relatively well established way to identify and characterize endosomes is to use specific molecular markers, which are known to act predominantly at one specific endomembrane compartment. Like in all eukaryotic cells, plant cells possess a broad range of highly conserved protein families known to be essential for proper protein sorting, directed vesicular trafficking and fusion of endosomal/ PM derived vesicles with the target membranes. All of these protein families can be divided into sub-classes, which often are associated specifically with only one endosomal compartment. The most common protein families used in this context are t-SNAREs/syntaxins (soluble *N*-ethyl maleimide sensitive factor attachment protein receptors), small GTPases and a set of diverse endosomal sorting receptors (for detailed description see Müller *et al.* 2007b). Additionally, there are some molecular markers which do not occur in plants but are used as heterologous markers, because they are known to define specific compartments or trafficking pathways in other eukaryotic cells. One actual example is the human transferrin receptor (hTfR) (Ortiz-Zapater *et al.*, 2006).

Using ultrastructural analysis as well as different molecular markers, a couple of endosomal compartments have been described during the past years in plants. They partially resemble those known from animals and yeast. Initially, it seemed to be difficult to integrate these structures into a functional endocytotic/secretory pathway. Nevertheless, recent studies provide first important insights into their functions, organization and interconnections. A model of the plant endosomal system based on recent findings, including a specification of the known endosomal markers is shown in Fig 3.

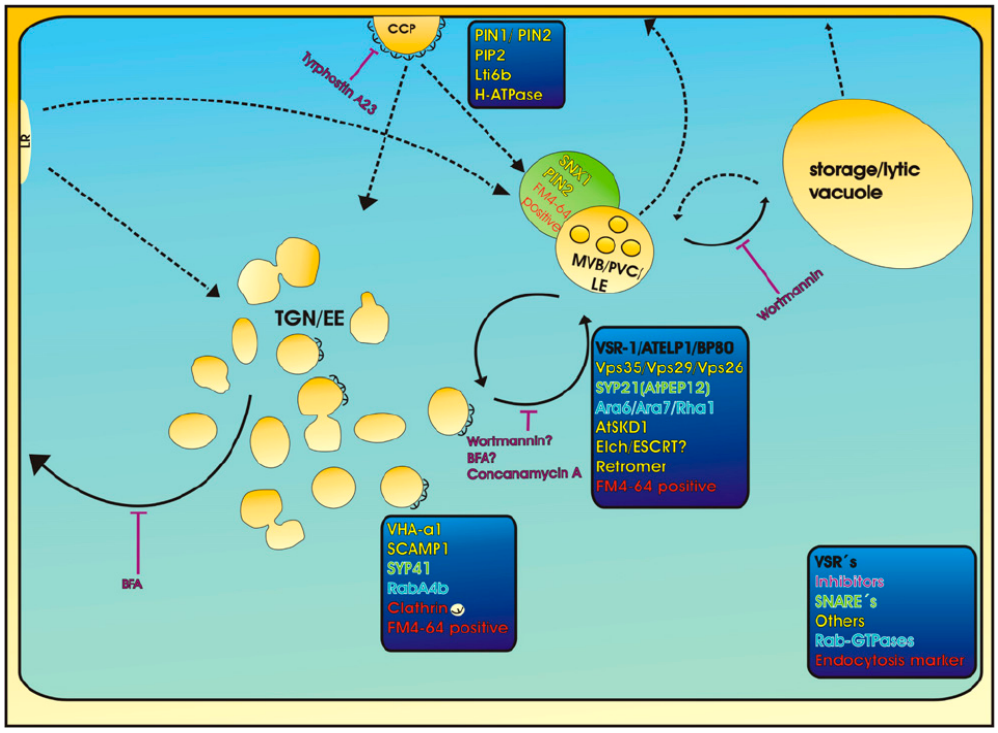

Figure 3. Endocytotic routes and compartments in plant cells. Components internalized by clathrin-dependent endocytosis (coated pits,CCP) are delivered to an early endosome (EE) that was proposed to be identical to the TGN (**Dettmer *et al.*, 2006; Lam *et al.*, 2007**). Internalized cargo is either recycled back to the PM or delivered to the MVBs/PVC, which are assumed to function as late endosomes (LE). From there, vacuolar proteins as well as proteins designated for degradation are transported to the vacuole, while cargo receptors may be recycled back to the TGN (**Oliviusson *et al.*, 2006**). Additionally, there is at least one endosomal compartment that is not identified yet. This compartment is labeled by SNX1 (sorting nexin 1) and might be a late endosome, since structural homologs of AtSNX1 in yeast are known to be part of a retromer complex residing on the MVB/PVC compartment (**Oliviusson *et al.*, 2006**). Both TGN and MVBs are labeled by FM4-64 and therefore clearly of endosomal nature. Molecular markers are depicted in different colors. Rab-GTPases: blue, SNAREs: green, VSRs: black, other molecules: yellow. Inhibitors with their inhibitory effects are shown in purple. Black arrows indicate established endocytotic routes, dashed arrows indicate putative pathways. The green colored compartment is not identified at the ultrastructural level, but it is labeled by endosomal markers visualized by confocal laser scanning microscopy. MVB = multivsicular body; PVC = prevacuolar compartment.

1.4.2 Pharmacological studies

Drugs affecting vesicular trafficking turned out to be very useful tools in determining the origin, assignment, and functional interconnections of distinct endosomal compartments within the endocytotic network. In addition to diverse drugs that are disturbing the dynamics of cytoskeletal elements and therefore affect the vesicular/organellar motility and organization, there are mainly two inhibitors extensively used in plants, which directly interfere with vesicular trafficking and fusion events, namely Brefeldin A (BFA) and Wortmannin.

Brefeldin A (BFA) is a fungal toxin from *Eupenicillium brefeldianum,* and it is commonly used as an inhibitor of membrane recycling by effectively inhibiting secretion (reviewed by Müller *et al.* 2007b). Whereas secretion is inhibited endocytosis not only

continues, but rather increases under BFA treatment (Emans *et al.* 2002; Wang *et al.* 2005). BFA was shown to inhibit ARF-GTPases by targeting ARF-GEF proteins resulting in disruption of the formation of COPI-coated vesicles, thereby stopping the membrane replenishment from the ER to the Golgi. There is at least one other ARF-GEF member called GNOM that is also sensitive to BFA. It is localized on an endosomal compartment and was proposed to be involved in membrane trafficking from endosomes to the PM (Geldner *et al.*, 2003). Secretion is stopped, whereas endocytosis may continue and produce a surplus of internalized membranes, which aggregate and form so-called BFA compartments in plants. In *Arabidopsis* roots, these BFA compartments consist mostly of accumulated TGN vesicles, which are surrounded by Golgi-stacks (Grebe *et al.* 2003; Šamaj *et al.* 2004a).

Wortmannin is the second inhibitor extensively used in studies on endosomal organization and trafficking. It is known to target phosphoinositide 3 kinase (Ui *et al.*, 1995) and it is inhibiting vacuolar/lysosomal trafficking at late endosomes in both mammalian (Bright *et al.*, 2001) and plant cells (Matsuoka *et al.*, 1995) in a dose-dependent manner. On the subcellular level, it has been shown that Wortmannin causes multivesicular bodies (MVB) / prevacuolar compartments (PVC) to form vacuolated structures, but it does not affect the Golgi (Tse *et al.*, 2004). However, results from Wortmannin treatments always have to be interpreted with some caution, because it is known to inhibit at higher concentrations also phosphoinositide 4 kinase (Matsuoka *et al.*, 1995).

In summary, BFA and Wortmannin can be used as valuable pharmacological tools for the study of secretory and endocytotic pathways. Because of the characteristic morphological changes which they cause at the level of TGN and MVB/PVC morphology and function, they can be further used to identify the localization of proteins within the endocytotic/secretory network.

1.4.3 Trans-Golgi network (TGN), an early endosomal compartment in plants

In animals, the TGN is described as a structure tightly associated with the trans-side of the Golgi apparatus and primarily responsible for the sorting of secretory and lysosomal proteins. However, in plants it seems that the TGN serves also, in addition to its role in the secretory pathway, as an early endosome in the endocytotic pathway.

One of the first molecular markers described as specific for the TGN was the *Arabidopsis* SNARE protein SYP41 (Uemura *et al.*, 2004). It has been shown, that a GFP-SYP41 fusion construct did not co-localize with Golgi- or PVC markers but aggregated under

the influence of BFA. Later, it was shown that the *Arabidopsis* membrane-bound V-ATPase subunit VHA-a1 is co-localized with SYP41 and resides in the TGN (Dettmer *et al.*, 2006). Interestingly, the endocytotic marker FM4-64 rapidly co-localizes with VHA-a1 in *Arabidopsis* root cells. This observation led to the conclusion that the TGN also serves as an early endosomal compartment. Moreover, it has been shown that the V-ATPase inhibitor Concanamycin A inhibits the endocytotic trafficking of FM4-64 to late endosomes and to the vacuole. Upon Concanamycin A treatment, FM4-64 and VHA-a1 were restricted to the TGN. Dettmer *et al.* (2006) also showed that BFA causes the VHA-a1 positive structures to aggregate within BFA-compartments. This clearly suggested that the TGN serves both, within the secretory/ vacuolar and the endocytotic pathway.

A recently published work describing the localization of secretory carrier membrane protein1 (SCAMP1) to the TGN (Lam *et al.*, 2007) supported and further strengthened previous conclusions. SCAMPs are endocytosis-mediating proteins in animals. Lam *et al.* (2007) localized the rice SCAMP1 in transgenic tobacco BY-2 cells both at the PM and within highly mobile, punctuated cytoplasmatic structures. Co-localization of SCAMP1 with V-ATPase, suggested that this organelle constitutes the TGN. Indeed, immunogold EM experiments revealed that SCAMP1 localizes to vesicular structures of TGN. Furthermore, it was shown that FM4-64 labels SCAMP1-positive organelles rapidly, and prior to the MVB/PVC. Together, these data provided evidence that SCAMP1 is localized to the TGN, an organelle which is serving as an early endosome in plant cells.

Additionally, RabA4b, an *Arabidopsis* homolog of the Rab11 family of mammalian small Rab-GTPase was shown to partially localize to the TGN compartment in growing tips of root hairs (Preuss *et al*., 2004a and 2006). Rab11 proteins in mammals are known to mediate recycling processes from early endosomal compartments to the PM by acting on recycling endosomes (Ullrich *et al*., 1996; Mohrmann *et al*., 1999). Interestingly, only the minor part of RabA4b seems to be associated with the TGN, while the major part labels a yet unidentified compartment (Preuss *et al.*, 2004a). These data provided the first indication for the existence of an additional early endosomal compartment, resembling the recycling endosome in mammals.

1.4.4 Multivesicular body as late endosomal compartment

In plants, similarly to other eukaryotic organisms, vacuolar/lysosomal protein degradation as well as the delivery of vacuolar proteins is mediated through a compartment

described as either prevacuolar compartment (PVC) or multivesicular body (MVB). Moreover, proteins of the secretory pathway as well as proteins delivered to protein storage vacuoles (PSV) apparently have to pass through such a compartment in the cell (for review see Mo *et al.* 2006). MVBs could be defined as round-shaped electron-transparent vesicular compartments enclosed by a limiting outer membrane and containing small internal electron dense microvesicles (Tse *et al.* 2004; Hause *et al.* 2006; Lam *et al.* 2007). In addition to the role of MVBs in the secretory/vacuolar pathway, it is known for a long time that organelles possessing multivesicular structures are also involved in endocytotic processes in plants. Already in the 1980s and the early 1990s uptake studies using electron dense tracers indicated their presence within MVBs (Hillmer *et al.* 1986 and 1988; Tanchak and Fowke 1987; Galway *et al.* 1993). During the last years, several molecular markers were developed and used to describe late endosomal/secretory compartments. Markers like vacuolar sorting receptors (VSRs) (Li *et al.* 2002; Tse *et al.* 2004), the *Arabidopsis* syntaxin SYP21/ PEP12p (da Silva Conceicao *et al.* 1997; Uemura *et al.* 2004), as well as small Rab-GTPases (Sohn *et al.* 2003; Kotzer *et al.* 2004; Lee *et al.* 2004) contributed significantly to the study of MVB/PVC functions. The use of these markers in combination with vital endocytotic marker dyes made it also possible to show that there are cross talks between the secretory/vacuolar and the endocytotic pathway on the level of MVB/PVCs (for review see Müller *et al.* 2007b; Robinson *et al.* 2008). Further, there is growing evidence for the existence of bidirectional trafficking also allowing retrograde transport from MVBs to the TGN via a cytosolic protein complex named retromer (Oliviusson *et al.* 2006; Shimada *et al.* 2006; Jaillais *et al.* 2006, 2007 and 2008).

1.5 Interactions between MAPKs and cytoskeleton in plants

Like in animals and yeast, the cytoskeleton in plants is involved in the establishment of cell polarity and regulated vesicular trafficking in endo- and exocytosis (reviewed by Šamaj *et al.* 2006; Boutte *et al.* 2007; Yang 2008) as well as in cell division, morphogenesis and in the general maintenance of intracellular motility (reviewed by Pollard and Borisy 2003; Panteris 2008; Wasteneys and Ambrose 2008). A precise regulation and high dynamic of actin filaments (AF) and microtubules (MT) are fundamental requirements in order to accomplish all these functions.

Importantly, the behaviour of AF and MT is mainly influenced by specific binding proteins called microtubule associated proteins (MAPs) and actin binding proteins (ABPs)

(reviewed by Hamada 2007; Higaki *et al.* 2007). From animal cells it is well known that MAPKs are involved in the regulation of the cytoskeleton either by direct association with cytoskeletal elements or by phosphorylation and regulation of cytoskeleton-binding proteins (for example Hai and Gu 2006; Pullikuth and Catling 2007; Gerthoffer 2008).

Over the recent years evidence has grown about crosstalk between MAPKs and MAPs/ABPs also in plants. Interestingly, MAPKs not only regulate the behaviour of these proteins by phosphorylation but seem to be regulated in turn by the cytoskeleton including the binding proteins. For example, it was shown that pharmacological inhibition of SIMK activity in *Medicago sativa* by the synthetic drug UO126 not only affects the arrangement of actin filaments and inhibits vesicle trafficking and polar growth of root hairs, but vice versa, the disturbance of actin dynamics by latrunculin B activates SIMK (Šamaj *et al.* 2002). Since actin cytoskeleton dynamic is regulated through actin binding proteins and the modulation of the G-actin pool, it is interesting to note the obvious connection between MAPKs and ABPs. For instance, it was found in tobacco by Limmongkon *et al.* (2004) that two tobacco MAPKs, namely $p45^{Ntf4}$ and SIPK, were able to phosphorylate profilin 2.

Apparently, SIMK not only interacts with the actin cytoskeleton but also with microtubules. It has been localized to the phragmoplast after salt stress (Baluška *et al.* 2000) and after stabilization of microtubules by taxol (Šamaj *et al.* 2004b). Other MAPKs were also shown to localize to the phragmoplast (Calderini *et al.* 1998; Bögre *et al.* 1999). This suggests that MAPKs connect the incoming stress signal with the microtubule system. One group of molecular players, which modulate MT-dynamics are the members of the MAP65 family. In *Arabidopsis*, it has been shown by *in vitro* phosphorylation assays that MAP65-1, which is associated with the cortical MT-system but is also involved in cytokinesis, is negatively regulated by MPK4 and MPK6 (Smertenko *et al.* 2006).

Another example for a tight association of a MAPK with the cytoskeleton is the tobacco NPK1, a MAP3K that is known to be essential for cell plate formation (Nishihama *et al.* 2001). During cytokinesis, NPK1 interacts with NACK1, a kinesin-like protein that is necessary to transport NPK1 to the equatorial region of the phragmoplast (Nishihama *et al.* 2002). Interestingly, the NACK1 binding domain of NPK1 contains a nuclear localization signal and it has been shown that NPK1 resides in the nucleus during interphase (Ishikawa *et al.* 2002). This was a first indication of spatial and temporal organization of distinct MAPK subpopulations in plants.

1.6 Aims

This thesis work aims to characterize the subcellular organization and function of three MAPKs in *Arabidopsis thaliana* roots, namely MPK3, MPK4 and MPK6, with the main focus on MPK6. The combined use of biochemical methods together with *in-vivo* and *in-vitro* localization techniques, such as the application of recombinant GFP-reporters and immunofluorescence co-labelling, should provide insight into the potential organization and function of MAPK subpopulations on specific organelles or the cytoskeleton. To this end, a set of specific antibodies against organellar marker proteins, cytoskeletal components and MAPKs are used. Where applicable, selective activation of MAPKs by well established elicitors and stimuli have been employed to examine the specific role of these subpopulations. Moreover, using Brefeldin A as an inhibitor of membrane trafficking, this work should test, whether one or more of these MAPKs are integrated in or regulated by the endocytotic / secretory pathway. These experiments will be supplemented by phenotypically characterizing a *mpk6* knockout mutant line and further studies on the cellular level. Finally, this work is aims at characterizing the cell type specific changes of the actin- and microtubule-cytoskeleton in course of heat shock, a type of physical stress, which is also known to activate MPK6. Live cell imaging of *Arabidopsis* lines transformed with GFP-fusion reporter constructs, are used in order to reveal the cell type specific behaviour of these cytoskletal components.

Arabidopsis thaliana is the best characterized experimental model system in plant biology. It has advantages such as the fully sequenced genome, availability of mutant lines, reliable transformation methods, established whole mount immuno-localization protocols and commercially and non commercially available antibodies against MAPKs as well as a set of organellar marker proteins.

Experimental work of this thesis is focused on the root of *Arabidopsis* seedlings representing an important organ for water and nutrition uptake and for plant – environment interactions. Moreover, roots are chosen, because of some practical advantages. They allow to use protocols for whole-mount immunofluorescence labelling and, because of their small size, they are suitable for microscopy without further embedding and sectioning. Further, they allow easy application of chemical probes such as vital dyes and drugs and the microscopic observation of effects caused by these probes.

2. MATERIAL AND METHODS

Plant growth conditions

If not stated otherwise, sterile *A. thaliana* seedlings of the Columbia 0 (Col-0) wildtype or the *mpk6-2* mutant line (SALK_073907) were grown on vertically oriented Phytagel plates containing ½ Murashige and Skoog (MS) medium (pH 5.7) under a 16-h-light/8-h-dark cycle at 22°C.

Seed sterilization

Seeds were sterilized for 15 min using 12% sodium hypochlorite solution in 0,1% v/v Triton X100. After successive washing with sterile double-destilled (MilliQ) water, seeds were dried on filter paper and stored at 4°C.

Extraction of proteins and isolation of cytosolic and microsomal fractions

For protein extraction, roots from 1-2 weeks old seedlings were homogenized in ice cold extraction buffer (30mM Tris at pH 8,3; 150mM NaCl; 10mM EDTA; 20%[V/V] Glycerol; 2mM DTT; 1mM PMSF; protease inhibitor cocktail (SIGMA-ALDRICH)) and subsequently filtered twice through Miracloth (CALBIOCHEM). To isolate cytosolic and microsomal fractions the resulting suspension was fractionated by the following centrifugation steps: (i) 15min at 10.000g resulting in a nuclear/waste sediment and a post-nuclear supernatant (PS); (ii) The PS was centrifuged for 60min at 100.000g (BECKMANN L8-70M ultracentrifuge) resulting in a microsomal pellet and a cytosolic supernatant. The pellet was resuspended in the extraction buffer.

Fractionation of microsomes

For the fractionation of microsomes *A. thaliana* (Columbia 0) seedlings were grown in liquid ¼ MS medium on a shaker for 2 weeks (16-h-light/8-h-dark at 22°C) and subsequently prepared as described above. The microsomal fraction was resuspended in extraction buffer and layered over a 30 to 55% continuous sucrose gradient prepared in centrifugation buffer (10mM Tris at pH 7,6; 30/55% [w/v] sucrose; 5mM EDTA; 2mM DTT; 1mM PMSF; protease inhibitor cocktail (SIGMA-ALDRICH)) and centrifuged using a SW40 swinging bucket rotor at 100.000g at 4°C for 18 h (BECKMANN L8-70M ultracentrifuge). Up to

twenty 0.5ml-fractions were collected from the top of the gradient. Sucrose concentration in the fractions was determined by refractometry.

Immunoblot analysis

Protein extract samples were precipitated by methanol and chloroform according to Wessel and Flügge (1984). First a MetOH:Sample:Chloroform (4:4:1) mixture was prepared in an Eppendorf tube and vortexed. After a centrifugation step (10min, 13.000rpm) the upper phase of the resulting three-phased sample was discarded. Another volume of MetOH was added and the sample was centrifuged a second time (10min, 13.000rpm). The resulting pellet was dried completely and resuspended in 1x SDS-PAGE sample buffer. SDS- PAGE was performed on a Minigel setup (MINI-Protean II cell system, BIORAD) using the Laemmli system (Laemmli 1970). Identical protein concentrations were loaded in all quantitative analyses and all fractions from sucrose density gradients. Proteins were transferred to a polyvinylidene difluoride (PVDF) membrane (PEQLAB) in a wet tank unit (BIORAD) at 100 V for 1,5 h using the transfer buffer according to Towbin *et al.* (1979). For immuno-detection of protein bands the membrane was blocked with 6% [w/v] bovine serum albumin (BSA) in Tris-buffer-saline (TBS, see buffer list below) for 1h, and subsequently incubated with a primary antibody diluted in TBS-T (TBS; 0,1% Tween 20) containing 1% [w/v] BSA at room temperature for 1,5h or at 4°C overnight. After washing in TBS-T the membrane was incubated with a secondary antibody diluted in TBS-T containing 1% [w/v] BSA at room temperature for 1,5h. Following at least six washing steps, proteins were detected by incubating the membrane in freshly prepared enhanced chemoluminescence (ECL) reagent for 2min. ECL reagent was prepared using the following solutions: 1ml of solution A (200 ml 0,1M Tris-HCl (pH 8,6); 50 mg Luminol (SIGMA-ALDRICH)), 100µl of solution B (11 mg para-Hydroxycoumarin acid (SIGMA-ALDRICH) in 10 ml DMSO) and 0.3µl H_2O_2 (37%). Luminescence was detected using Hyperfilm ECL (AMERSHAM) in a dark room.

Antibodies used for SDS-PAGE

The following primary antibodies were used: rabbit polyclonal anti-AtMPK3 (diluted 1:3500, SIGMA-ALDRICH); rabbit polyclonal anti-AtMPK4 (diluted 1:3500, SIGMA-ALDRICH); rabbit polyclonal anti-AtMPK6 (diluted 1:7500, SIGMA-ALDRICH), rabbit polyclonal anti-SCAMP1 (diluted 1:1000; provided by Liwen Jiang, University of Hong-Kong, China), rabbit polyclonal anti-phosphoenol pyruvate carboxylase (PEPC) (diluted 1:2000; ROCKLAND); mouse monoclonal anti-clathrin LC (diluted 1:1500; SIGMA-ALDRICH); rabbit polyclonal

anti-alpha-mannosidase1 (diluted 1:1000; provided by Sebastian Bednarek, Wisconsin University, USA); rabbit polyclonal anti-FLS2 (diluted 1:5000; provided by Silke Robatzek, MPI, Cologne, Germany) rabbit polyclonal anti-AtSec12 (diluted 1:1000; see Bar-Peled and Raikhel 1997); rabbit polyclonal anti-AtPEP12/SYP21 (diluted 1:1500; see Preuss *et al.* 2004); mouse monoclonal anti-actin (MabGPa) (diluted 1:1500; provided by Richard Meagher, University of Georgia, USA); mouse monoclonal anti-alpha-tubulin (diluted 1:500; SIGMA-ALDRICH) and rabbit polyclonal anti-PIP2;2 (diluted 1:2000; provided by Anton Schäffner, Helmholtz Zentrum München, Germany).

Secondary antibodies were anti-mouse and anti-rabbit IgGs conjugated with horse radish peroxidase (diluted 1:2000; CELL SIGNALLING).

Statistical distribution analysis of proteins in microsomal and cytosolic fractions

The average grey value intensity of the immunoreactive band of each fraction was measured using the ImageJ software (http://rsbweb.nih.gov/ij/). In order to prevent false-positive values, the background of the surrounding membrane was additionally measured and subtracted individually for each band. The sum of the resulting values of cytosolic and microsomal fractions was defined as 100%. The relative portion of each fraction was subsequently calculated. Each experiment was repeated 3-4 times and the final values presented as the average of these multiple experiments. The standard deviation represents the differences between the repeated experiments.

Phos-tag™ SDS-PAGE

Phos-tag™ acrylamide was used on a normal SDS-PAGE at a concentration of 25-37µM. For reference see Kinoshita *et al.* 2006. General information about this reagent and for a detailed list of references see the homepage of the developer (http://www.phos-tag.com/english/) and the product description (http://www.phos-tag.com/english/shouh/pt_page_e_ver3.pdf).

Reverse transcriptase PCR analysis of *Arabidopsis mpk6-2* mutant and wild-type line

For RT-PCR analysis frozen root tissue from two weeks old Col-0 and *mpk6-2* mutant (SALK_073907) seedlings were homogenized in a 1,5ml Eppendorf tube and RNA was isolated using plantrna-OLS kit (OLS, Germany). RT-PCR analysis was performed with the help of the SuperScriptTMIII One-Step RT-PCR kit (INVITROGEN) using the following

specific primers: MPK6 forward 5`gc gga tcc atg gac ggt ggt tca agg 3` and reverse 5`gc act agt cta ttg ctg ata ttc tgg att g 3`.

The following run parameters were used for RT-PCR analysis:

One Step RT-PCR	**Temperature**	**Time**
reverse transcriptase	55°C	30min
denaturation	94°C	2min
denaturation	94°C	15sec
annealing	55°C	30sec
extension	68°C	1min
final extension	68°C	5min
cycles	26-30	

GUS staining procedure

Samples were processed according to Block and Debrouwer (1992) with 1 mM of 5-bromo-4-chloro-3-indolyl-D-glucuronide (X-Gluc) in staining buffer consisting of 0,1 M NaH_2PO_4; 0,1M Na_2HPO_4; 10 mM EDTA; 2 mM $FeK_3[CN]_6$; 2mM $FeK_4[CN]_6$ x $3H_2O$; 0.1% v/v Triton X100; pH 7.0 at 37°C for 2-18 hrs. To extract chlorophylls of aerial parts of the seedlings, samples were transferred to ethanol/acetic acid (1:1) with two or three changes. Specimen were examined with a stereo microscope (Leica MZFL III) equipped with a CCD camera. For image documentation a Diskus-program (Carl Hilgers, Königswinter, Germany) was used.

Whole mount immunofluorescence labelling

A. thaliana (Columbia 0) seedlings or the respective transgenic lines (all 4-6 days old) were fixed *in vacuo* using 1,5% formaldehyde and 0,5% glutaraldehyde in half strength microtubule stabilizing buffer (1/2 MTSB, see buffer list below) at pH 6,8. After successive washing (at least 4 times) with 1/2 MTSB followed by Phosphate buffered saline (PBS, see buffer list below), free aldehyde groups were reduced by 0,1% borohydrite in PBS. Cell walls were permeabilized by a mixture of cell wall digesting enzymes containing 2% [w/v] cellulase (CALBIOCHEM); 1% [w/v] pectinase, and 2% [w/v] driselase (SIGMA-ALDRICH) at 37°C

for 30min. Subsequently, the samples were permeabilized by 10% [v/v] DMSO and 2% [v/v] Nonidet P40 in PBS for 1h. For subsequent immunolabelling, samples were blocked using 1% [w/v] BSA in PBS for 1h and incubated with primary antibody (diluted in PBS containing 1% BSA) at 4°C overnight. Samples were washed with PBS and incubated with fluorescently labelled secondary antibody (also diluted in PBS containing 1% BSA) for 3h (1,5h at 37°C and 1,5h at room temperature). Finally, samples were mounted in one drop of mounting medium (0,1% [w/v] para-phenylenediamine prepared in 90% [v/v] glycerol in PBS). In the case that primary antibodies were raised in different host animals double labelling was performed using both primary antibodies simultaneously followed by secondary antibodies which were also applied simultaneously. If antibodies were raised in the same animal, immunolabelling was done successively and with increased washing periods between steps. In this case additional negative controls were performed using only one primary antibody and successive incubation with two fluorescent secondary antibodies.

Antibodies used for single and double labellings:

Rabbit polyclonal anti-AtMPK3 (diluted 1:350, SIGMA-ALDRICH); rabbit polyclonal anti-AtMPK4 (diluted 1:350, SIGMA-ALDRICH); rabbit polyclonal anti-AtMPK6 (diluted 1:750, SIGMA-ALDRICH); rabbit polyclonal anti-SCAMP1 (diluted 1:300, kindly provided by Liwen Jiang, University of Hong-Kong, China); mouse monoclonal anti-clathrin LC (diluted 1:300, SIGMA-ALDRICH); mouse monoclonal anti-Golgi 58k (diluted 1:350, SIGMA-ALDRICH); mouse monoclonal anti-GFP (diluted 1:500, ROCHE); rat monoclonal anti-tubulin (YOL1/34) (1:300-500, SEROTEC); plant specific mouse monoclonal anti-actin (1:100, SIGMA-ALDRICH, A0480)

Secondary antibodies were: AlexaFluor®488 and AlexaFluor®546, both goat anti-rabbit IgG (H+L) and goat anti-mouse IgG (H+L) (diluted 1:500, INVITROGEN). AlexaFluor®488 anti-rat IgG (1:500, INVITROGEN)

Transgenic *Arabidopsis* lines

For visualization of microtubules an *Arabidopsis* line expressing a fusion-construct of GFP with the microtubule-binding domain (MBD) of the animal MAP4-protein (Marc *et al.* 1998) was used. Control experiments were done with a line expressing a fusion-construct of YFP with TUA5, an isoform of *Arabidopsis* alpha-tubulin (Shaw *et al.* 2003). For visualization of the actin cytoskeleton another *Arabidopsis* line was used expressing a fusion-construct of

GFP with the actin-binding-domain 2 (ABD2) of the plant actin binding protein fimbrin (Voigt et al. 2005). For visualization of MPK6 a transgenic line was used expressing a *35S:GFP:MPK6* construct (generated by Martina Beck in our laboratory). For whole mount labelling of the endoplasmic reticulum, a transgenic line expressing a *mGFP5-ER* construct was used (kindly provided by Jim Haseloff, University of Cambridge, UK).

Confocal microscopy

For heat stress experiments:

The cytoskeleton in living *A. thaliana* roots was observed with a LEICA TCS 4D confocal laser scanning microscope (LEICA, Germany), equipped with an argon/krypton laser, using a 40x oil immersion objective. GFP fluorescence of chimeric MT and actin constructs (see above) was imaged using the 488nm excitation line of the laser and a 515nm long pass or 530nm band pass emission filter. Time-lapse series were generated from single optical sections of cells or tissues, which were captured at defined time intervals. Serial confocal optical sections were taken for Z-stack projections at different step sizes. The projection of image stacks and further image processing was done with the Scion Image software package (Scion Corporation) and Adobe Photoshop, respectively (Adobe Systems Inc.).

For all other studies:

Microscopical analysis was performed using an Olympus FV1000 upright confocal laser scanning microscope. All images were acquired with 4x/0.16 (dry), 10x/0.4 (dry) and 60x/1.35 (oil immersion) UPlanSApo objectives (Olympus). GFP as well as Alexa488-conjugated antibodies were excited at 488nm and detected between 505-530nm. Alexa546-conjugated antibody was excited at 543nm and detected at 550-650nm. Fluorescent vital dyes FM4-64 and AM4-65 were excited at 515nm or 488nm and detected at 650-750nm. To avoid bleed-through in double labelling experiments, all images were captured using line-sequential scanning mode. Post-processing of images was done with the aid of Olympus software FV1000 (Ver.1.7a), Image J 1.38x, Photoshop 6.0/CS, Microsoft Powerpoint and Open office applications.

Heat treatment and recovery

Slides with mounted plant seedlings were placed on a float in a water bath with temperatures set between 35°C and 42°C for 5 min up to 6 hours. Recovery took place at room temperature (20°C) for up to 2 days.

Inhibitor and stress treatments for biochemical analysis

In order to prevent unspecific stress reactions, plants grown on vertically oriented plates were layered horizontally and slightly covered with liquid ¼ strength Murashige & Skoog (¼MS) medium, prior to any treatment, for several hours. Brefeldin A (BFA, 50µM; 1,5h), H_2O_2 (10mM; 10min) and bacterial flagellin elicitor peptide, flg22 (10µM; 10-15min) were diluted in ¼ MS medium and carefully applied by exchanging liquids. Controls were identically treated by exchanging liquid medium.

Phenotype analysis of the *mpk6-2* mutant

Mutant seedlings were grown as described above. As a control, Col-0 seedlings were always grown in parallel on the same phytagel plate. Root and hypocotyl length of wild type versus mutant seedlings were measured after 5 days using the stereo microscope Leica MZFL III. Lateral roots were counted on 8 days old seedlings. Root length was only measured in those plants, which developed a visible root.

Dyes, inhibitors and elicitors

The following dyes, inhibitors and elicitors were used:

Name	**Company**	**Application**
FM4-64 (SynaptoRed)	BIOTIUM	1:2000
AM4-65 (fixable FM4-64)	BIOTIUM	1:1000
Brefeldin A (BFA)	SIGMA-ALDRICH	50µM / 1.5h
Wortmannin (WM)	SIGMA-ALDRICH	33µM / 1.5h
PD 98059	SIGMA-ALDRICH	20µM / 0.5-2h
Flg22	Provided by Silke Robatzek, MPI, Cologne, Germany	10µM / 10-15min
Hydrogen peroxide (H_2O_2)	SIGMA-ALDRICH	10mM / 10min

Frequently used buffers and solutions

½ MS medium

MS basal salt mixture (without vitamins)	2,3 g
sucrose	10 g
add Aqua dest.	1 l

pH 6, autoclaved

for solid medium incl. 4 g/l Phytagel

PBS

0,14 M NaCl	8,0 g
2,7 mM KCl	0,2 g
6,5 mM Na_2HPO_4 x H_20	1,15 g
1,5 mM KH_2PO_4	0,2 g
add Aqua dest.	1 l

pH 7,3

MTSB (1x)

50 mM PIPES	15,1 g (PIPES free acid MW = 302,4)
5 mM $MgSO_4$ x $7H_2O$	1,23 g
5 mM EGTA	10 ml of a 0,5 M stock solution
add Aqua dest.	1 l

pH 6,9 (with KOH)

Mounting Medium

p-Phenylenediamine	100 mg
Glycerol	90 %
PBS	10 %

pH 8,0; adjusted with carbonat/bicarbonate or Tris

Solutions for SDS-PAGE and Western-Blotting

Resolving gels (10-15 %)

Acrylamide/Bis (30%/2,67)	3.3 - 5.0 ml

Aqua dest.	2.4 - 4.1 ml
1,5 mM Tris-HCl, pH 8,8	2,5 ml
10 % SDS	100 µl
10 % ammonium persulfate	50 µl
TEMED	5 µl

Stacking gel (4 %)

Acrylamide/Bis (30%/2,67)	1,3 ml
Aqua dest.	6,1 ml
0,5 mM Tris-HCl, pH 6,8	2,5 ml
10 % SDS	100 µl
10 % ammonium persulfate	50 µl
TEMED	5 µl

4 x sample buffer

(62,5mM Tris-HCl, pH 6.8, 20% glycerol, 2% SDS, 5% β-mercaptoethanol)

Aqua dest.	3,0 ml
0,5M Tris-HCl, pH 6,8	1,0 ml
glycerol	1,6 ml
10 % SDS	1,6 ml
β-mercaptoethanol	0,4 ml
0,5% (w/v) bromphenol blue	0,4 ml

SDS-running buffer (10x)

250 mM Tris	30 g
1,92 M Glycine	144 g
10 % SDS	10 g
add Aqua dest.	1 l

Transfer buffer (1x)

20 mM Tris	9,68 g
150 mM glycine	45,05 g
10% methanol	400 ml
add Aqua dest.	4 l

TBS-buffer (10x)

100 mM Tris-HCl (pH 7,4)	12,1 g
1,5 mM NaCl	87,6 g
Add. A. dest.	1 l

TBS-T buffer

0,1 % Tween 20	500 µl
TBS buffer	500 ml

Solutions for molecular biology methods

Sample buffer for agarose gel electrophoresis

Brome phenol blue	0,25 %
Xylene Cyanole FF	0,25 %
Ficoll 400	15 %
in Aqua dest. (MilliQ)	

TAE (Tris acetate EDTA) buffer (50x)

Tris	242 g
0,5 M EDTA, pH 8,0	100 ml
Acetic acid 100 %	57,1 ml
add Aqua dest. (MilliQ)	1 l

TBE (Tris Borate EDTA) buffer (10x)

Tris	53 g
Boric acid	27,5 g
0,5 M EDTA, pH 8,0	20 ml
add Aqua dest. (MilliQ)	1 l

3. RESULTS

3.1 Specificity of antibodies against *Arabidopsis* MPK3, MPK4 and MPK6

In order to characterize the antibodies used for the detection of MPK3, MPK4 and MPK6, immunoblots of protein extracts from *Arabidopsis* roots were performed. Each antibody detected its specific MAPK at the predicted molecular weight of 43kDa for MPK3, 41kDa for MPK4 and 47kDa for MPK6 (Fig 4 A). However, the antibody against MPK4 but not MPK3 and MPK6 detected an additional band at ~55kDa. This additional band most likely represents a cytosolic protein, because it solely appeared within the cytosolic but not within the microsomal fraction (Fig 4 B).

Taken together, each antibody detected an individual protein band of predicted molecular size for the respective MAPK without cross-reacting with the other two MAPKs.

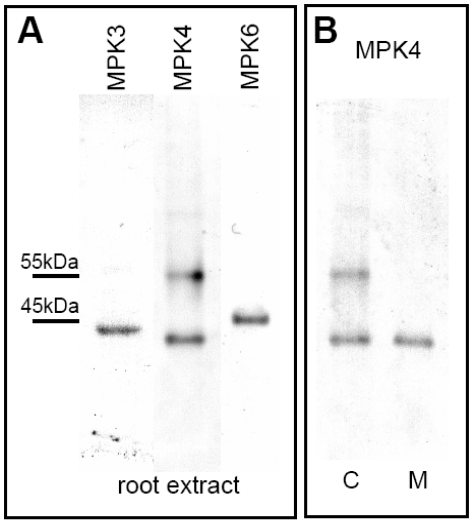

Figure 4. Characterization of MAPK-specific antibodies. (**A**) Immunoblot detection of MPK3 (43kDa), MPK4 (41kDa) and MPK6 (47kDa) using crude protein extracts from roots of one week old *Arabidopsis* seedlings. Note that each antibody detects a specific band at the predicted molecular size. (**B**) Immunoblot detection of MPK4 on isolated cytosolic and microsomal fractions prepared by differential centrifugation using a postnuclear extract of root proteins. Note that the additional 55kDa band only appears within the cytosolic fraction.

3.2 MPK3, MPK4 and MPK6 associate with microsomal and cytosolic fractions

To analyze the subcellular distribution of MPK3, MPK4 and MPK6, a quantitative immunoblot evaluation of cytosolic and microsomal protein fractions was performed. Previous to the measurement, cross-contamination of isolated fractions was excluded in both fractions by western blot analysis using marker antibodies against: (i) cytosolic phosphoenol pyruvate carboxylase (PEPC) and (ii) against PEP12, a transmembrane protein known to reside at late endosomes and pre-vacuolar compartments (PVC) (da Silva Conceição *et al.*

1997; Tse *et al.* 2004) (Fig 5 A). Although these results suggested relative purity of the fractions, both fractions were further tested by microscopic analysis. For this purpose the fluorescent lipophilic marker FM4-64 was directly applied on isolated fractions as a marker for microsomal membranes (Fig 5 B). FM4-64 stained only the microsomal but not the cytosolic fraction.

Subsequent immunoblotting experiments using antibodies against MPK3, MPK4 and MPK6 revealed high abundance of all three MAPKs in both cytosolic and microsomal fractions (Fig 6 A). Quantification of the intensity of immunoreactive protein bands from four independent experiments (Fig 6 B-C) revealed 55.1% of the total MPK3 signal to be associated with the microsomal and 44.9% with the cytosolic fraction. This suggests a major microsomal association of MPK3 with a difference of 10.2 % between both fractions. In contrast, MPK4 and MPK6 showed slightly different distributions. The respective average microsomal association was 40.5% for MPK4 and 44.8% for MPK6. This represents 19% difference between these two fractions for MPK4 and 10.4% for MPK6, suggesting a small majority of cytosolic localization. Taken together, all three MAPKs can be characterized as partially associated with the microsomal fraction.

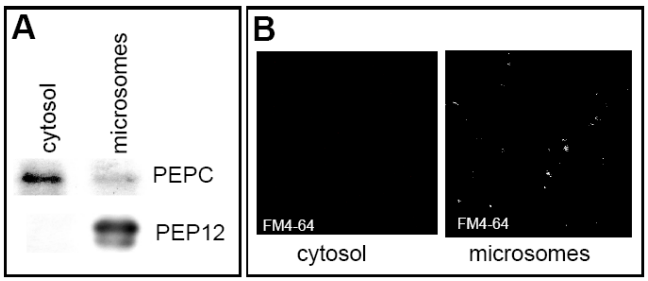

Figure 5. Purity test for cytosolic and microsomal fractions. (**A**) Immunoblot detection of the cytosolic protein PEPC and the transmembrane protein PEP12 on cytosolic and microsomal protein fractions prepared by differential centrifugation of a post-nuclear root extract. Note that there is almost no cross-contamination. (**B**) Microscopical analysis of cytosolic and microsomal fractions directly labeled with FM4-64 (5µg/ml for 10min). White spots represent labelled microsomal structures. Note that there is no labelling within the cytosolic fraction.

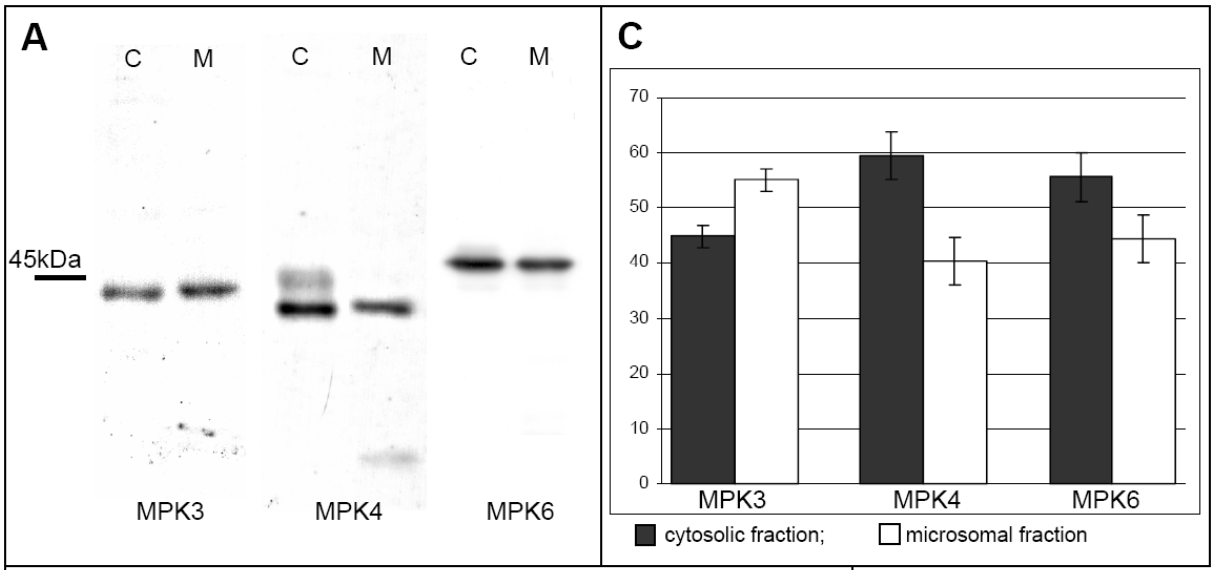

B

Average MAPK distribution in %				
MAPK	cytosolic	microsomal	std. deviation	difference
MPK3	44.9	55.1	± 2.0	10.2
MPK4	59.5	40.5	± 4.3	19
MPK6	55.2	44.8	± 4.3	10.4

Figure 6. Representative cytosolic and microsomal distributions of MPK3, MPK4 and MPK6. (**A**) Immunoblot detection of MPK3, MPK4 and MPK6 on cytosolic and microsomal protein fractions isolated from *Arabidopsis* roots. Note that all MAPKs are abundant within both fractions. (**B**) Average distribution of all three MAPKs. Abundance was calculated from four independent experiments for each MAPK. Note that MPK3 was most abundant within the microsomal fraction while the majority of MPK4 and MPK6 was detected within the cytosolic fraction. The overall difference between both fractions ranged between 10.2 % and 19 %. (**C**) Graphical presentation of values shown in B. C=cytosolic fraction; M=microsomal fraction. n=4

3.3 MPK3, MPK4 and MPK6 co-localize with PM, clathrin-, TGN- and Golgi-markers in isolated subcellular fractions

The association of all tested MAPKs with the microsomal fraction raised the question as to the identity and composition of microsomal membrane compartments. To address this, microsomal extracts of 2-week-old plants were sub-fractioned by density gradient centrifugation on a continuous sucrose gradient (30-55% sucrose). Total proteins of the different fractions were prepared for immunoblotting and probed with MAPK antibodies and with antibodies specific for different organellar marker proteins. Due to the fact that fractionation of microsomal extracts only yields relatively small amounts of protein per fraction, two gradients were prepared (Fig 7 A and B). Results obtained from the first gradient showed that all three MAPKs noticeably co-fractionated with the clathrin light chain recognized by monoclonal antibody specifically binding to a 28-29 kDa protein band

corresponding to one of three *Arabidopsis* CLCs, which were shown to functionally interact with clathrin heavy chain (CHC) (Scheele and Holstein 2002) (Fig 7 A). MPK3, MPK4 and MPK6 also co-fractionated with secretory carrier membrane protein1 (SCAMP1), representing a reliable marker for the trans-Golgi network (TGN), a tubular-vesicular secretory/endocytotic compartment partially coated by clathrin (Lam *et al.* 2007a). Further, all three MAPKs co-fractionated with two bands (63,5kDa and 66kDa) that were detected by an antibody against α-1,2-mannosidase I, a commonly used Golgi marker (for example Preuss *et al.* 2004a). On the other hand, MAPKs did not co-fractionate with SEC12, an ER-resident protein (Bar-Peled and Raikhel, 1997) or with PEP12, a marker of prevacuolar compartments (PVC).

Data from the second gradient shown in Fig 7 B revealed that the tested MAPKs co-localized with plasma membrane-intrinsic protein2;2 (PIP2;2), used as PM marker. Overall, there was only a negligible contamination with PEPC within the first fractions (30-40% sucrose) representing cytosolic protein. Because distribution of all three MAPKs was almost identical in all experiments, MPK6 was used as a representative MAPK in the second gradient.

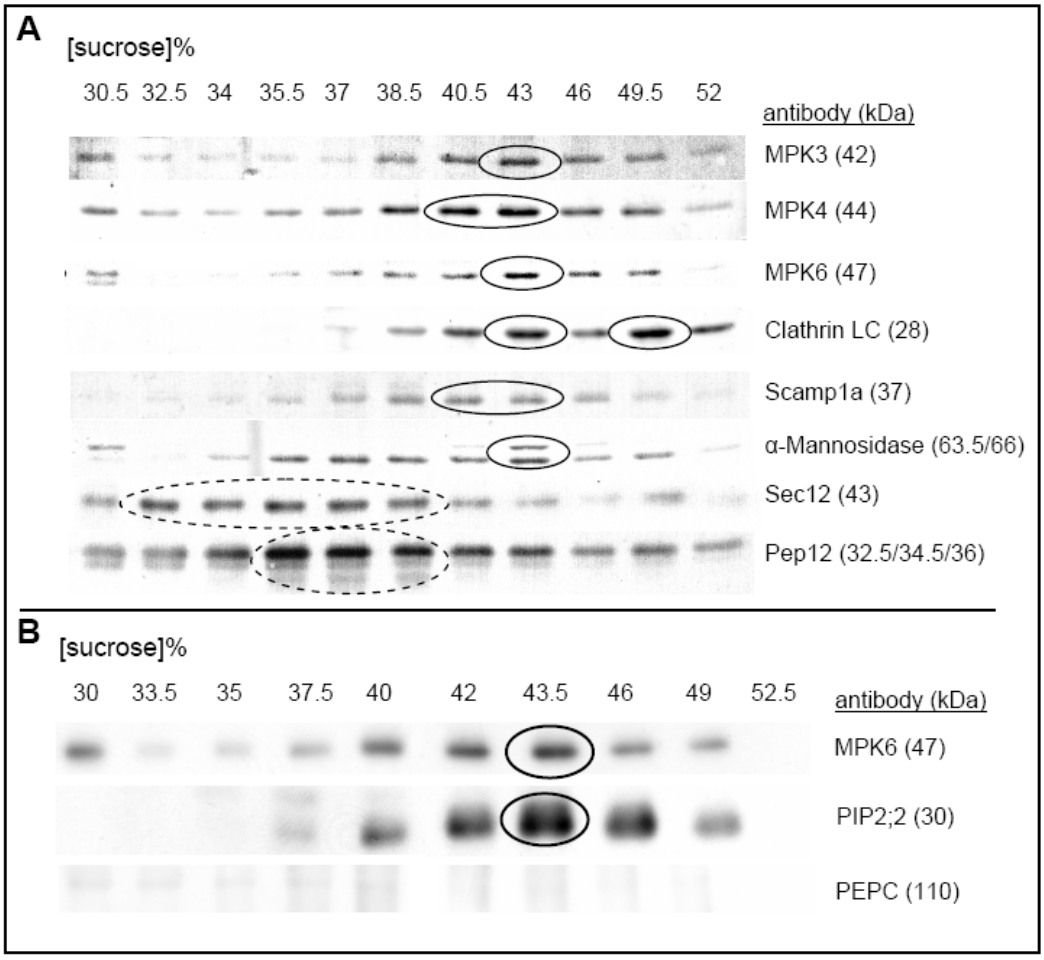

Figure 7. Distribution of microsomal MPK3, MPK4 and MPK6 within sucrose density gradients. (**A-B**) Immunoblot detection of microsomal MAPKs within single fractions of specific density after organelle separation by density gradient centrifugation. The localization of all MAPKs is shown in direct comparison to the distribution of specific organellar marker proteins. Among them, clathrin LC mainly represents PM, CCVs and TGN; SCAMP1a represents clathrin coated TGN; alpha mannosidase represents Golgi; Sec12 represents ER; Pep12 represents late endosomes/PVC; PIP2;2 represents PM. In addition, the cytosolic marker protein PEPC was tested to exclude cytosolic contaminations. All MAPKs and all tested marker antibodies showed unique distributions within gradient fractions. Circles mark fractions that showed the highest abundance (main peak) for each respective marker. Punctuated circles mark such peaks that did not overlap with the main peak of the MAPKs. Note that all MAPKs are similarily distributed and mainly overlap with marker proteins against clathrin, TGN, PM and Golgi.

3.4 MPK3, MPK4 and MPK6 localize to distinct spots/patches in the cytosol, at the cell cortex and in the nucleus of root cells

To further investigate the localization of all three MAPKs at the subcellular level, whole-mount immunolabellings on fixed *Arabidopsis* roots were performed using MAPK antibodies. To exclude unspecific labelling, control experiments were done using solely the secondary antibody. No signal was detected in such controls (Fig 8).

Microscopical analysis of several root tips from at least three independent experiments and for each MAPK revealed multiple localizations (Fig 9). Besides a diffuse cytosolic background, a multitude of spot-like and patch-like structures were labelled by all MAPK antibodies. Nuclear localization was found to be present in all cell types but showing some variability from cell to cell. Moreover, all MAPKs showed pronounced labelling at the PM (Fig 9 A, D and G; overviews).

Nevertheless, some clear differences among the MAPKs could be described. Thus, MPK3 showed the strongest microsomal labelling supporting the results from quantitative immunoblotting experiments. In meristematic cells, MPK3 labelling occurred all-over the surface of the PM (Fig 9 B, arrows) and was highly abundant within cytosolic spot-like and rod-shaped microsomal structures in post-meristematic elongating cells (Fig 9 C, arrowheads). Labelling of the PM did not change significantly within the different cell types. In contrast, both MPK4 and MPK6 generally labelled round shaped spot- and/or patch- like structures (Fig 9 E-F and H-I). Interestingly, dense spots often appeared along the PM in meristematic and post-meristematic epidermal cells (Fig 9 E and H, arrows), while both MPK4 and MPK6 seemed to be distributed randomly within cytosolic spots and patches in elongating cells (Fig 9 F and I, arrowheads). Both MAPKs sometimes lost clear association with the PM in elongating cells.

Taken together, these localization experiments strongly support the results from immunoblotting experiments (chapter 3.2) showing a clear association of MPK3, MPK4 and MPK6 with the microsomal fractions and microsomal subcellular structures in intact roots.

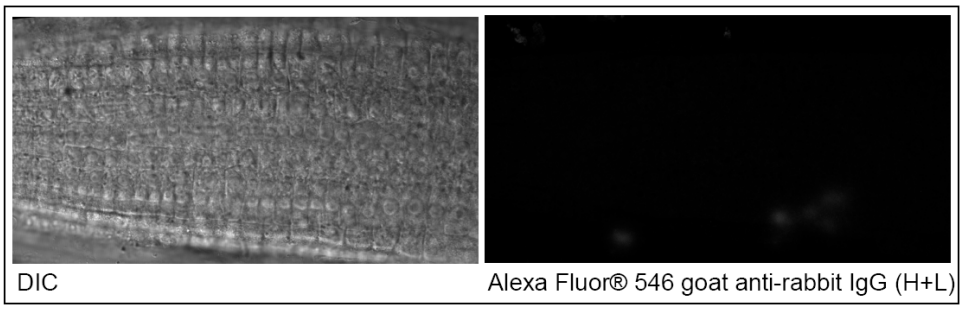

Figure 8. Secondary antibody control. Overview of a whole-mount labelled root-tip of a 6 days old *Arabidopsis* seedling. Labelling was done with the secondary antibody only in order to exclude detection of an unspecific signal caused by this fluorescent antibody. The figure shows a DIC image on the left and the corresponding immunolabelling on the right side. Note that there is no unspecific labelling. DIC= differential interphase contrast.

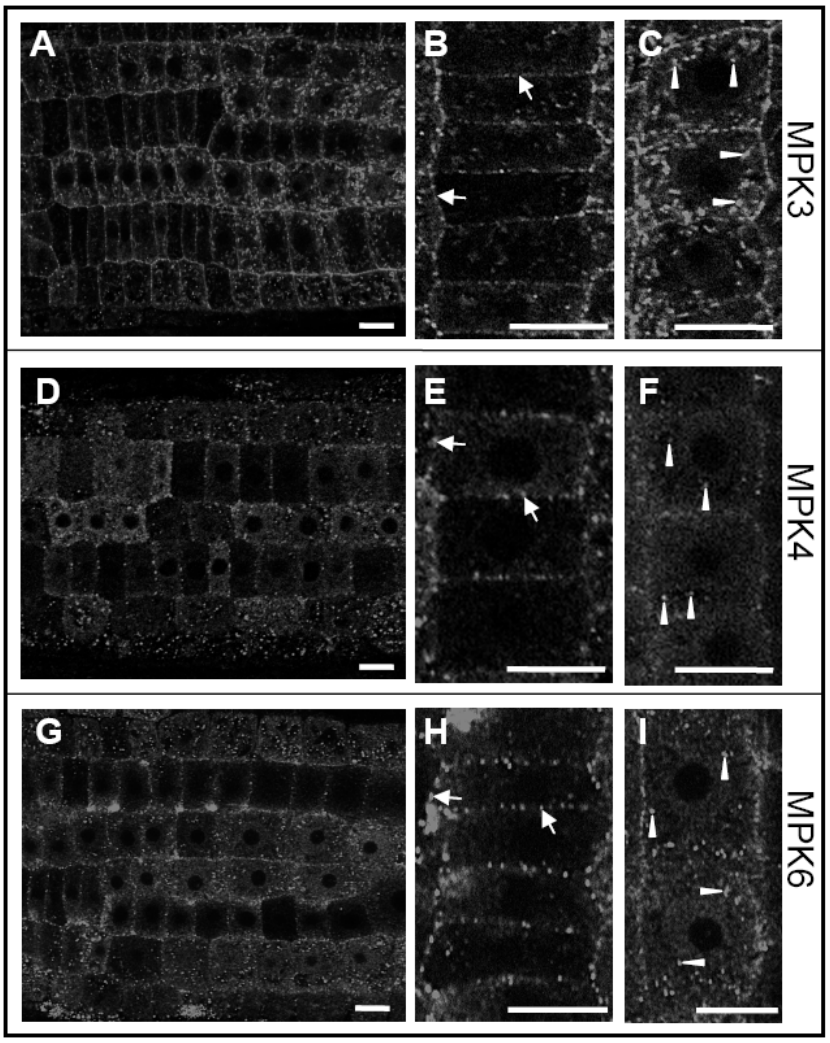

Figure 9. Whole-mount immunofluorescent localization of MPK3, MPK4 and MPK6. (**A, D, G**) Overview of fixed, antibody-labelled root tips of 6 days old *Arabidopsis* seedlings. All pictures show labelling of meristematic and post-meristematic elongating cells using specific MAPK antibodies. Note that there is a multitude of spot-like structures at cell peripheries and in the cytosol. (**B, E, H**) Detail of the distribution of MAPKs in meristematic cells. Arrows indicate punctuated labelling of the PM, which was found for all three MAPKs. (**C, F, I**) Detail showing typical distribution of MAPKs in post-meristematic elongating cells. Arrowheads indicate spot-like structures that often appeared within the cytosol of these cells. Note that the labelling of the PM is weaker in cells labelled with antibodies against MPK4 and MPK6 but not in cells labelled with MPK3.

3.5 Immunofluorescence double-labelling studies

In order to reveal the identity of the microsomal structures labelled by MAPK antibodies, whole-mount co-localization studies were performed using rabbit polyclonal MAPK antibodies in combination with the specific mouse monoclonal clathrin light chain (CLC) antibody, which was previously used for immunoblotting (chapter 3.3). Because this work mainly focusses on the characterization of MPK6, further double-labelling with marker antibodies against Golgi and TGN compartments were done only for this MAPK.

To avoid unspecific labelling and detection of unspecific signals, all experiments included negative controls with the two secondary antibodies alone (Fig 10) followed by microscopic analysis using the sequential scanning mode in a confocal laser scanning microscope (Olympus FV1000).

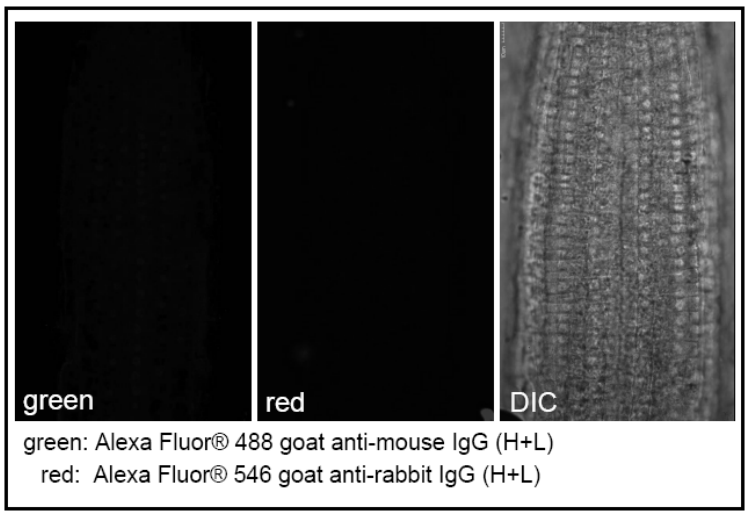

Figure 10. Secondary antibody control. Overview of a whole-mount labelled root-tip of a 6 days old *Arabidopsis* seedling. Labelling was done with a combination of red and green fluorescent secondary antibodies in order to exclude detection of an unspecific signal. The figure shows green and red channel and the corresponding DIC image on the right. Note that there is no fluorescence signal detected.

3.5.1 MPK3 and MPK4 co-localize with clathrin at the PM

Further supporting the above immunolabelling data, MPK3 was found to co-localize with CLC all along the PM (Fig 11 A-C, arrows). Interestingly, only the MPK3-positive spot-like but not the rod-shaped cytosolic microsomal structures partially associated with clathrin-labelled organelles (Fig 11 A-F, white arrowheads). In some cases, instead of a clear co-localization, MPK3-positive spots appeared only at specific domains of bigger compartments labelled by the CLC antibody (Fig 11 A-F, red arrowheads).

In contrast, MPK4 did not co-localize with CLC along the whole PM surface but rather within distinct spot-like domains (Fig 11 G-I, arrows). Similar to MPK3, cytosolic spots often associated with CLC-positive compartments (Fig 11 G-L, white arrowheads). As

in the case of MPK3, MPK4-positive spots were also sometimes overlapping with domains of CLC positive organelles (Fig 11 G-L, red arrowheads).

In summary, these experiments suggest an association of MPK3 and MPK4 with the PM and within specific domains of clathrin-labelled intracellular compartments.

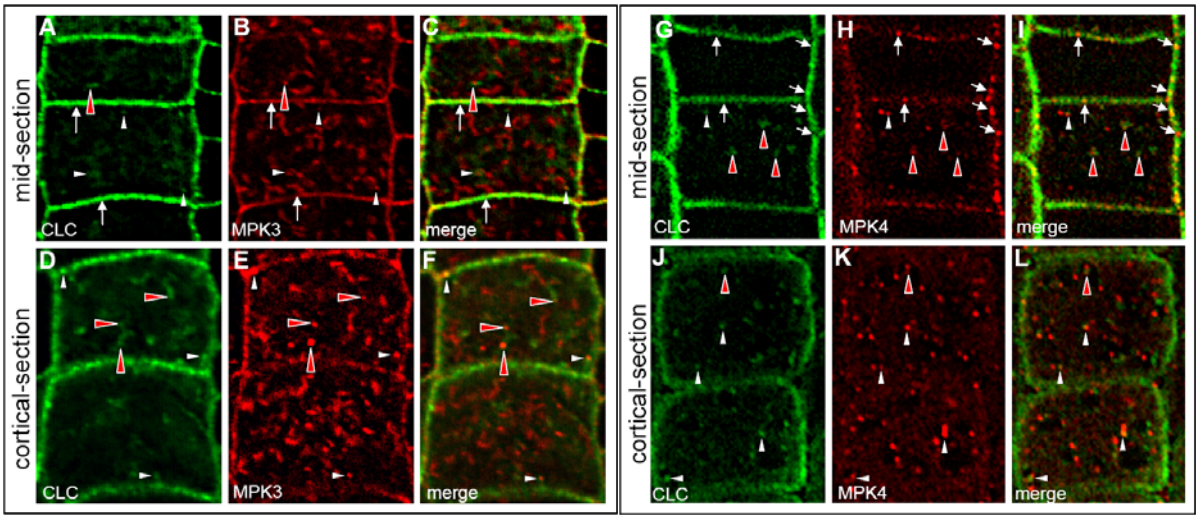

Figure 11. Whole-mount co-immunolabelling of clathrin light chain (CLC) and MPK3 or MPK4, respectively. (**A-C and G-I**) Single mid-sections of postmeristematic elongating root epidermal cells, showing typical distribution of CLC and MPK3 or MPK4, respectively. (**D-F and J-L**) Single cortical-sections directly underneath the PM. Arrows indicate co-localization of both proteins at the PM. Arrowheads indicate partial co-localization at spot like structures within the cytosol. Bigger red arrowheads indicate such MPK3- or MPK4-positive spot-like structures that partially co-localize with domains of bigger CLC positive compartments.

3.5.2 MPK6 co-localizes with clathrin at the PM and at the TGN

Two different approaches were used for co-localization of MPK6 with clathrin-coated subcellular structures. First, double co-immunolabelling was performed on wild-type seedlings according to the above method used for MPK3 and MPK4. Second, transgenic *Arabidopsis* seedlings stably expressing a *CLC:GFP* construct (using the At2g40060 CLC sequence, which is coding for the 28,8 kDa light chain protein) (Konopka *et al.* 2008) were used to visualize clathrin:GFP in combination with MPK6. In this case, seedlings were co-labelled with rabbit MPK6 antibody and with a monoclonal mouse GFP antibody (Fig 12 A-I).

Microscopic analysis revealed that MPK6 co-localized *in-situ* with both native CLC (Fig 12 A-F) as well as with the CLC:GFP fusion protein (Fig 12 G-I). As in the case of MPK4, this co-localization occurred mainly in spot-like structures/domains directly at the PM

(Fig 12 A-I, arrows) or within the cytosol (Fig 12 A-I, arrowheads). In comparison to the *in-situ* CLC labelling, CLC:GFP fusion protein strongly labelled spot-like cytosolic organelles that often clearly co-localized with MPK6 (Fig 12 G-I, arrowheads).

To further test, whether these spot-like structures represent the partially clathrin-coated TGN, antibodies against the TGN localized secretory carrier membrane protein1 (SCAMP1) (Lam *et al.* 2007a) were used for co-localization with MPK6. Double labelling of MPK6 and SCAMP1 clearly revealed their co-localization at the TGN (Fig 13 J-O, arrowheads). Because MPK6 and SCAMP1 were both raised in rabbit, specific negative controls were performed in order to exclude unspecific labelling (Fig 13).

In order to localize Golgi-stacks a specific commercial mouse monoclonal antibody against Golgi resident 58k protein was used (Li and Yan 2000; Baluska *et al.* 2002). As shown in Fig 12 P-U, epidermal cells contained widely dispersed Golgi-stacks within the cytosol. In analogy to the TGN, which is known to be closely attached to the Golgi-stacks in some cases (reviewed by Staehelin and Kang 2008), MPK6-positive spots showed no direct co-localization but were occasionally found in association with Golgi-stacks. This further supports the conclusion of MPK6 being localized at the TGN.

In summary, these experiments suggest an association of MPK6 with clathrin at the PM and at the TGN.

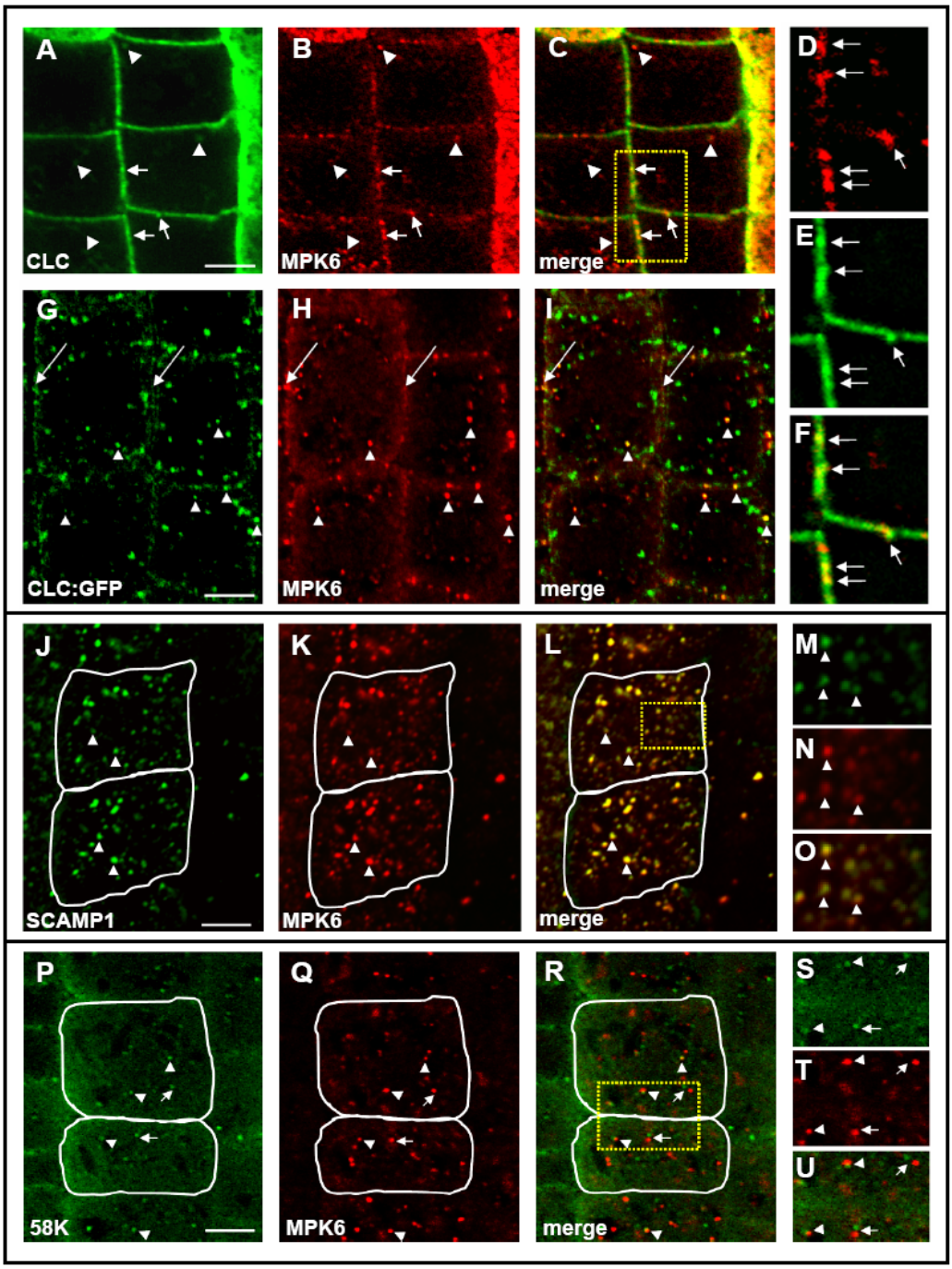

Figure 12. Co-localization of MPK6 with clathrin, TGN and Golgi in *Arabidopsis* root epidermal cells using whole-mount immunofluorescence labelling. (A-C) Co-localization of CLC and MPK6. **(D-F)** Magnification of boxed area in C. **(G-I)** Co-localization of CLC:GFP and MPK6 in transgenic root epidermal cells expressing a *35S::CLC:GFP* construct. Arrows indicate co-labelling at the PM, arrowheads indicate co-localization on cytosolic microsomal spots. Note that MPK6 massively co-localizes with clathrin at spot-like structures along the PM and within the cytosol. **(J-L)** Co-localization of MPK6 and TGN marker SCAMP1. **(M-O)** Magnification of boxed area in L. Note that both proteins almost completely co-localize on spot-like structures within epidermal cells. Arrowheads indicate some of the spots that are co-localizing. **(P-R)** Co-localization of MPK6 and Golgi marker 58k. **(S-U)** Magnification of boxed area in R. Arrowheads indicate spots that are tightly associated with each other. Arrows indicate spots that are clearly unconnected. Note that there is partially a tight association but no direct co-localization of spots labelled by both antibodies. Images A-I show single midplane sections of the cells in order to better illustrate PM localization, while images J-U show single cortical section of the cells in order to illustrate cytosolic, spot-like localization. Bars are 5µm.

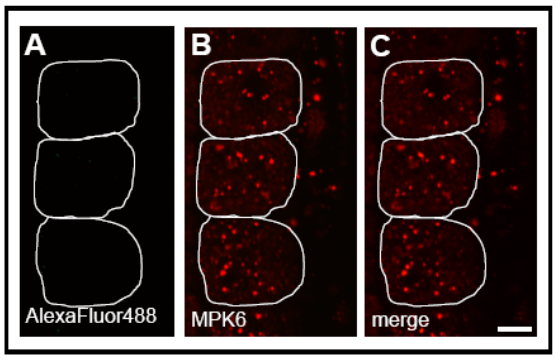

Figure 13. Negative controls for double immunolabeling with MPK6 and SCAMP1 antibodies. Postmeristematic root epidermal cells (A-C) were successively labelled by a combination of (i) rabbit anti-MPK6 as primary antibody and the red fluorescent secondary anti-rabbit AlexaFluor546 antibody followed by (ii) the green fluorescent anti-rabbit AlexaFluor488 as control. Note that there is no unspecific labelling with the green fluorescent secondary antibody. Bar is 5µm.

3.6 GFP:MPK6 co-localizes with the vital endocytotic tracer FM4-64

To further characterize the identity of MPK6-positive subcellular compartments, a transgenic *Arabidopsis* line stably expressing a *35S::GFP:MPK6* construct (developed by Martina Beck in our lab) was used for *in-vivo* and *in-situ* microscopic co-immunolabelling studies. Additionally, these transgenic plants were incubated with the endocytotic tracer FM4-64. FM4-64 is a red fluorescent amphiphilic styryl dye that, if applied exogenously, incorporates into the PM. Following the endocytotic pathway, this marker sequentially labels early endosomes, late endosomes and vacuolar membranes (tonoplast) in plants (Bolte *et al.* 2004). Therefore, it is commonly used to determine, if a protein is associated with the subcellular endocytotic network (for review see Müller *et al.* 2007b).

Immunoblotting analysis of microsomal and cytosolic protein fractions from these transgenic plants using antibodies against MPK6 and GFP revealed that the GFP:MPK6 (74kDa) fusion protein was clearly present in both fractions (Fig 14 A). This suggests that the GFP-tag does not disturb the microsomal association of MPK6. Moreover, the fact that the MPK6 antibody but not the GFP antibody specifically detects two bands representing the fusion protein and native MPK6 (47kDa), again demonstrates the antibody specificity.

In-vivo microscopic analysis showed that GFP:MPK6 co-localizes with FM4-64 at the PM and on spot-like endosomes within root epidermal cells (Fig 14 B-D). Further, time-lapse imaging provided evidence that these spots are moving along selective tracks throughout the cell (Fig 14 E-J). Therefore, these experiments strongly support the biochemical fractionation and co-immunolabelling data presented in chapters 3.2 - 3.5.

In contrast to growing epidermal root cells, which mainly showed spot-like structures embedded in an overall diffuse cytoplasmic fluorescence of GFP:MPK6, fully grown epidermal cells often showed labelling of a network like structure strongly resembling the ER-

network of such cells (Ridge *et al.* 1999) (Fig 15). Bright fluorescent spots that co-localized with FM4-64 labelled endosomes appeared within this network (Fig 15, arrows). To further test, whether MPK6 localizes to the ER, transgenic seedlings stably expressing a mGFP5-ER construct (kindly provided by Jim Haseloff, University of Cambridge, UK) were co-immunolabelled with a mouse GFP antibody and with the antibody against MPK6. mGFP5-ER is a fusion protein containing an N-terminal signal peptide derived from the *Arabidopsis* vacuolar basic chitinase and the C-terminal amino acid sequence HDEL. HDEL is a tetrapeptide sequence that acts as an ER retention signal and therefore specifically labels ER structures.

Microscopical analysis of fully grown root epidermal cells showed that MPK6 did not localize to the ER network (Fig 16) but several MPK6-positive spots were clearly embedded in gaps within this network (Fig 17, arrows). These spots probably represent those bright fluorescent spots, which co-localized with FM4-64 (Fig 15).

Taken together, these experiments supported the biochemical results, excluding an association of MPK6 with the ER and it provides further evidence that native MPK6 localizes to endosomal structures.

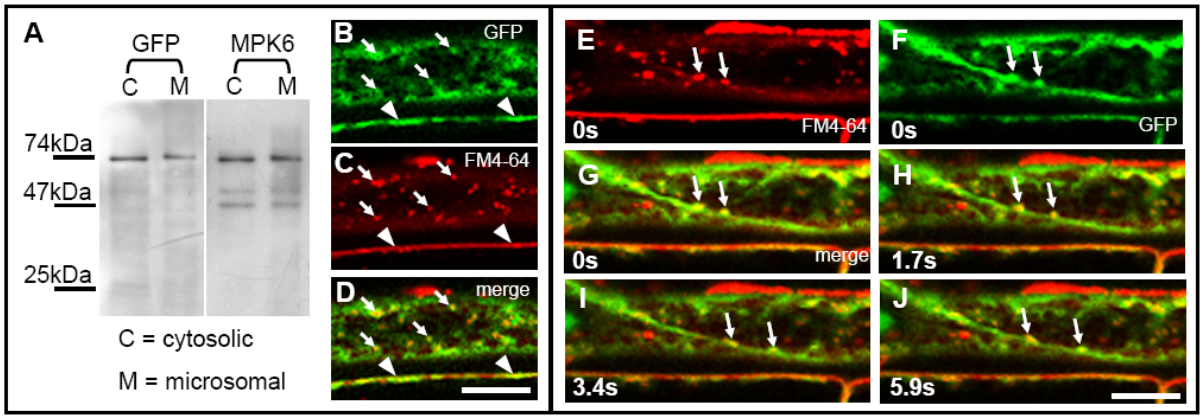

Figure 14. ***In vivo*** **localization of GFP:MPK6 in transgenic** ***Arabidopsis*** **roots. (A)** Distribution analysis of GFP:MPK6 (74kDa) in cytosolic and microsomal fractions using MPK6- and GFP- specific antibodies. Note that the GFP:MPK6 fusion protein is abundant in both fractions. (B-D) Co-localization of GFP:MPK6 and FM4-64 on endosomal organelles (white arrows) and at the PM (arrowheads) in root epidermal cells. (E-J) Time series showing co-labelled mobile GFP:MPK6 and FM4-64 positive endosomes (arrows). Time is indicated at the bottom of each image. Bars represent 10µm.

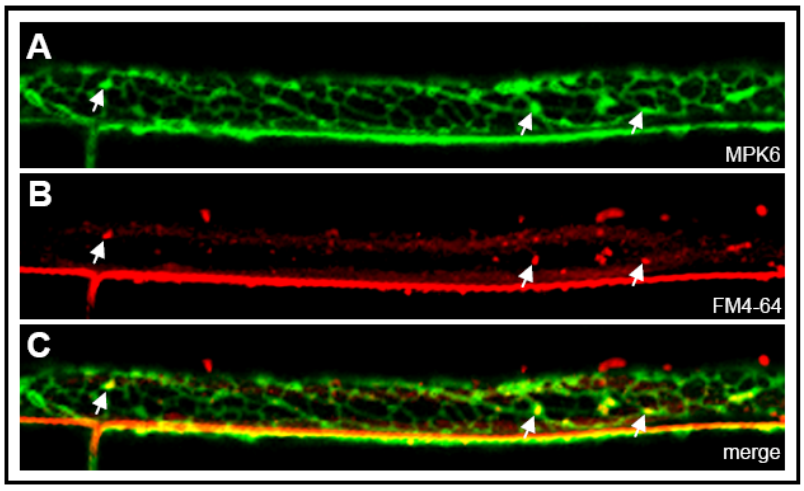

Figure 15. ***In vivo*** **localization of GFP:MPK6 in fully grown root epidermal cells of transgenic** ***Arabidopsis*** **roots. (A)** Localization of GFP:MPK6 within an ER-like network in fully grown root epidermal cells. Arrows indicate bright fluorescent spots within the network. (**B**) Labelling of endosomes (arrows) by the endocytotic marker FM4-64. (**C**) Merged image of A and B. Note that FM-labelled endosomes co-localize with the bright fluorescent spots visualized by the GFP:MPK6 fusion protein.

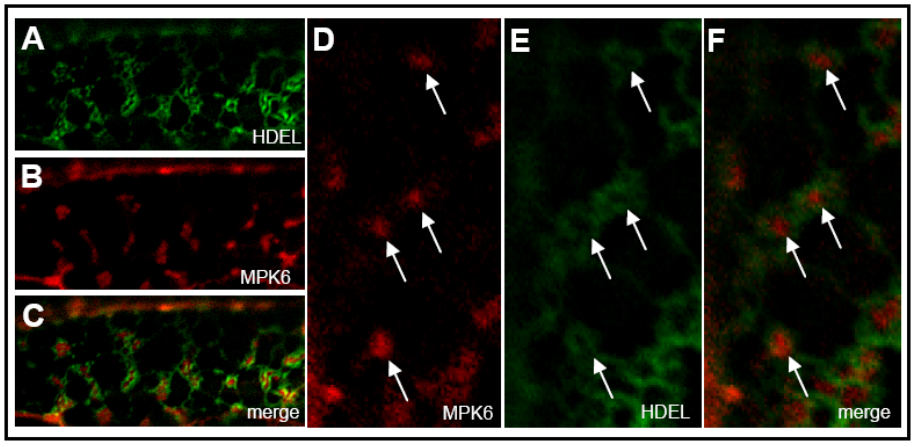

Figure 16. Whole-mount co-immunolabelling of mGFP5-ER and MPK6 in fully grown root epidermal cells of transgenic ***Arabidopsis*** **roots. (A; E)** Labelling of the ER network by a GFP-specific antibody detecting **mGFP5-ER.** (**B; D**) Labelling of MPK6 using MPK6-specific antibody. (**C; F**) Merged images. Arrows indicate MPK6 positive spots and their localization with respect to the ER network. Note that almost all MPK6 labelled spots are located in gaps within this ER network.

3.7 Oxidative stress causes phosphorylation of cytosolic but not microsomal MAPKs

In order to test the phosphorylation status of microsomal and cytosolic MPK3, MPK4 and MPK6 under oxidative stress conditions, 6-8 days old seedling roots were treated with 10mM H_2O_2 for 10 minutes (Noriega *et al.* 2009) and compared to control plants by immunoblot analysis using Phos-tag™ acrylamide gels. Phos-tag™ is a phosphate binding tag that is embedded in the acrylamide network of the SDS-gels. By loosely binding phosphorylated proteins, this tag is able to slow down their movement during electrophoresis. This causes the appearance of multiple bands with each band representing a specific phosphorylation status of the detected protein (see also Material and Methods).

Application of H_2O_2, which is thought to act as a general upstream activator of MAPKs (reviewed by Colcombet and Hirt 2008) affected the phosphorylation status of all three MAPKs (Fig 17). In untreated plants, the MPK3 antibody detected multiple phosphorylated bands of different intensity and size in both cytosolic and microsomal fractions. Interestingly, the intensity of some bands in the microsomal fraction significantly decreased, while those in the cytosolic fraction became significantly stronger in H_2O_2 treated plants.

A similar result was found also for MPK4 and MPK6. Phosphorylated bands were clearly detected within the cytosolic but not the microsomal fraction after H_2O_2 application for both MAPKs. Taken together, these experiments indicate that H_2O_2 -induced activation of all three MAPKs mainly occurs in the cytosol.

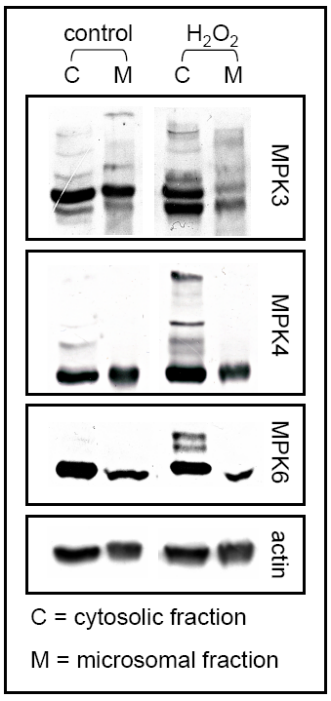

Figure 17. Phosphorylation analysis of MAPKs after H_2O_2 treatment using Phos-tag™. Immunoblots from cytosolic and microsomal fractions using antibodies against MPK3, MPK4 and MPK6 of control versus H_2O_2 treated plants (10mM for 10 min). SDS-PAGE was done using Phos-tag™ gels. Each protein band, detected by the respective MAPK antibody represents one specific phosphorylation status. Higher bands represent multiple phosphorylations. Note that all three MAPKs show multiple additional bands after treatments with H_2O_2. Actin was detected as a loading control.

3.8 Treatment with Brefeldin A (BFA) alters MAPK distribution but does not affect MAPK activity

Brefeldin A (BFA) is a fungal toxin that is extensively used as a general inhibitor of secretion and membrane recycling, which causes the accumulation and aggregation of early endocytotic TGN vesicles in *Arabidopsis* (for detailed overview see chapter 1.4.2). Because proteins residing on organelles of the early endocytotic pathway mostly show some sensitivity to BFA (see below) it can be used as an indicator to identify the specific localization of those proteins.

Immunoblotting experiments on isolated cytosolic and microsomal fractions of control and BFA-treated roots (50µM for 1.5h) of 6-8 days old seedlings were performed to test, whether MPK3, MPK4 and MPK6 distribution is affected by this pharmacological disturbance of membrane recycling. BFA treatment caused a significant increase in all MAPKs within the cytosolic fraction accompanied by a comparable decrease in the microsomal fraction (Fig 18 A). Distribution analysis combined from three independent experiments revealed an average amount of 61.3 % (MPK3), 64.4 % (MPK4) and 68.7 % (MPK6) of cytosolic MAPK protein in treated roots (Fig 18 B and C). According to the previous measurements done on non-treated plants (see Fig 6), this values represent a cytosolic shift of 32.8 % for MPK3, 9.8 % for MPK4 and 27 % for MPK6 (Fig 18 B).

In summary, all three MAPKs seem to partially loose their association with microsomes upon BFA treatment. To further check, whether the observed reaction is accompanied by activation the phosphorylation status of microsomal and cytosolic MAPKs in BFA-treated versus control plants was compared by immunoblot analysis using Phos-tag™ Acrylamide gels. No significant additional phosphorylated bands could be detected upon BFA treatment (Fig 19).

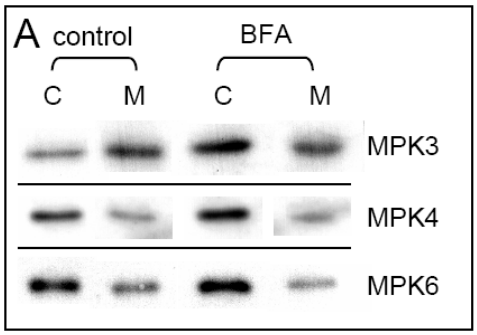

C = cytosolic ■ M = microsomal □

[ ] = distribution in control plants

B Average MAPK distribution in %

MAPK	cytosolic	microsomal	std. deviation	difference	cytosolic shift
MPK3	61.3	38.7	± 1.3	22.6	32.8
MPK4	64.4	35.6	± 6.2	28.8	9.8
MPK6	68.7	31.3	± 4.4	37.4	27

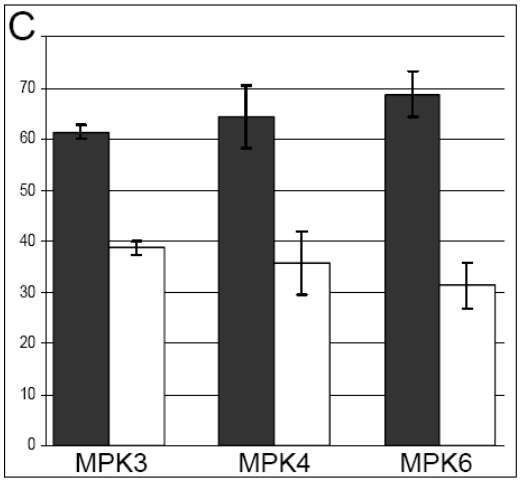

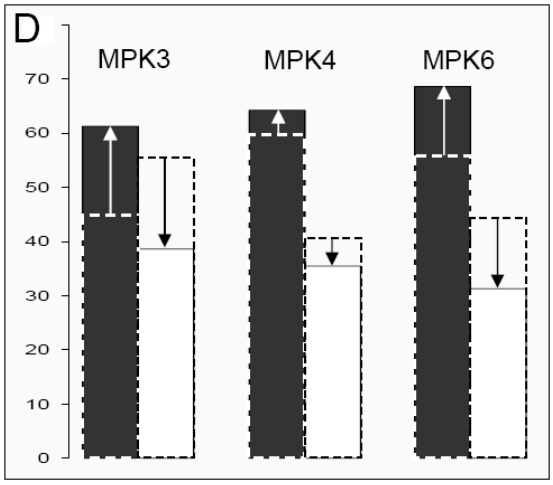

Figure 18. Distribution analysis of MPK3, MPK4 and MPK6 in BFA treated roots. (A) Immunoblot analysis of the distribution of cytosolic (C) and microsomal (M) MAPKs in control versus BFA treated (50µM/1.5h) roots of 6-8 days old seedlings. (**B**) Average cytosolic and microsomal distribution of all three MAPKs after BFA treatment, calculated from 3 independent experiments. Also shown are the values for the cytosolic shift for each MAPK, calculated by direct comparison with values from untreated plants shown in Figure 6. (**C**) Graphical view of the average MAPK distribution after BFA treatment. (**D**) Graph showing changes in the distribution of all MAPKs after BFA in comparison to untreated cells.

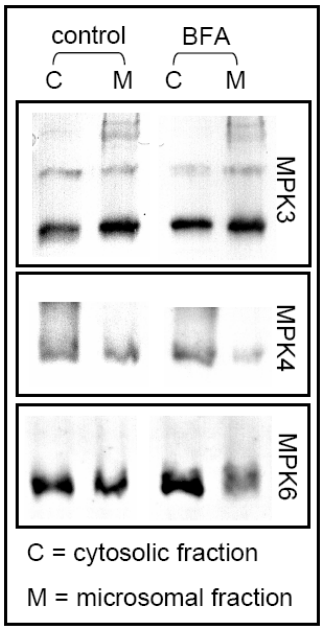

Figure 19. Phosphorylation analysis of MAPKs after BFA treatment using Phos-tag™. Immunoblots on cytosolic and microsomal fractions using antibodies against MPK3, MPK4 and MPK6 of control versus BFA treated plants (50µM / 1.5h). Each protein band detected by the respective MAPK antibody represents one specific phosphorylation status. Higher bands represent multiple phosphorylations. Note that the phosphorylation status of all three MAPKs did not change after BFA treatment.

3.9 Microsomal MPK6 participates in flagellin signalling

3.9.1 Microsomal and cytosolic MPK6 becomes phosphorylated in flg22-treated plants

Until now, flagellin induced internalization of FLS2 is the only experimentally proven example of receptor-mediated endocytosis (RME) in plant cells (see also chapter 1.3). To investigate, whether microsomal MPK6 is specifically involved in the flagellin-triggered stress response, *Arabidopsis* seedlings were treated with the 22-amino-acids long flagellin peptide flg22, which is known to activate MPK6 (Nühse *et al.*, 2000). When the phosphorylation status of both cytosolic and microsomal MPK6 fractions was tested upon flg22 treatment, two phosphorylated bands appeared in the cytosolic fraction and a weaker single band of phosphorylated MPK6 in the microsomal fraction (Fig 20), suggesting that differently phosphorylated MPK6 subpopulations are associated with different cellular compartments.

Because H_2O_2 was shown to activate cytosolic but not microsomal MPK6 (see Fig 17) this experiment provided a first indication that stimulus-specific signalling of MPK6 is coupled with its spatial cellular organization.

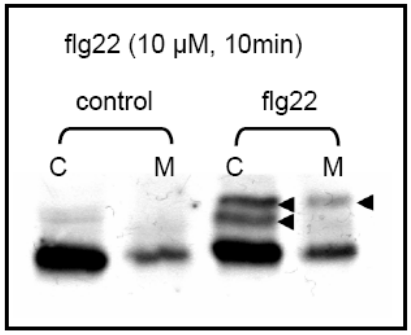

Figure 20. Phosphorylation analysis of MPK6 after flg22 treatment using Phos-tag™. The figure shows immunoblots of cytosolic and microsomal fractions prepared from control versus flg22 treated roots (10µM for 15min) using the antibody against MPK6. SDS-PAGE was performed with Phos-tag™ gels. Note that the antibody clearly detects additional bands within both fractions of flg22 treated roots.

3.9.2 FLS2 redistributes to early endosomal fractions after flagellin treatment

In *Arabidopsis* leaves it was shown previously that a FLS2:GFP fusion protein localizes to the PM, but becomes rapidly internalized to yet unidentified endocytotic organelles after flagellin triggered activation (Robatzek *et al.* 2006). In order to test, whether FLS2 and MPK6 associate with the same endocytotic organelle, plant cells were treated with the elicitor epitope flg22. Microsomal extracts from flg22-treated plants were fractionated in sucrose density gradients and FLS2 distribution was determined in treated versus control plants and this was compared with previously described localization of MAPKs and organellar markers. For this purpose, a polyclonal FLS2 antibody was used (kindly provided by Silke Robatzek, MPI, cologne, Germany). As shown in Fig 21 A, the FLS2 antibody specifically detected one band at the predicted size of around 170kDa (Chinchilla *et al.* 2007).

Untreated plants showed the strongest localization within fractions of 35.5-38.5 % sucrose. A second, small maximum was additionally found in the 49.5 % sucrose fraction (Fig 21 B and D). In contrast, flg22-treated plants showed an extended distribution including the fractions between 39-43 % sucrose (Fig 21 C-D). Compared with previous results (see Fig 7), untreated plants showed an FLS2 distribution corresponding with the localization of the late endosomal marker PEP12. Moreover, the much smaller maximum at 49.5 % sucrose corresponds with one of the two CLC maxima. In contrast, flg22 treated plants showed an additional distribution that also included fractions typically accumulating MAPKs and early endosomal compartments, indicating that activated FLS2 partially relocates to the same organelles, MAPKs are associated with.

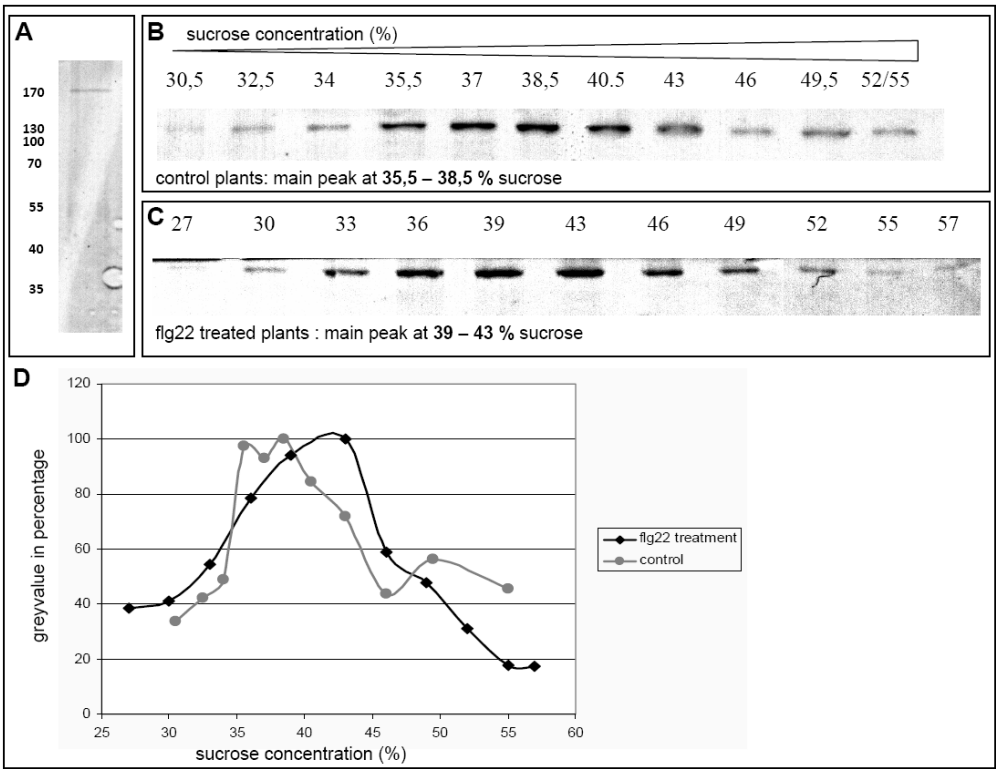

Figure 21. Distribution of FLS2 using sucrose density gradients. (A) Immunoblot of crude protein extract from 2 weeks old *Arabidopsis* seedlings using polyclonal anti-FLS2 antibody. Note that there is only one specific band at the predicted molecular size of ~170 kDa. **(B-C)** Immunoblot detection of FLS2 in fractions of specific density after microsome separation by density centrifugation. (**B**) Distribution in untreated control plants. Note that FLS2 is mostly present in fractions between 35.5 % and 38,5 % sucrose, corresponding to the distribution of the late endosomal marker PEP12 (**Figure 7**). (**C**) Distribution of FLS2 in flg22-treated plants (10µM for 15min). Note that FLS2 is most abundant in fractions with 39 % and 43 % sucrose, corresponding to the detection of MAPKs and the endosomal marker SCAMP1. (**D**) Graphical view of the FLS2 distribution shown in B-C. The mean greyvalue of each band was measured and the value of the strongest band was taken as 100% for each gradient. The percentage of all other fractions was calculated proportional to this maximum.

3.9.3 FLS2-GFP localizes to the PM and co-localizes with FM4-64 in Arabidopsis roots

To further characterize the localization of FLS2 in roots, a transgenic *Arabidopsis* line stably expressing FLS2-GFP under the control of its native promoter (kindly provided by Silke Robatzek, MPI, Cologne, Germany) were microscopically analyzed. In order to test, whether FLS2 is associated with the membrane compartments of the endocytotic pathway, transgenic plants were co-labelled with FM4-64 and additionally treated with BFA (50µM/1.5h). As shown in Fig 22 A, FLS2-GFP clearly localized to the PM and in cytosolic spots and co-localized with the endocytotic marker FM4-64 at the PM (Fig 22 A-C, arrows) but not within endosomal compartments (Fig 22 A-C, arrowheads).

Interestingly, when treated with BFA FLS2-GFP accumulated within BFA compartments and partially co-localized with FM4-64 on smaller cytosolic spots (Fig 22 D-F). However, some of the FLS2-GFP labelled spots clearly did not co-localize with FM4-64.

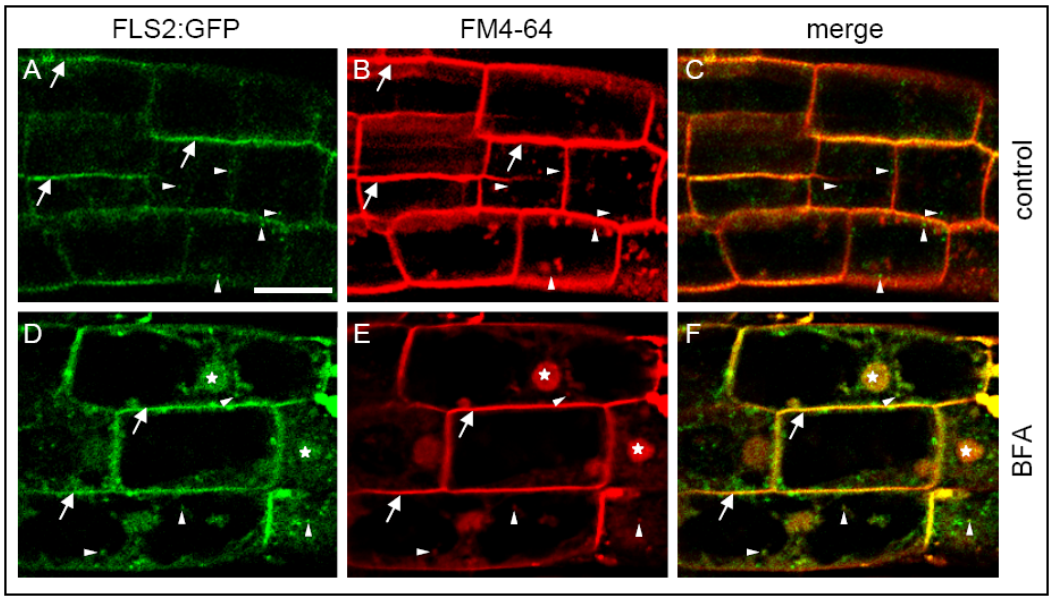

Figure 22. Subcellular distribution of FLS2-GFP in roots of transgenic *Arabidopsis* seedlings. (**A-C**) Co-localization of FLS2-GFP and FM4-64 (1.5h). Arrows indicate co-localization at the PM. Arrowheads indicate cytosolic spots containing FLS2-GFP. Note that these spots do not co-localize with FM4-64 labelled endosomes. (**D-F**) Co-localization of FLS2-GFP and FM4-64 after BFA treatment (50µM/1.5h). Arrows indicate co-localization at the PM. Arrowheads indicate co-localization in spot-like structures. Stars indicate co-localization within BFA compartments. Bar in A represents 10µm.

3.10 Cytoskeletal association of MPK6

Growing evidence suggests that MAPK activity is also involved in the regulation of cytoskeletal arrangement and dynamics in plants (Šamaj *et al.* 2002 and 2004). Interestingly, several studies described MAPK regulation of tubulin- and actin-binding proteins such as kinesins (Ishikawa *et al.* 2002; Nishihama *et al.* 2001 and 2002), MAP65 proteins (Smertenko *et al.* 2006) or profilins (Limmongkon *et al.* 2004).

In order to check, whether MPK6 is directly associated with cytoskeletal elements in *Arabidopsis* roots whole-mount co-localization studies were performed on 5-6 days old seedlings using the rabbit MPK6 antibody in combination with a specific rat derived antibody against α-tubulin or with a mouse derived antibody against plant actin, respectively.

3.10.1 MPK6 co-localizes with mitotic and cortical MTs

Microscopic analysis revealed that the α-tubulin antibody clearly labelled all known microtubular structures, namely cytokinetic microtubules (MTs) (Fig 23 B, E, H and K), subcortical MTs (Fig 23 N) as well as a dense, well defined cortical array directly underneath of the PM (Fig 23 U). MPK6 was found to associate with mitotic microtubules including the

preprophase band (PPB) and the phragmoplast but not or only weakly with the mitotic spindle (Fig 23 A-L, arrows). Further analysis revealed that MPK6 also localizes within spot-like structures at the level of the maturing cell plate (Fig 23 G-I). Moreover, MPK6 co-localized within spot like structures in the subcortical area of elongating postmeristematic cells (Fig 23 M-O, arrowheads). In contrast, non dividing meristematic cells did not show cytosolic spots but revealed close association of MPK6 with the PM (Fig 23 P-R, arrowheads).

MPK6 also co-localized with MTs of the cortical array. In most cases this localization appeared in a spot like manner though less clearly defined because of a higher diffuse cytosolic background (Fig 23 S-V). However, in some cases MPK6 clearly labelled the complete cortical MT array (Fig 23 W-Y).

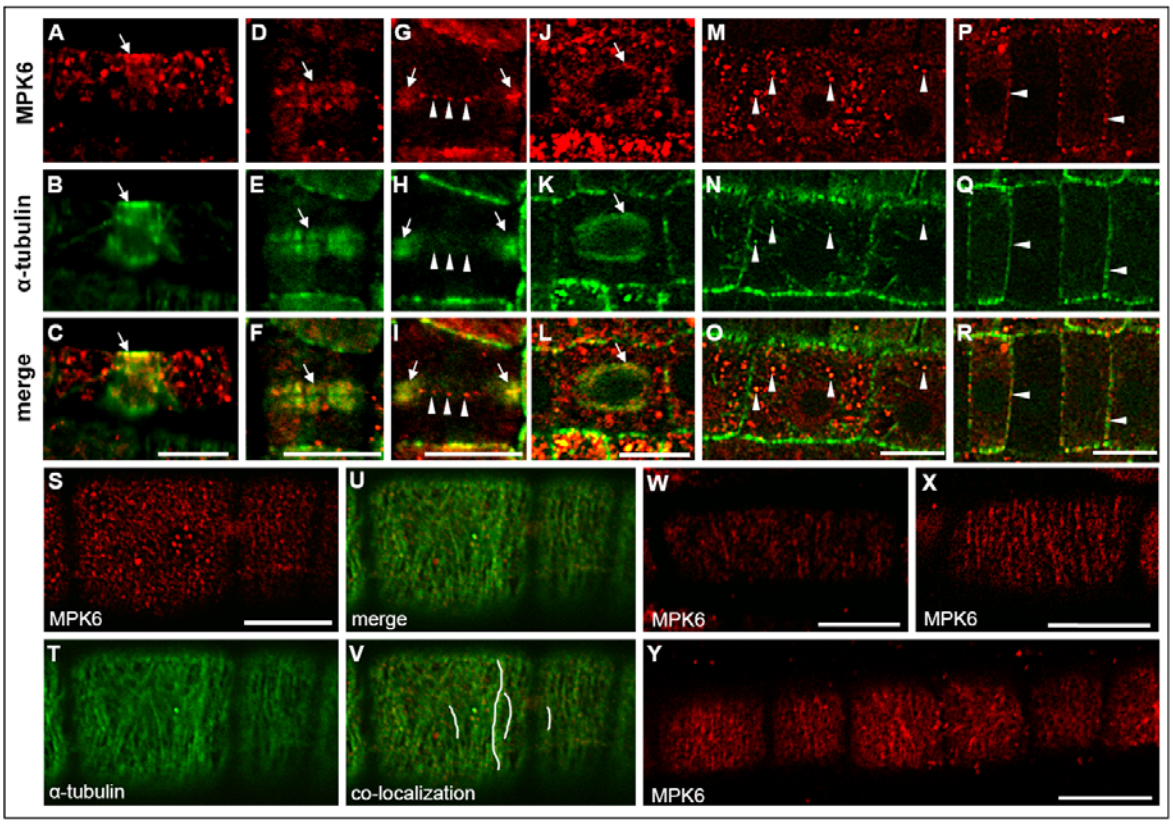

Figure 23. Whole-mount co-immunolabeling of MPK6 and α-tubulin in root epidermal cells. (**A-C**) Co-localization of MPK6 and α-tubulin at the preprophase band (arrows). (**D-F**) Cortical section showing co-localization at the phragmoplast (arrows). (**G-I**) Subcortical section of the cell from D-F showing localization of MPK6 at the phragmoplast (arrows) and in spots at the level of the mature (arrowheads) and growing cell plate (right hand arrows). (**J-L**) Metaphase cell showing only very weak localization of MPK6 to the spindle (arrow). (**M-R**) Co-localization of MPK6 and α-tubulin in the subcortical area of postmeristematic cells (M-O) and non-dividing, meristematic cells (P-R). Arrowheads in M-O indicate co-localization with spot-like structures. Arrowheads in P-R point to the close association of MPK6 and α-tubulin at the PM. (**S-V**) Co-localization of MPK6 and cortical MTs in postmeristematic elongating cells. Lines in V are drawn to highlight some MTs that are obviously associated with MPK6. Note that co-localization is hard to distinguish from the cytotolic background. (**W-Y**) Single labelling of MPK6 at the cortical array of postmeristematic elongating cells. Note, that sometimes MPK6 nicely labelles the cortical array in these cells. Bars represent 10μm.

3.10.2 MPK6 does not co-localize with the actin cytoskeleton

In contrast to the well defined microtubule network with its dense cortical array and only a few subcortical bundles or single MTs, which connect the nucleus with the PM, actin filaments are organized as a complex and dense network becoming more or less longitudinally oriented in postmeristematic elongating cells. This network runs through the center of the cell (Fig 24 E and H), through the cortical area directly underneath the PM (Fig 24 K) and is also present in the subcortical area underneath of the cortical MT array (Fig 24 N). Co-labelling of MPK6 with actin filaments revealed only partial and weak association in the different subcellular areas of both non dividing meristematic and postmeristematic elongating epidermal cells (Fig 24 D-O). Within early stage phragmoplasts actin mostly resided in the central part which probably contains the young cell plate while MPK6 localized to the whole phragmoplast except the mid-zone. Nevertheless, in a small area MPK6 overlapped with actin in the phragmoplast (Fig 24 A-C). Moreover, because MPK6 was found to localize within spot-like structures at the level of the maturing cell plate (Fig 23 J-L) it can not be excluded that there is also a partial co-localization.

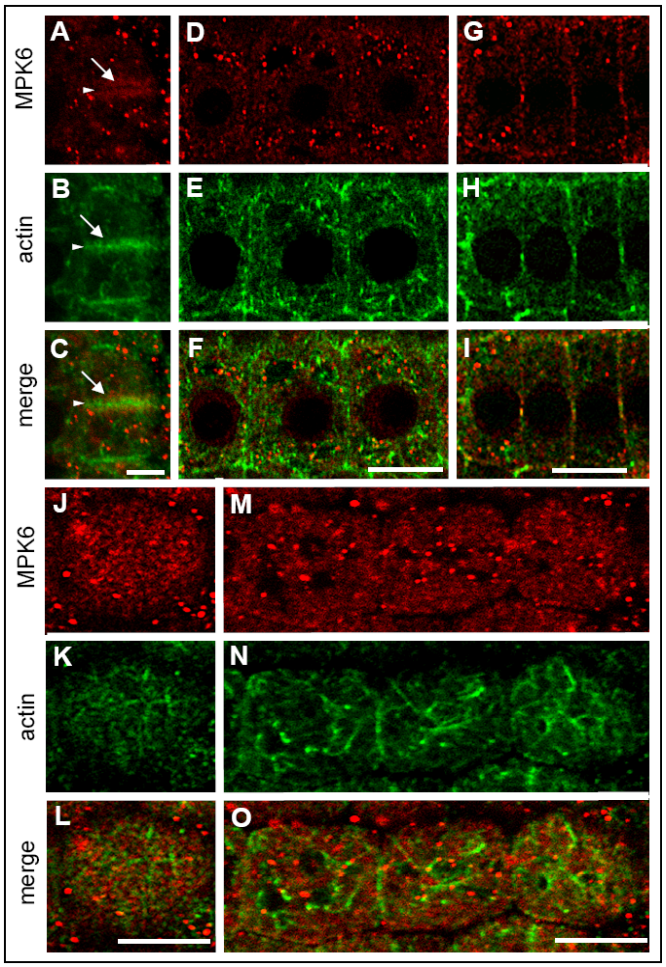

Figure 24. Whole-mount co-immunolabeling of MPK6 and actin in root epidermal cells. (**A-C**) Co-labelling of MPK6 and actin in a cytokinetic cell at the stage of cell-plate formation. Note that the entire phragmoplast is clearly labelled by MPK6 (arrow) while actin mainly labels the mid-zone representing the area of cell-plate maturation (arrowhead). (**D-I**) Co-labelling in the subcortical area in the centeral parts of meristematic cells. Note that there is only weak co-localization of actin and MPK6 within the observed cell types and subcellular areas. (**J-L**) Co-labelling of MPK6 and actin at the cortical array directly underneath the PM. (**M-O**) Co-labelling at the early subcortical area directly underneath the area, which contains the cortical microtubules. Bars represent 5µm in A-I and 10µm in J-O.

3.11 Treatment with BFA alters arrangement of actin and subcellular distribution of microtubules

3.11.1 α-tubulin and MAPK behave similarily in BFA-treated cells

Microsomal and cytosolic fractions were prepared from roots of control and BFA-treated 5-6 days old *Arabidopsis* seedlings in order to test the effects of BFA on the plant cytoskeleton. Subsequent immunoblotting of these fractions using antibodies against actin and α-tubulin revealed that tubulin but not actin followed the behavior of MAPKs by showing a clear shift towards the cytosolic fraction (Fig 25).

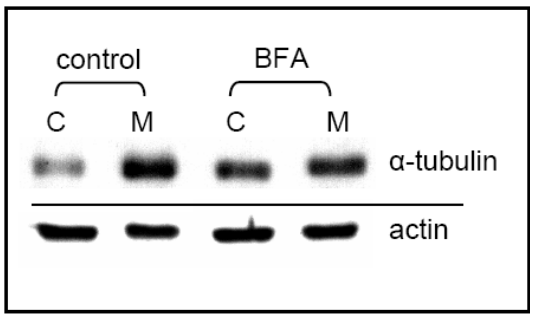

Figure 25. Cytosolic and microsomal distribution of α-tubulin and actin in control versus BFA-treated roots. Immunoblot on cytosolic and microsomal fractions of untreated and BFA-treated (50μM/1.5h) roots using antibodies against actin and α-tubulin. Note, that the strong microsomal fraction of α-tubulin decreased while the cytosolic one increased after BFA treatment. In contrast, no significant changes were observed for actin. C=cytosolic fraction; M=microsomal fraction.

3.11.2 BFA causes rearrangement oft actin but not of MT and MPK6

To test whether there is a significant and visible change in the arrangement and/or distribution of the cytoskeletal elements and of MPK6, whole-mount immunolocalization and *in-vivo* localization experiments on control and BFA-treated plants were performed.

For co-visualization of MTs and MPK6 BFA treated *Arabidopsis* seedlings were co-immunolabelled with antibodies against MPK6 and α-tubulin. However, except a minor reduction of the number of MPK6 and α-tubulin labelled spots that could be observed sometimes, no significant visible changes were found on the arrangement or distribution of MPK6, the cortical MT array, the subcortical MTs or the cytokinetic structures like the phragmoplast (Fig 26).

To study the actin cytoskeleton, a transgenic line was used stably expressing a GFP:ABD2 fusion protein under the control of the constitutive 35S promoter (Voigt *et al.* 2005). ABD2 (actin binding domain2) is one of the two binding domains of the actin bundling protein fimbrin 1 and known to specifically visualize the actin cytoskeleton in *Arabidopsis* (for example Sheahan *et al.* 2004; Wang *et al.* 2004; Voigt *et al.* 2005). This transgenic line

was chosen because it allowed dynamic *in vivo* visualization of the actin cytoskeleton upon BFA treatment. In this case, observations were focused on elongating cells because they also allowed the tracking of BFA induced compartments.

Untreated cells showed a fine, dense and highly dynamic network of actin filaments and bundles within root epidermal cells (Fig 27 A). Embedded within this network, a prominent actin cage around the nucleus was visible in each cell (Fig 27 A, arrows), consistent with our previously published results (Voigt *et al.* 2005). After BFA treatment, especially the fine actin network strongly disintegrated and only a few thick bundled filaments as well as the prominent actin cage around the nucleus remained (Fig 27 B-D, arrows). Interestingly, actin accumulated within another type of cage that was observed around the BFA compartments (Fig 27 B-D, arrowheads). This was evident when plants were additionally pre-treated with the red fluorescent endocytotic marker FM4-64, which labels early endosomal TGN that is known to accumulate in BFA compartments in *Arabidopsis* root cells (for example Jaillais *et al.* 2006). FM4-64 clearly labelled the core of BFA compartments surrounded by newly formed actin cages (Fig 27 E-G, arrowheads). It remained unclear, whether the changes in the structure of the filamentous actin network were the consequence of a non-regulated disintegration of the dense filaments or whether the BFA-induced disturbance in vesicular trafficking causes a regulated modulation of the arrangement of the actin network. A non-regulated disintegration most likely would be accompanied by a breakdown of the ability of actin filaments to build motility tracks throughout the cells. Time series were performed to analyse the ability of BFA-treated cells to maintain actin-dependent subcellular movements. The newly formed BFA induced compartments were highly mobile and moved along actin bundles throughout the cell with a velocity up to 2.2µm per second as shown in Fig 27 H-M. This velocity is within the typical range described for vesicular structures in plant cells (for example Voigt *et al.* 2005).

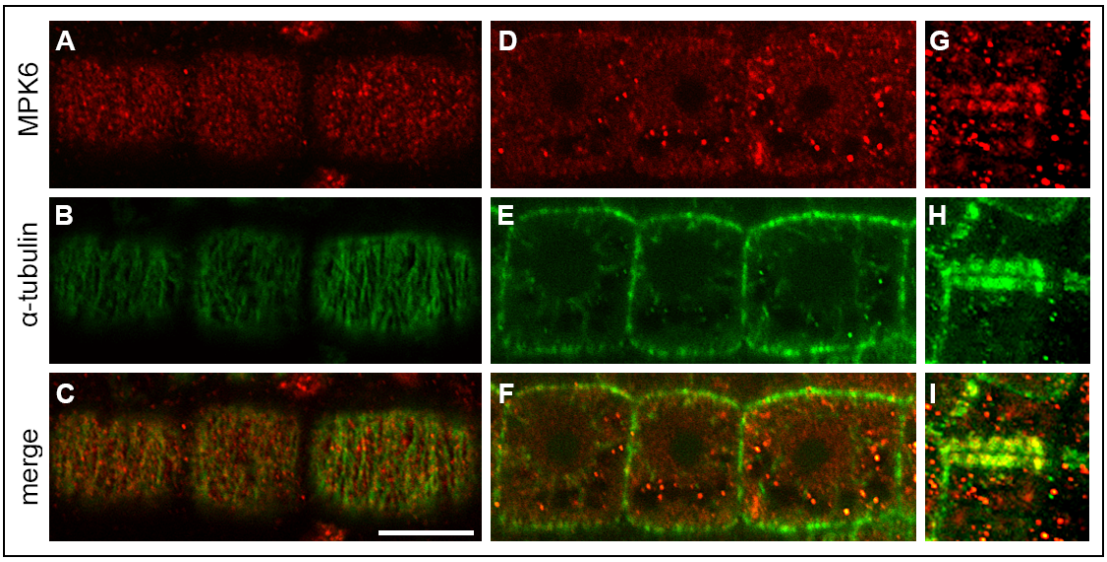

Figure 26. Whole-mount co-immunolabelling of MPK6 and α-tubulin in root epidermal cells treated with BFA. (**A-C**) Co-labelling of MPK6 and cortical MTs in the area directly underneath of PM. (**D-F**) Co-labelling of MPK6 and α-tubulin in the subcortical area. (**G-I**) Co-labelling of MPK6 and MTs in the phragmoplast. Note that, except a minor increase in diffuse MPK6 labeling, there is no significant visible difference between BFA treated cells and the control cells showed in Figure 23. Bar represents 10µm.

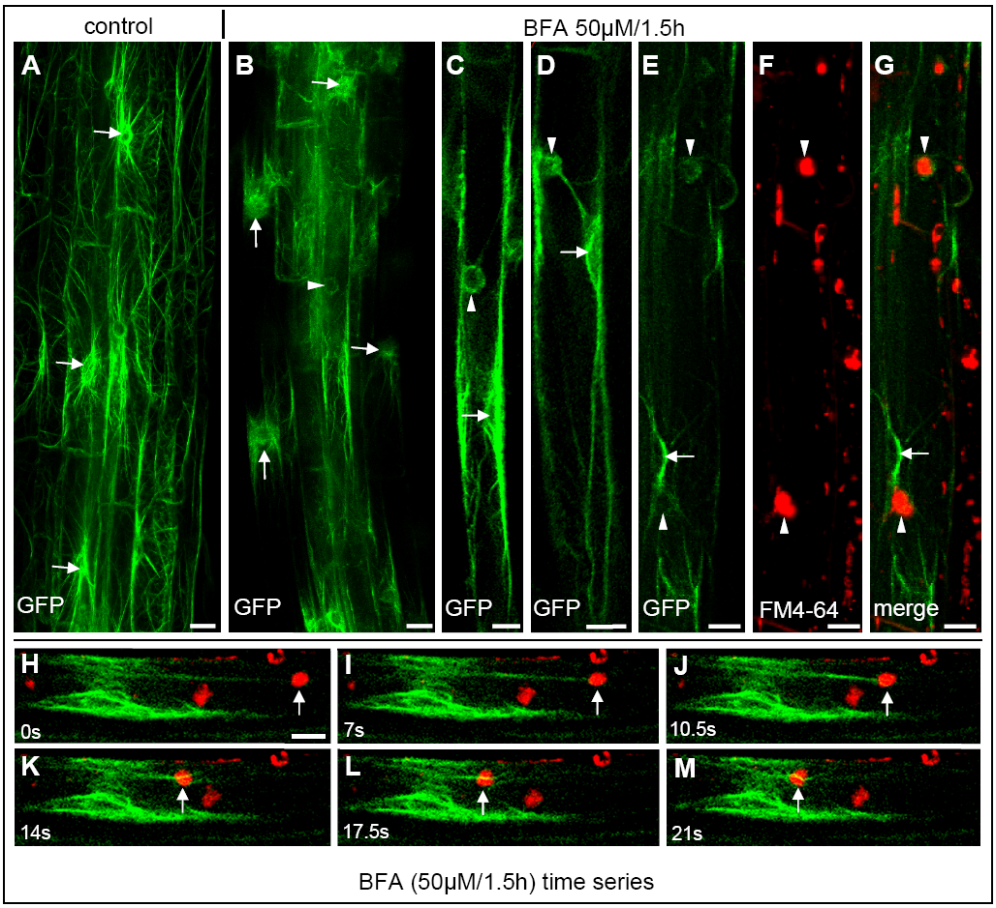

Figure 27. *In-vivo* localization of actin in control versus BFA-treated root epidermal cells using a stably transformed GFP:ABD2 *Arabidopsis* line. (**A**) Overview of elongating epidermal cells from a control plant showing the dense network of actin filaments and bundles in all epidermal cells. Note the typical actin cage surrounding the nucleus (arrows). (**B-D**) Overview of elongating epidermal cells in a BFA-treated plant. Note that the fine actin network strongly disintegrates and accumulates at the actin cage that surrounds the nucleus (arrows) and around putative BFA induced compartments (arrowheads). (**E-G**) Co-visualization of actin and FM4-64 in BFA-treated roots. (E) Prominent actin cages surrounding the nucleus (arrow) and (F) FM4-64 labeled BFA-induced compartments (arrowheads) as shown in merged image (G). (**H-M**) Time series imaging showing actin (green) and a FM4-64 labelled BFA compartment (red) that moves along an actin bundle through the cell (arrows). The average velocity of the BFA compartment in this video was 2.2µm/sec. Bars represent 10µm.

3.12 *MPK6* gene expression pattern in *Arabidopsis* roots

In order to analyze the expression pattern of *MPK6* in root tissues in greater detail, wild type *Arabidopsis* seedlings stably transformed with a *MPK6prom::GUS* construct (generated by Martina Beck in our laboratory) were examined. As shown in Fig 28 A-B most roots showed the strongest *MPK6* promoter activity in the early apical root meristem and lateral root cap as well as in the post-meristematic, transition zone of primary roots. The transition zone (also called distal elongation zone) is defined as the region of isotropic growth directly following the meristem (for review see Verbelen *et al.* 2006). On the other hand, the *MPK6* promoter was less active in fully elongated differentiated cells of the root. This result indicates a role of MPK6 in meristematic and in young post-meristematic root tissues.

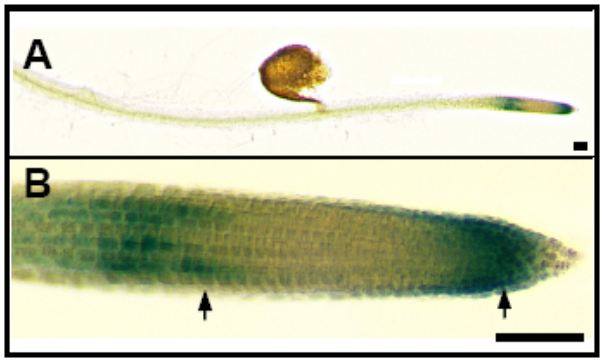

Figure 28. GUS staining of the transgenic *PromMPK6::GUS* root. (A) Overview of a root; (B) Detail on a tip of a primary root. Arrows indicate the approximate position of the stem cell niche at the root tip and transition zone following the root meristem. Bars represent 100µm.

3.13 *mpk6-2* knockout mutant shows disturbed post-embryonic root growth

Previous studies on *mpk6-2* and *mpk6-3* knock out mutant lines described a weak phenotype such as reduction of fertility and a decrease in the size of siliques and internodes between flowers (Bush and Krysan, 2007). These authors also described an aberrant embryo development in the mutant lines, sometimes causing embryos to burst out of their seed coat

during development. However, nothing was reported about the early post-embryonic development of seedling roots so far.

Because this thesis is mainly focused on the analysis of MAPKs, and especially of MPK6 in roots, further analysis was focused on the root phenotype of the *mpk6-2* mutant line (SALK_073907).

To prove that this mutant was a homozygous knock-out, RT-PCR and immunoblotting experiments were performed. As shown in Fig 29, both mRNA and MPK6 protein were detected only within the wild type but not in the *mpk6-2* mutant. This result showed that the mutant line used was homozygous. Additionally, the immunoblotting experiment further demonstrated the specificity of the MPK6 antibody, which was used in previous experiments described in this thesis.

To perform phenotypic studies, wild-type Col-0 and *mpk6-2* knock-out mutants (in the Col-0 background) were grown on ½ MS phytagel plates for 5 days and compared with each other. Interestingly, some *mpk6-2* mutant seedlings showed serious defects in the initial growth of roots but not in the green tissue. Direct comparison with wild-type seedlings revealed only a minor difference in the development of hypocotyls and cotyledons but *mpk6-2* mutants sometimes almost completely lacked roots or roots were significantly shorter, especially during early post-embryonic development (3-8 days after germination) (Fig 30, A-C). Altogether, five experiments were performed comprising at least 350 seedlings for each Col-0 control and mutant plants. Depending on the experiment, the number of mutant seedlings that completely lacked root development was in the range between 16% and 44%. In contrast, no single wild-type seedling showed such an aberrant development. Interestingly, mutant seedlings with this phenotype did not permanently lack root development but most of these plants rather showed a significant delay in root growth. If those plants were measured again after 8 days, seedlings started to develop short roots (compare Fig 30 C with D).

Quantitative analysis of the average size of 5 days old seedlings revealed an average decrease of 34.44% of hypocotyl length and an average decrease of about 50.99 % in the length of primary roots in the *mpk6-2* mutant line as compared to the Col-0 wild-type (Fig 30 H and I). Thus, there is likely a general growth inhibition during the first days of post-embryonic development after germination. Moreover, a noticeable difference in the development of lateral roots was found in *mpk6-2* mutant plants after 8 days of growth. While there was almost no difference in the average number of developed lateral roots, mutant plants showed a significant increase in the formation of adventitious roots (Fig 30 E-G, arrows). Quantitative analysis revealed that while the average number of lateral roots per plant

(including adventitious roots) was only slightly decreased in the *mpk6-2* line the average portion of adventitious roots increased from 20.45% to 44.26% in the mutant compared to the Col-0 wild type (Fig 30 J).

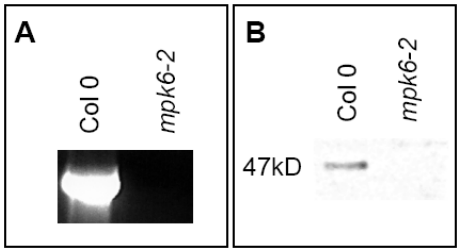

Figure 29. RT-PCR and immunoblot analysis on wild type Col-0 and *mpk6-2* mutant line. (**A**) RT-PCR analysis using isolated RNA from roots and MPK6 specific primers. Note that mRNA for MPK6 is only detected in the wild-type (**B**). Immunoblot of crude extract from roots using the MPK6 antibody. Note that protein is only detected in the wild-type (Co-0) but not in the mutant line.

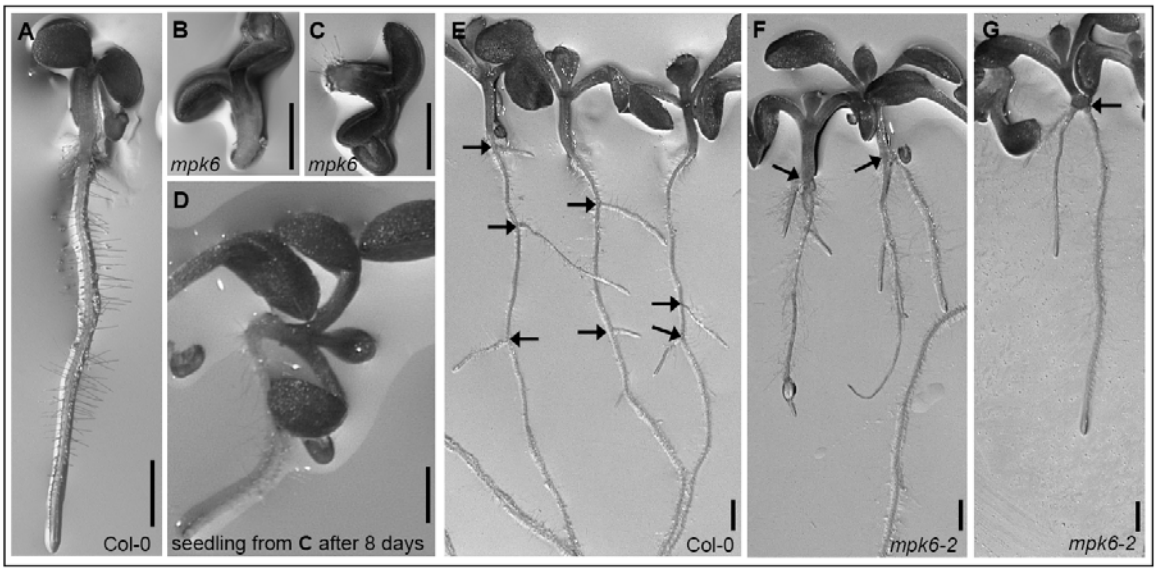

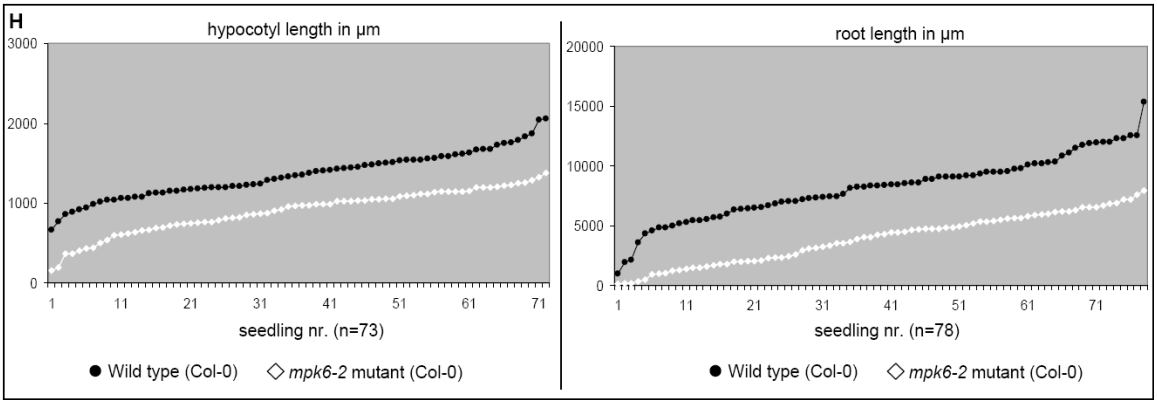

I	hypocotyl	std. deviation	
Col-0	1353 µm	291 µm	hypocotyl n= 73
mpk6-2	887 µm	273 µm	
	root	std. deviation	root n= 78
Col-0	8163 µm	2680 µm	
mpk6-2	4001 µm	2068 µm	

J 8 days old plants	Col-0	*mpk6-2*
total nr. of plants	68	90
total nr. of lateral roots	220	244
average nr. of lateral roots/plant	3.23 ± 1.77	2.71 ± 1.41
total nr. of adventitious roots	45	108
quotient of adventitious roots	20.45%	44.26%

Figure 30. Phenotype and growth analysis of wild-type Col-0 and *mpk6-2* mutant seedlings. (**A-C**) Five days old seedlings grown on ½ MS medium containing phytagel. (A) Wild-type Col-0 seedling showing normal development. (B-C) Representative images of *mpk6-2* mutant seedlings that showed a normal development of cotyledons and slightly shorter hypocotyls but almost completely lack roots. (**D**) Image of the same seedling shown in C after eight days of growth. Note that this seedling started to develop a root. (**E-G**) Eight days old seedlings. (E) Wild-type Col-0 seedlings showing normal development of lateral roots along the primary root (arrows). (**F-G**) *mpk6-2* mutant seedlings showing development of long adventitious roots (arrows). (**H**) Graphical presentation of the measurement of hypocotyl (left graph) and root length (right graph) in wild-type versus mutant plants after 5 days of growth. 73 and 78 seedlings of each line were used for measurement of hypocotyls and roots, respectively. The respective size for each seedling is marked by a dot directly on the graph. Black lines represent wild-type and white lines represent mutant seedlings. Note that the average length is significantly reduced in all seedlings. (**I**) Average length of hypocotyls and roots in 5 days old wild-type and mutant seedlings calculated from the values shown in H. Note that there is a significant decrease in the growth of mutant seedlings, especially in roots. (**J**) Comparison of average number and origin of lateral roots in 8 days old wild-type versus mutant seedlings. Note that there is only a slight decrease in the number of lateral roots but a strong dominance of adventitious roots in *mpk6-2* seedlings. Bars represent 1mm.

3.14 *mpk6-2* mutant shows irregular cell divisions and disturbed cell division planes

Arabidopsis root tips have a simple and invariable architecture with distinct and highly ordered cell files originating from non-differentiated meristematic cells (Fig 31 A) called initials. All initials are in contact with four central cells called the stem cells or quiescent center (QC) (Fig 31 A; C-D). Together, QC cells and initials are called the stem cell niche. In early post-embryonic root development the QC is characterized by strict mitotical inactivity and it was shown that QC cells directly control division and differentiation of the surrounding meristematic initials (for review see Doerner 1998; van den Berg *et al.* 1998; Jiang and Feldmann 2005). The stem cell niche is followed by meristematic tissue of around 200µm in length which is followed by the so called transition (distal elongation) zone (for review about nomenclature and partitioning of zones see Verbelen *et al.* 2006), a zone of very slow cell elongation where postmitotic cells undergo several physiological changes in order to prepare for rapid elongation and differentiation (Verbelen *et al.* 2006).

In order to further characterize the *mpk6-2* root phenotype on the cellular level 5-6 days old seedlings were stained with the red fluorescent membrane marker FM4-64 and microscopically analyzed. Examination of the root tip revealed disturbances in the cell division planes as well as additional irregular cell divisions within the quiescent center (QC) and in the transition zone (Fig 31). The extent of this phenotype was directly correlating with the degree of disturbance in root development and elongation. Seedlings with extensively reduced root growth showed a strong disturbance in the alignment of cells and the control of cell size and division in the area of the stem cell niche (Fig 31 E-G).

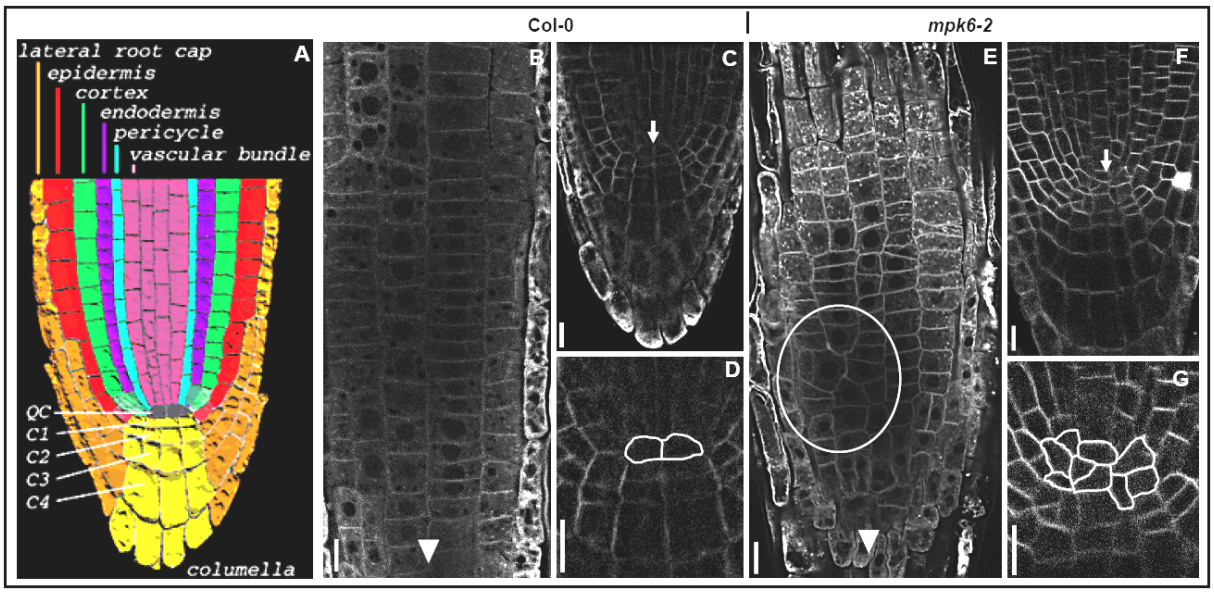

Figure 31. FM4-64 staining of 5 days old *mpk6-2* mutant roots. (**A**) Schematic graph of the typical, invariable distribution of cells within the meristematic zone of the *Arabidopsis* root tip. The image was taken from http://www.plantsci.cam.ac.uk/Haseloff/biosystems/Arabidopsis/anatomy.htm. Note that in a longitudinal section typically two cells of the quiescent center (QC) are visible (**B**) Late meristematic and transition zone of a wild type Col-0 root (**C**) Root tip of a wild type Col-0 root. (**D**) Detail of the QC from C. Cells belonging to the area of the QC are encircled. (**E**) Late meristematic and transition zone of a mutant root. Note that the strict order of cell file alignment is partially disturbed in the mutant root showing an area with disoriented cell division planes (circle). (**F**) Root tip of a mutant that shows strongly reduced root growth. Note that cell divisions in the cells of the QC and the surrounding initials are disoriented. The arrow indicates the area of the QC (**G**) Detail of the QC from F. Cells putatively belonging to the area of the QC are encircled. Arrowheads point toward the root tip. Bars represent 10µm.

It is known that mitotic and cortical MTs regulate cell division, cell growth and morphology (for review see Müller *et al.* 2009; Wasteneys and Ambrose 2009). Because the previous results (chapter 3.10) revealed a direct association of MPK6 with cytokinetic and cortical MTs (see Fig 23) it is likely that the inhibited growth and the irregular cell divisions in the *mpk6-2* mutant resulted from deficient organization of MTs. In order to test this hypothesis, whole-mount immunolabellings were performed on mutant seedlings using the α-tubulin specific antibody. Microscopic analysis of epidermal and cortex cells of the root tip showed clusters of irregularly dividing cells in the transition zone in strongly shortened *mpk6-2* mutant roots (Fig 32 A-D). Careful examination revealed no cytokinetic defect, because all cells were able to build and finalize a normal cell plate. However, within these clusters and partially also in single cells of the surrounding tissue a multitude of cells showed redundant cell divisions with abnormal division planes caused by disoriented alignments of PPBs, mitotic spindles and phragmoplasts (Fig 32 E-G). In summary, these experiments revealed that the *mpk6-2* knockout mutant is disturbed in the control of cell division planes, specifically in the stem cell niche and in the transition zone. These abnormalities are mainly

due to the appearance of redundant/abnormal mitotic activity and disturbances in the cell division plane caused by an aberrant alignment of mitotic microtubules in mutant root cells.

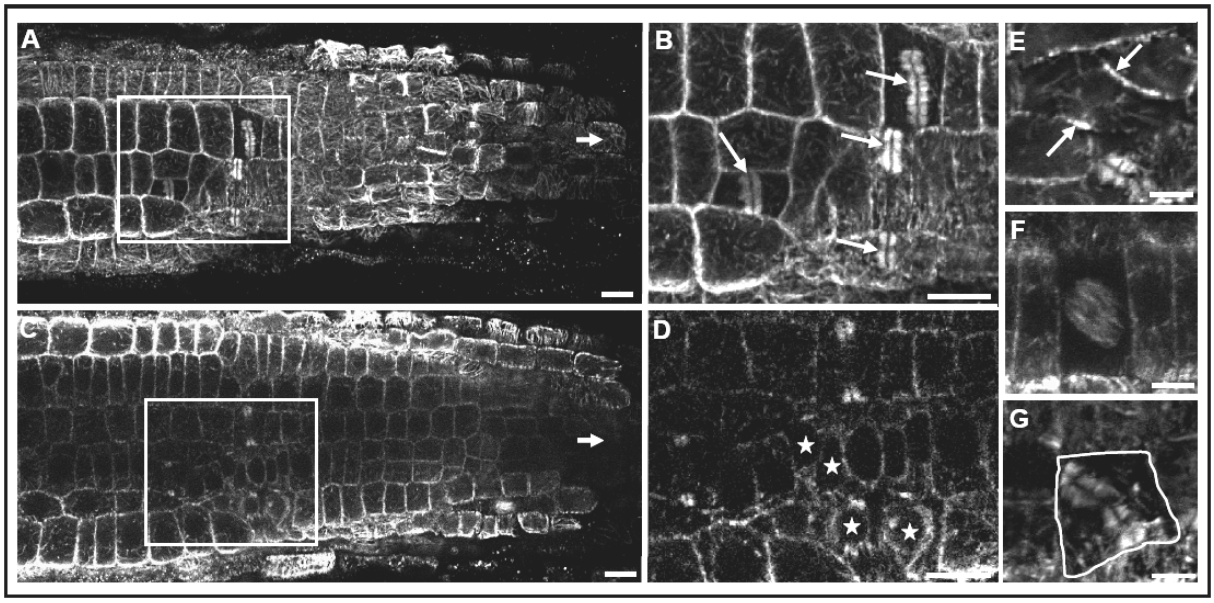

Figure 32. Whole-mount immunolabelling of α-tubulin in roots of the *mpk6-2* mutant. (**A**) Longitudinal section of epidermal cells in the transition root zone showing irregular clusters of dividing cells (rectangle). (**B**) Detail of the rectangle in A. Phragmoplasts of dividing cells are indicated by arrows. Note the abnormal orientation and the variable size of the cells in this area. (**C**) Longitudinal section of deeper tissue from the root in A showing also cells in the root cortex. (**D**) Detail of the rectangle in C. Stars indicate cells with preprophase bands. (**E-G**) Detail of cells with disoriented preprophase band (E), spindle (F) and phragmoplast (G). Bars represent 10µm in A-D and 5µm in E-G.

3.15 Inhibition of MAPK activity affects distribution of cortical MTs

In order to test, whether the general inhibition of MAPK activity affects the distribution and alignment of cortical MTs, transgenic seedlings stably expressing a GFP:MBD fusion protein under the control of the constitutive 35S promoter were treated with PD98059. MBD (microtubule binding domain) is part of the microtubule binding protein MAP4 (microtubule-associated protein 4) from mammals and it is known to visualize MTs in *Arabidopsis* (Marc *et al.* 1998; Müller *et al.* 2007a). PD98059 is a cell permeable highly specific inhibitor of MAPKKs and therefore represents a useful tool to generally inhibit downstream MAPK activity (for example Alessi *et al.* 1995, Dudley *et al.* 1995).

In untreated elongating root epidermal cells, cortical MTs showed their typical uniformly oriented transversal orientation (Fig 33 A and B). In contrast, when treated with PD98059 those cells showed bundling of cortical MTs (Fig 33 C and D, arrows). Interestingly, this bundling did not affect the ability of cells to rearrange the overall MT array towards a transversal alignment in young, elongating cells (Fig 33 E-F).

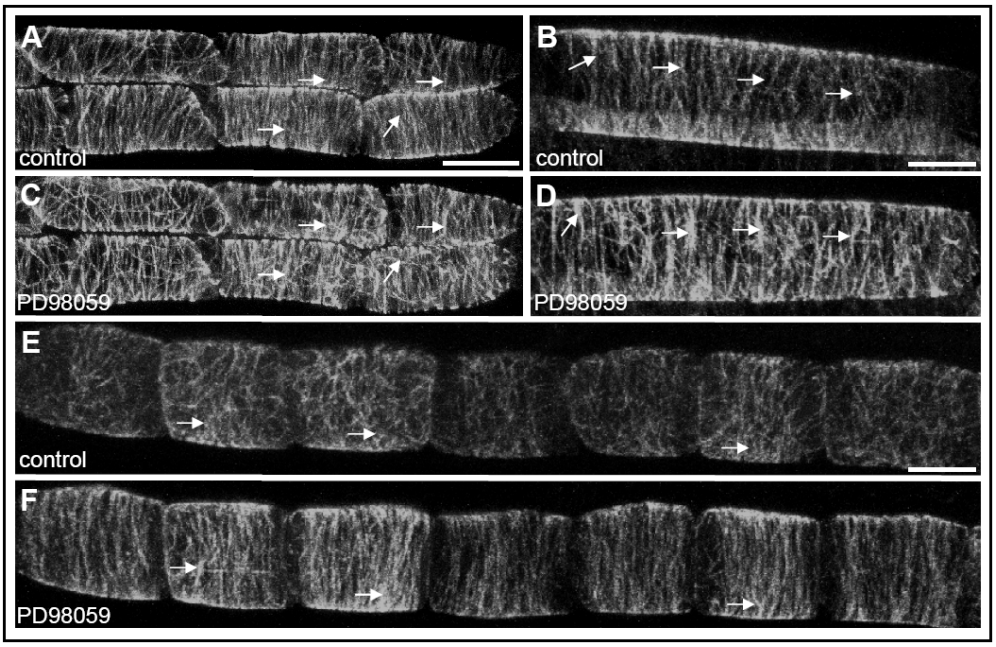

Figure 33. Microtubule arrangements in untreated versus PD98059-treated epidermal root cells using a stably transformed 35S::GFP:MBD *Arabidopsis* line. (**A, B**) Transversal arrangement of cortical MTs in untreated elongating root cells. (**C, D**) Bundling of transversal cortical MTs in the same cells as in A and B after 1h of PD98059 treatment. Note that the overall alignment of MTs did not change. (**E**) Young cells showing non-parallel alignment of cortical MTs. (**F**) Same cells as in E after 1h PD98059 treatment showing rearrangement to transversal and parallel cortical MT and their increased bundling. Arrows in all images show bundled MTs in treated cells and the respective area in untreated cells. Bars represent 10μm.

3.16 Cell-type specific disruption and recovery of the cytoskeleton upon heat stress

In the recent years, studies indicated that transient depolymerization of MTs, induced by cold and aluminium, is involved in the adaptation to these environmental changes (Abdrakhamanova *et al.* 2003; Sivaguru *et al.* 2003). Additionally, it was predicted that MT depolymerization causes the release and activation of signalling molecules and complexes (Wasteneys 2003 and 2004). Further, self incompatibility (SI) related programmed cell death (PCD) was shown to be related to rapid F-actin depolymerization/reorganization, and transient actin disruption was sufficient to activate MAPK in Papaver pollen tubes (Rudd *et al.* 2003; Thomas *et al.* 2006; Li *et al.* 2007; Bosch and Franklin-Tong 2008).

In general, rapid changes in temperature represent a major environmental factor, plants have to cope with. Previous work in our laboratory showed that MPK6 gets activated after short-term heat shock (Samaj, unpublished). However, very little is known about *in vivo* reactions of the cytoskeleton to abiotic stress, especially to heat. In order to characterize the cytoskeletal behaviour and to check, whether heat shock stress also causes transient depolymerization of the actin- and/or microtubule- networks, transgenic plants were treated

under different heat stress conditions followed by observation using confocal laser scanning microscopy. Stable lines expressing the 35S::GFP:ABD2 or the 35S::GFP:MBD construct were used for visualization of F-actin and MTs, respectively.

3.16.1 Reaction of MTs to heat stress and their recovery

As expected for living organisms, the intensity of the reaction under heat stress conditions was somewhat variable from seedling to seedling and clearly dependent on the cell type. Heat shock resulted in cell-type-dependent disruption of the cortical MT array. The parallel transverse MT pattern (Fig 34 A) disappeared, while an increasing number of brightly fluorescent spots appeared within the cortical region (Fig 34 B). This reaction was mainly observed under temperature conditions of 40–42 °C and an incubation time between 7 to 25 min. Higher temperature and/or longer incubation time caused more severe damage leading to cell death, whereas lower temperatures did not result in changes of the MT patterns. For example, there was no obvious reaction of MTs at 34 °C for an incubation time of 70 min. This is consistent with results of Smertenko *et al.* (1997) reporting that MTs in tobacco suspension cells disappeared at an incubation temperature of 42 °C but not at 38 °C. The experiments also showed that there was a difference in the level of disruption and depolymerization of MTs, depending on the developmental stage and the cell identity of root epidermal cells. While there was an almost complete MT destruction in younger fast-growing epidermal cells (Fig 34 B), only a partial destruction of MTs occurred in elongated non root hair cells (Fig 35). Surprisingly, root hair cells showed an almost complete depolymerization of MTs (Fig 35). Time-lapse observations of the heat-stressed seedlings revealed a full recovery of the original pattern of the parallel MT array, when plants were returned to normal growth conditions, starting a few minutes after heat shock treatment and completed after about 1–3 h (depending on the cell type). This was observed for both undifferentiated young epidermal cells (Fig 34) and differentiated ones (Fig 35). The mode of recovery depended on the developmental stage of the cell or rather on the level of MT depolymerization. In young fast-growing cells and in root hair cells, where almost all MTs were depolymerized due to stress, a non-ordered network of MTs appeared first. Subsequent to this, the cells were able to restore the natural order of parallel MT array (Fig 34 C–E). In contrast, mature (elongated) non root hair cells showed no such disordered state. Instead, a full reconstitution of parallel obliquely oriented MTs took place during the first step of recovery (Fig 35 C–D).

This raises the question as to whether there is some kind of template, which defines the orientation of MTs. The unique behavior of MT ends growing perpendicularly to existing MTs seems to support this contention. Time series showed that the moment, when a MT touches another MT with its growing end, it starts to depolymerize (Fig 36; for example, microtubules marked by arrows 1 and 4). Such MT behavior was reported before (Van Bruaene *et al.* 2004) and it indicates that existing MTs at least indirectly control parallel alignment by the fact that MTs straying out of alignment get destroyed. Such episodes suggest that dynamic instability of microtubules works in the context of living plant cells.

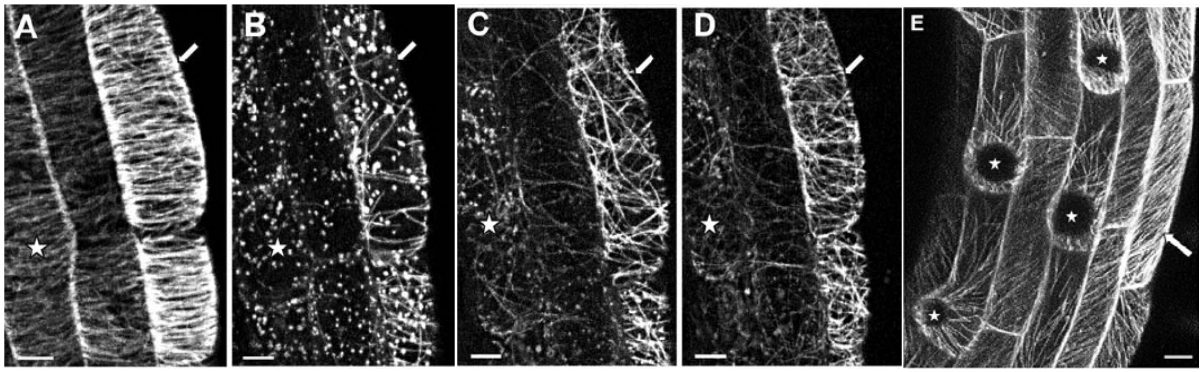

Figure 34. *In vivo* localization of MTs in young root epidermal cells of stably transformed *Arabidopsis* seedlings (GFP:MBD) (**A**) control cells showing transversal, parallel array of cortical microtubules; (**B**) cells from A directly after heat shock treatment (41°C, 25 minutes). Most of the cortical microtubules are destroyed. Instead there is a high number of brightly fluorescent spots within these cells; (**C**) 30 minutes after treatment the cells reconstitute a dense network of disordered microtubules traversing the cortical region. Most of the fluorescent spots disappeared; (**D**) 60 minutes after treatment the disordered network starts to get reorganized into a parallel array again. (**E**) 17 hours after treatment. The cells have grown and differentiated. The dense MT-arrays are completely recovered. Differentiated root hair cells are marked by stars, non root hair cells are marked by arrow. (A-B) projection of 10 optical sections; (C-D) projection of 6 optical sections; (E) projection of 15 optical sections. Bars represent 10 μm.

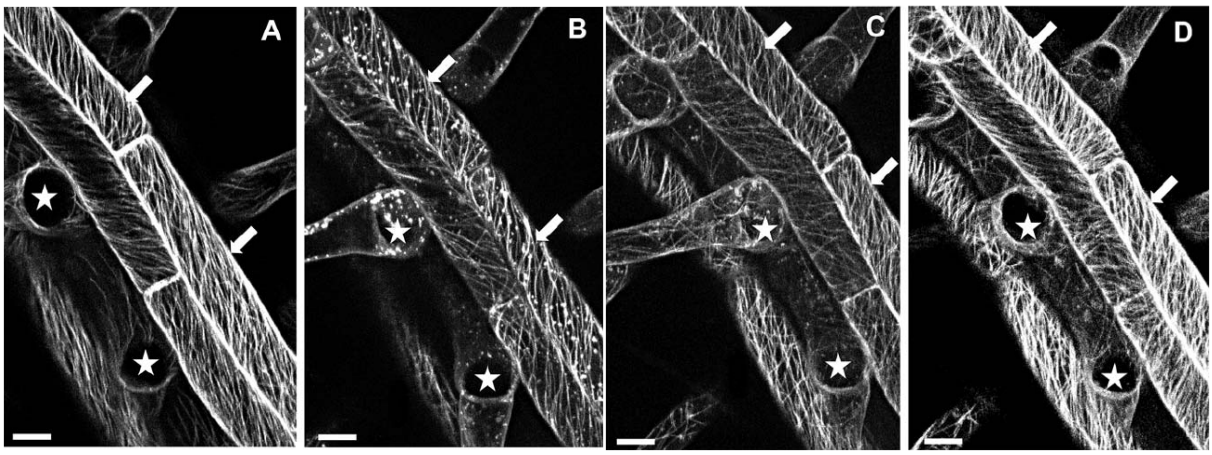

Figure 35. *In vivo* localization of MTs in almost mature root epidermal cells of stably transformed *Arabidopsis* seedlings (GFP:MBD) (**A**) control cells showing a mostly oblique, parallel array of cortical microtubules; (**B**) right after treatment (41°C, 25 minutes) only some of the microtubules are depolymerized, leaving gaps within the dense parallel MTs of non root hair cells. (**C**) 50 minutes after treatment new microtubules have been formed, building an parallel array; (**D**) 110 minutes after treatment a very dense array of parallel microtubules is clearly visible, that seems to be identical to the control cells. Root hair cells are marked by stars, non root hair cells are marked by arrows. (A, C-D) projection of 9 optical sections; (B) projection of 6 optical sections. Bars represent 10 μm

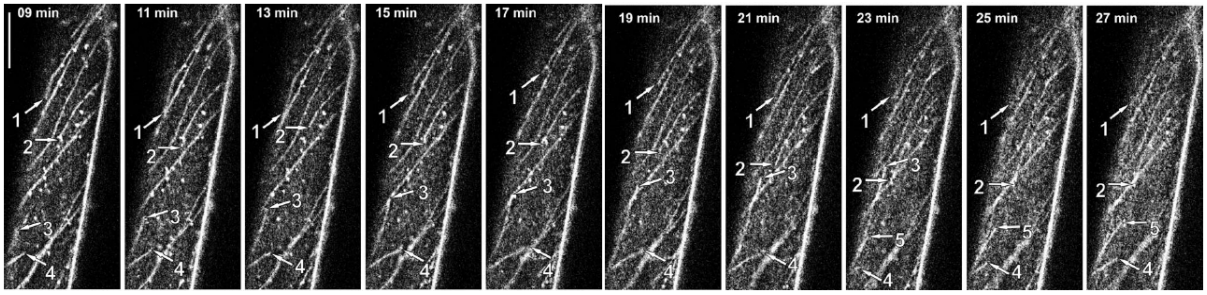

Figure 36. Time-lapse images showing dynamics of MTs after heat-stress (41°C for 11 minutes). The figure shows growing microtubules in a root epidermal cell starting 9 minutes after heat treatment. Every 2 minutes a new image was taken. Numbered arrows are marking plus-ends of growing microtubules. Some microtubules show catastrophe events, when their plus-ends get in contact with already existing microtubules. Bar is 10 μm.

Another interesting aspect is the origin of the brightly fluorescent spots. These are clearly linked to the heat treatment, because their quantity seems to be directly correlated to the rate of MT depolymerization and because they subsequently disappear as MT recovery is in progress (Fig 34 C and Fig 35 C). To clarify this point further, control experiments were done using transgenic plants overexpressing an YFP:TUA5 construct, which directly visualizes tubulin (Shaw *et al.* 2003). In this case MTs in non root hair cells disassembled almost completely, which was accompanied by enhanced overall diffuse fluorescence, however, no fluorescent spots could be observed after heat treatment (Fig 37). Unfortunately, the YFP:TUA5 construct did not visualize MTs in root hair cells (only diffuse fluorescence was found in these cells) indicating that the construct is not suitable for cell-type specific studies in the root. Therefore, it was not possible to clarify, if there are any differences between trichoblasts/root hair cells and atrichoblasts/non root hair cells. Nevertheless, this result leads to the conclusion that spots observed in root hair cells of GFP:MAP4 transgenic line during previous experiments are most likely aggregates of this construct which accumulate upon progressive heat-induced disruption of MTs.

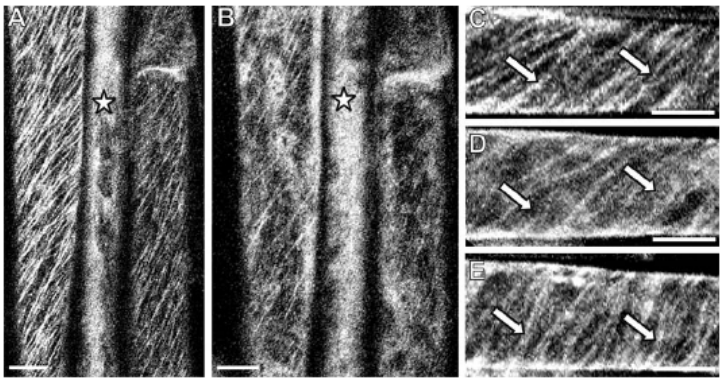

Figure 37. *In vivo* localization of MTs in root epidermal cells of stably transformed *Arabidopsis* seedlings (YFP:TUA5 construct). (**A-B**) Epidermal cells showing no recovery after stress. (**C-E**) Epidermal cell showing recovery. (**A, C**) control; (**B, D**) directly after heat-shock stress (41°C, 8 minutes); (**E**) during recovery (75 minutes at room-temperature). (**A-E**) projection of 5 optical sections. (A, C) Control cells showing an oblique, parallel array of cortical microtubules. Root hair cells (marked by white star) do not show distinct MTs. (B, D) Cortical microtubules are partially destroyed directly after treatment. Note the overall fluorescent background and lack of any fluorescent spots in these cells. (E) 75 minutes after treatment new microtubules have been formed, building a parallel array. Some MTs are marked by arrows. Bars represent 10 μm.

Heat stress experiments under different conditions revealed that the degree of MT destruction depends on the exposure time (Fig 38). Interestingly, some of the MTs seem to be resistant against heat shock treatment, because within the critical time limit of 25 minutes (beyond this time-point most seedlings died) there were always some MTs left intact (Fig 38 D). At this stage and within young, fast growing cells mainly a few oblique and longitudinal MTs seem to be insensitive to heat. On the other hand, parallel transverse arrays of MTs, which are predominant within these cells, were almost always destroyed (Fig 39). In mature cells, where the bigger part of cortical MTs is aligned in an oblique up to longitudinal manner, most MTs seem to be resistant. Thus, it is suggested that longitudinally and obliquely oriented cortical MTs are more resistant to heat-depended depolymerization. On the other hand, this is not so in root hair cells, where MTs are mainly aligned longitudinally (as shown in Fig 34 E and Fig 35 A). These MTs are depolymerized completely due to the heat shock treatment.

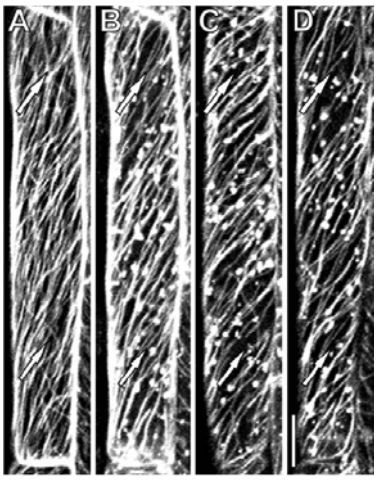

Figure 38. *In vivo* localization of MTs in a nearly full-grown root epidermal cell of a stably transformed *Arabidopsis* seedling (GFP:MBD) after heat-stress. Images A-D show the same cell after different incubation times at 41°C. The seedling was first treated with heat for 11 minutes and after the first image was taken, it was treated again each time for another 7 minutes and each time an image was taken. (**A**) control; (**B**) after 11 minutes of treatment; (**C**) after 18 minutes of treatment; (**D**) after 25 minutes of treatment. Note that there are still some MTs left after 25 minutes of treatment. Because 25 minutes is a critical limit, beyond which most seedlings die, some MTs seem to be resistant against heat. Arrows indicate points where progressively evolving gaps between MTs are visible. Figs. A-D are projections of 9 optical sections. Bar represents 10 μm.

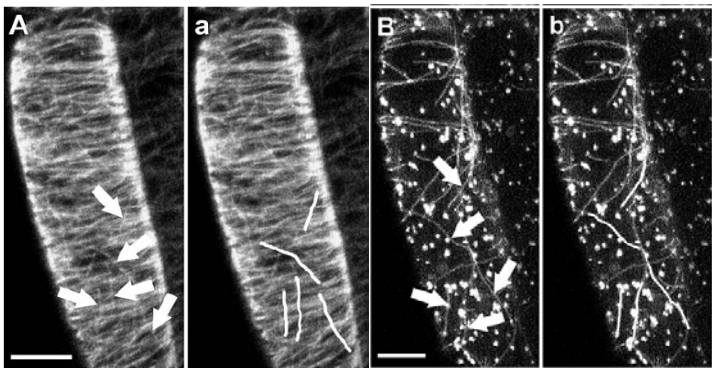

Figure 39. Detail on cortical MT disruption by heat. (**A**) control cell. (**B**) the same cell after 25 minutes of heat treatment (41°C). Arrows indicate such microtubules which can be observed before and after stress. Pictures a and b represent duplicates of A and B. white lines depict microtubules which are marked by the arrows in order to better illustrate them. Bar is 10 µm.

3.16.2 Reaction of actin microfilaments to heat stress and their recovery

Due to heat stress conditions the actin cytoskeleton nearly completely disappeared in all kinds of root epidermal cells. Instead of well-organized networks of actin filaments (Fig 40 A), a diffuse fluorescent background appeared within the cytoplasm, while only a few thick and short actin-bundles remained intact (Fig 40 B, C). Such reorganization/disruption of the actin cytoskeleton can be achieved by the same conditions that destroy MTs (40-42°C, and an incubation time of about 7-25 minutes). However, unlike MTs, the reaction of actin to heat was independent of the cell type and developmental stage. The fact, that almost all F-actin is depolymerized as a consequence of heat shock indicates a higher sensitivity of actin compared to MTs. F-actin recovery starts around 30 minutes after treatment and it could be observed that, under the described conditions, most cells start to rebuilt a new dynamic network of F-actin (Fig 40 D-G). During the first two hours of recovery young non-differentiated epidermal cells (Fig 40 H) as well as all non root hair cells (Fig 40 I, J) built up aberrantly thick and rigid bundles of F-actin winding around the cell cortex (indicated by white arrows) along with a new dynamic F-actin network. This phenomenon was not that pronounced in root hair cells. Interestingly, only nearly full-grown root hair cells of the late root hair zone infrequently and temporarily formed thick bundles (Fig 40 J, indicated by arrowheads), while such bundles were not observed in young root hair cells (Fig 40 I, root hair cells are marked by stars). Surprisingly, the difference between different cell types became more pronounced with prolonged recovery time. Thus, it was possible to clearly distinguish between different F-actin arrays within different cell types after several hours of recovery. Fig 40 K shows the young root hair zone 17 hours after treatment. It is clearly visible, that all young non root hair cells possess thick actin-bundles (marked by white arrows) with an underlying dynamic actin network (marked by transparent arrows), while surviving root hair cells reconstitute F-actin

networks very similar to that of control cells (marked by stars). The experiments revealed that especially young non root hair cells keep their aberrantly thick bundles even after a period of several hours (Fig 40 K and Fig 41 B), whereas most other cells reconstituted a fine F-actin network as it was seen in control cells (Fig 40 L and Fig 41 C). Furthermore, it was observed that the major part (71%) of young root hair cells died due to the treatment, while for mature root hair cells it was only 14%. On the other hand, in the case of non root hair cells less than 1% of dead cells was found, regardless of root hair zone. Interestingly, either nearly all young root hair cells survived and recovered normal, fine F-actin networks without thick actin-bundles (Fig 40 K) or most of these cells died due to the treatment (Fig 41 B) in a particular single experiment. Fig 41 shows representative images of root epidermal cells from different root zones 20 hours after heat-shock treatment. It is clearly visible, that particularly young root hair cells show heat-shock dependent cell death. Thus, it seems that especially young root hair cells are not able to build up thick F-actin bundles, and as a consequence they are only sparsely resistant to the heat shock treatment. At least 374 cells, containing 69 young root hair cells, have been scored in these experiments. All surviving root hair cells showed the F-actin network without abnormally thick bundles. In contrast, at least 50% of 90 observed non root hair cells from the early root hair zone still showed thick F-actin bundles after recovery overnight. In the older root hair zone (Fig 40 L) all epidermal cells (at least 50 cells) almost completely lack thick actin-bundles after recovery overnight with no difference between root hair- and non root hair cells. The experiments showed, that only young, fast growing epidermal cells as well as young non root hair cells keep their aberrantly thick and rigid bundles of F-actin over a longer period, while older cells and root hair cells tend to rebuild a dynamic F-actin network, which did not differ from that in control cells. In cells of the meristematic and post-meristematic zones such thick F-actin bundles were only sparsely observed and mostly restricted to endoplasmic F-actin enwinding the nucleus (Fig 41 A, arrow).

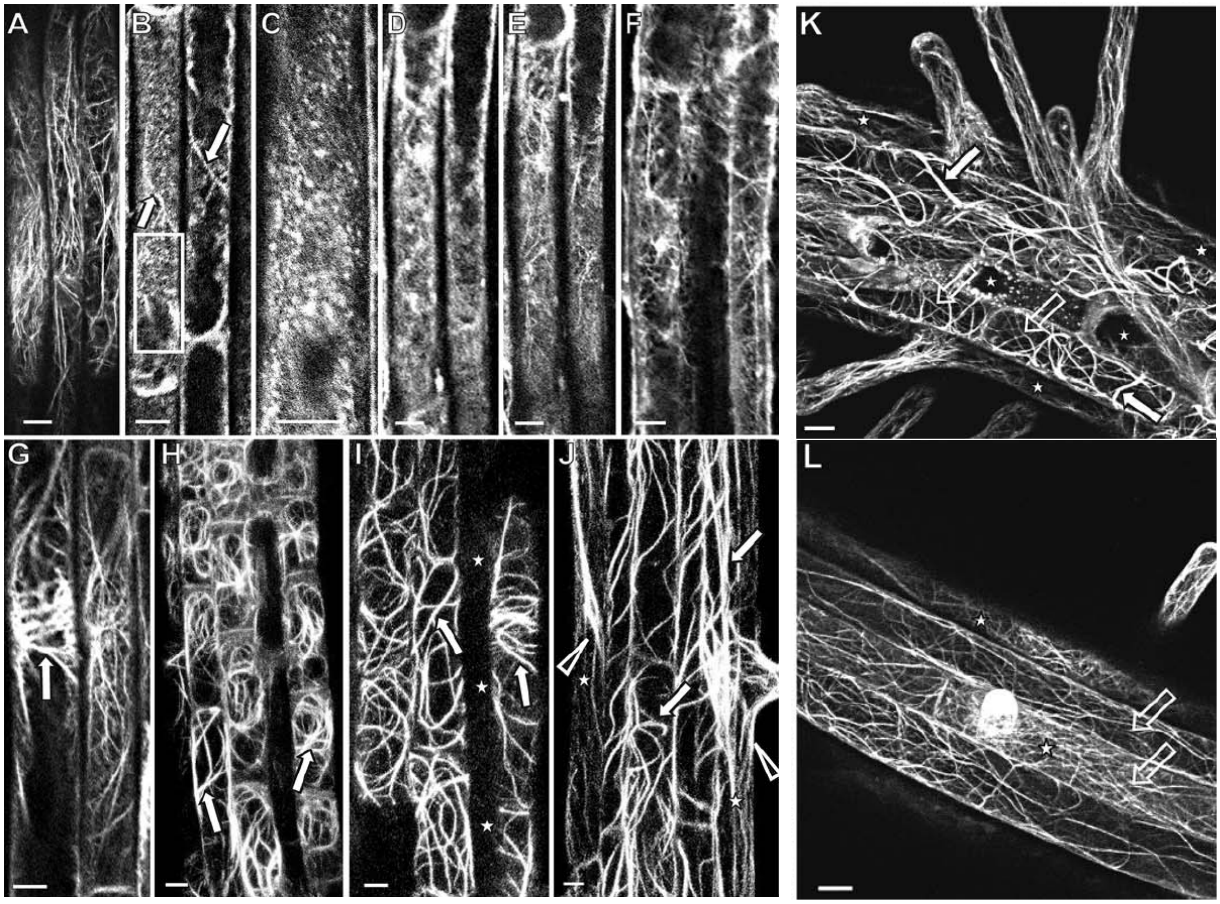

Figure 40. *In vivo* localization of AFs in root epidermal cells of stably transformed *Arabidopsis* seedlings. (**A**) Control showing dense network of F-actin. Projection of 6 optical sections. (**B, C**) Right after treatment (41°C, 10 minutes), the F-actin network is almost completely depolymerized except for a few thick and short actin bundles (indicated by arrows). Instead, there is a strong, diffuse background fluorescence. Boxed area in B is shown in higher magnification in C. (**D**) 15 minutes after treatment. (**E**) 45 minutes after treatment the first reconstituted actin-filaments are visible. (**F**) 65 minutes after treatment first signs of a new F-actin network are visible. (**G**) After 165 minutes a complete new F-actin network is build up and thick actin-bundles are visible surrounding the nucleus in some cells (indicated by arrow). (**H-J**) Epidermal cells from different tissues, 2 hours after heat treatment. Non root hair cells of all tissues, as well as root hair cells of the mature root hair zone show the generation of thick bundles (indicated by white arrows in non root hair cells (**H-J**) and transparent arrowheads in mature root hair cells (**J**). (**H**) Undifferentiated, young epidermal cells. Projection of 8 optical sections. (**I**) Young root hair zone. Projection of 8 optical sections. (**J**) Mature root hair zone. Projection of 9 optical sections. (**K**) 17 hours after treatment young non root hair cells show thick actin-bundles winding around the cell-cortex, while root hair cells rather show fine F-actin networks without thick bundles. Projection of 17 optical sections. (**L**) Mature non root hair cells do not possess this kind of thick actin bundles 17 hours after treatment. Projection of 10 optical sections. Actin-bundles in non root hair cells are marked by white arrows, actin-bundles in root hair cells are marked by arrowheads, fine F-actin is marked by transparent arrows. Root hair cells are marked by stars. Bars are 10 µm.

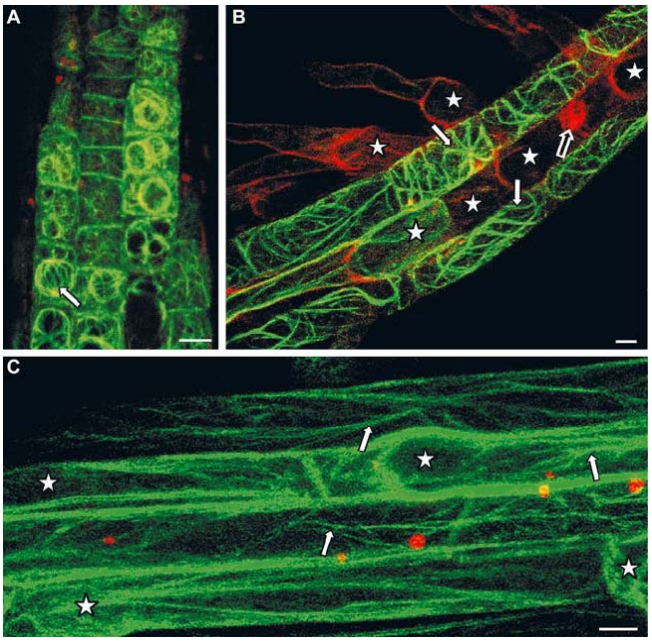

Figure 41. *In vivo* localization of AFs in root epidermal cells of stably transformed *Arabidopsis* seedlings in different tissues 20 hours after heat-shock treatment (41°C, 10 minutes). F-actin is shown in green colour, autofluorescence of dead cells is shown in red colour. (**A**) Meristematic and postmeristematic cells. The arrow indicates AF bundles surrounding a nucleus. Most cells show a normal, fine F-actin network. Projection of 6 optical sections. (**B**) Young root hair zone. Most non rot hair cells keep their abnormal, thick bundles, while the majority of the root hair cells died. Cell death was ascertained through the lack of cytoplasmic streaming, cell fragmentation and disability to grow. In most cases dead cells were clearly visible through an enhanced red autofluorescence as shown here. Projection of 9 optical sections. (**C**) Mature root hair zone. Root hair- and non root hair cells show a normal F-actin network. Red dots are plastids from the deeper tissue, detected by their autofluorescense. Projection of 11 optical sections. F-actin bundles are marked by white arrows, cell fragments are marked by transparent arrows and root hair cells are marked by stars. Bars represent 10 µm.

In order to test, whether long-term treatments at more moderate conditions also lead to the reorganization of F-actin, plants were exposed for several hours to temperatures between 35-38°C. These experiments revealed that F-actin depolymerization is not necessary for subsequent actin reorganization, since thick bundles were formed without previous F-actin disruption under these conditions (Fig 42).

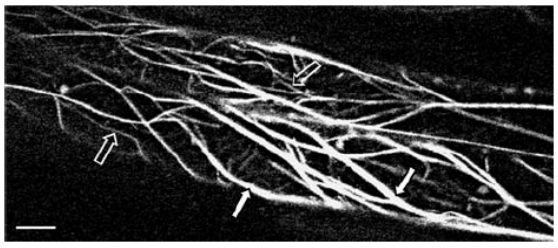

Figure 42. *In vivo* localization of AFs in root epidermal cells of a stably transformed *Arabidopsis* seedling after heat-stress (35°C, 6 hours). Thick actin-bundles are formed winding through the cell cortex (white arrows). There is a network of fine and dynamic F-actin underneath of these bundles (transparent arrows). Bar is 10 µm.

4. DISCUSSION

4.1 MPK3, MPK4 and MPK6 associate with microsomes and co-fractionate with plasma membrane and organelles of the early endocytotic / secretory pathway

By fractionation and enrichment of cytosolic and post nuclear microsomal fractions this work shows that MAPKs, namely MPK3, MPK4 and MPK6 not only localize in the cytosol but also with the microsomal fraction in root tissue of *Arabidopsis* seedlings.

This conclusion was supported by whole mount immunolabelling on fixed *Arabidopsis* roots. All three MAPKs showed a diffuse cytosolic as well as a variable nuclear labeling (Nagatani 1998; Mishra *et al.* 2006). Additionally, all MAPKs localized to spot like and patch like subcellular structures that where either arranged along the PM or randomly distributed within the cytosol. While MPK4 and MPK6 had a very similar distribution, MPK3 showed a stronger PM localization and a type of rod-shaped structures were also labeled. Moreover, MPK4 and MPK6 but not MPK3 showed a clear tendency to redistribute from the PM to cytosolic spots in elongating cells, compared to non dividing meristematic and postmeristematic cells. The identity of the labeled structures was further investigated by co-fractionation and co-immunolabelling experiments (see below).

In animal cells, tightly regulated spatial subcellular organization of MAPK module assembly is essential for proper signalling, and it is one major factor dictating signal specificity. In this respect, association of MAPKs with PM, CCV and endosomes were described to strongly influence cellular behavior including the regulation of endocytotic trafficking and mitosis (see Introduction chapter 1.2). In contrast, very little is known about subcellular organization of plant MAPK modules. Until now, some plant MAPKs were described as residing in the cytosol with the ability to relocate to the nucleus in order to phosphorylate transcription factors (for example Ligterink *et al.* 1997; Coronado *et al.* 2002 and 2007; Ahlfors *et al.* 2004). However, these translocation studies mostly based on the detection of a stimulus-induced nuclear accumulation and/or activation of MAPKs and disregarded a closer observation of the MAPK localization outside the nucleus. Only a few studies provided some indications for a more complex subcellular organization of plant MAPKs. For example, Baluška *et al.* (2000) described the translocation of SIMK (*Medicago sativa*) homolog of *Arabidopsis* MPK6 from the nucleus to the cell plate in dividing root cells. Interestingly, the same MAPK was co-localized with cytokinetic microtubules and its

localization at tips of growing root hairs was found to be sensitive to BFA (Šamaj *et al.* 2002 and 2004b).

This thesis shows for the first time that there is at least one microsomal subpopulation for each of the investigated MAPKs.

Subfractionation of isolated microsomes using liquid density sucrose gradient centrifugation allowed the separation of different organelles and provided the chance to compare the fractionation pattern of MAPKs with those of highly specific organellar marker proteins. All three MAPKs showed an almost identical distribution sharing a maximum enrichment within the same fraction. This suggests that they localize to identical organelles. However, minor differences in the range of the signal across the fractions might also indicate some variability. Strongest co-fractionation was found in fractions that were positive for a TGN specific marker (SCAMP1), for markers against plasma membrane (PIP2;2) and Golgi stacks (α-mannosidase) as well as for one of two maxima of clathrin light chain. No co-fractionation was found with the well established ER marker, SEC12, and a commonly used marker for late endosomal compartments (PEP12).

As described in *chapter 1.4.3*, several investigations recently documented that in plant cells the TGN simultaneously serves both as an early endocytotic compartment as well as a secretory organelle (e.g. Dettmer *et al.* 2006; Dhonukshe *et al.* 2007; Lam *et al.* 2007a; Tahara *et al.* 2007). Both TGN and PM are sites of the formation of clathrin-coated vesicles (Barth and Holstein 2004). Thus, co-fractionation of MPK3, MPK4 and MPK6 with TGN, PM and CLC suggests an association of those MAPKs with the early endosomal and/or secretory pathway. Co-fractionation with α-mannosidase might also indicate an association with Golgi stacks. Interestingly, although widely used as Golgi marker, only the 63,5kDa band detected by the antibody against α-mannosidase was previously described to co-fractionate with other typical Golgi markers (PD3-5c and 180598E) while a second 66kDa band was previously shown to co-fractionate with the same fraction that was positive for TGN-localized syntaxins SYP41 and SYP51 (Preuss *et al.* 2004a). Because the maximum accumulation of all three investigated MAPKs was detected in the fractions with the strongest signal of the 66kDa band, this result might rather indicate an association with the TGN.

The results from the subfractionation experiments were further supported by co-immunolabeling studies, which revealed that all MAPKs co-localized with CLC at the PM. MPK3 and MPK4 were shown to partially co-localize with bigger CLC-positive organelles

and MPK6 localized to organelles labelled with both native CLC and with a CLC:GFP fusion construct.

In mammalian and yeast cells, the early endosomal (EE) compartment has a pleiomorphic organization consisting of tubular and globular/vesicular structures. It is well known that these pleiomorphic organization resembles the existence of specific functional subdomains for receiving, sorting and recycling of proteins from and to the PM and lysosomes as well as for maturing into late endosomes (for review see Gruenberg 2001). The plant TGN was also described as a tubular-vesicular structure (Staehelin and Moore 1995) and it was proposed that it also constitute specific subdomains (Lam *et al.* 2007b). Recently, Chow *et al.* (2008) showed that the two Rab-GTPases RabA2 and RabA3 only partially overlap with the TGN-resident V-ATPase, VHA-a1, on one domain of an endosomal post-Golgi compartment. Thus, the observation that the investigated MAPKs partially co-localize with a clathrin positive organelle most likely indicates an association with specific domains of an early endosomal/secretory TGN.

Rab-GTPases were extensively used as specific molecular markers for the identification of endosomal organelles and their subdomains in animals (for example Sönnichsen *et al.* 2000). Although, members of the plant Rab-GTPase family seem to be organized in a different way as their homologs in mammalian and yeast cells, they represent a valuable tool to identify endosomal organelles (for review see Müller *et al.* 2007b). Future work should address, whether they can be also used to identify putative functional domains on early endosomal TGN compartments.

4.2 MPK6 localizes to the TGN

Co-immunolabelling experiments revealed that MPK6 co-localizes with organelles labelled by antibodies against SCAMP1. SCAMP1 is known to specifically localize to the early endosomal, clathrin-coated TGN (Lam *et al.* 2007a). On the other hand, MPK6 did not co-localize with the 58K Golgi marker, which seemed to be an appropriate tool, since it was previously described to label Golgi-stacks in lily pollen and in maize root cells (Li and Yan 2000; Baluska *et al.* 2002). Instead, MPK6-positive organelles were occasionally found in close association with Golgi-stacks. Because the TGN is known to be closely attached to the Golgi-stacks in some cases (reviewed by Staehelin and Kang 2008), this result further supports the idea of MPK6 localization at the TGN.

Finally, *in-vivo* localization experiments were preformed using stably transformed *Arabidopsis* seedlings that expressed a GFP:MPK6 construct under the control of the constitutive 35S promotor (generated by Martina Beck in our laboratory). GFP:MPK6 was found to co-localize with the endocytotic marker dye FM4-64 on highly mobile organelles as well as on the PM in root epidermal cells. FM4-64 is a red styryl marker dye which, if exogenously applied, incorporates into the PM and passes through the diverse endosomal compartments on its way to the tonoplast (Vida and Emr 1995; Bolte *et al.* 2004). The combined application of this membrane marker with proteins tagged to GFP is widely used and helped substantially to localize proteins and to define and characterize intracellular endosomal compartments in plants (for example Ueda *et al.* 2001 and 2004; Tse *et al.* 2004; Voigt *et al.* 2005; Dettmer *et al.* 2006). Thus, the results obtained by co-visualization of MPK6 and FM4-64 provided evidence for the endosomal nature of MPK6 labelled organelles. However, interpretation of these data has to be made with caution because overexpression of the GFP:MPK6 fusion protein also seemed to partially produce unspecific artificial labelling of the endoplasmic reticulum. Future experiments using the native promoter might help to further characterize the nature of MPK6 localization in living cells.

4.3 Phosphorylation analysis of MAPK after oxidative stress using Phos-tag™

The use of Phos-tag™ as a novel tool to identify phosphorylated isoforms of a particular protein brought clear advantages, because it allowed the identification of the general phosphorylation status of the investigated MAPKs by using the same commercially available and specific antibodies that were characterized previously and extensively used in this work. However, for an appropriate interpretation of the data shown in this work, some basic characteristics regarding the utilization of Phos-tag™ gels have to be considered. First, the use of Phos-tag™ in a normal SDS-PAGE does not allow the identification of the number of phosphorylated sites, because they are not related to a specific molecular size or a defined mobility shift (for reference see Kinoshita *et al.* 2006). Therefore, no prediction could be made with respect to the putative different phosphorylation states from each of the bands that appeared after treatment. Second, in the course of multiple repeats of each experiment it became apparent that the number and molecular size of bands that appear after a particular stimulus is variable. Nevertheless, the tendency, whether a protein shows additional bands and therefore can be defined as phosphorylated, was consistently reproduced. Thus, despite its

restrictions, Phos-tag™ Acrylamide turned out to be a useful tool and allowed clear predictions, as to whether a tested protein occurs as a phosporylated variant or not.

Immunoblotting experiments using Phos-tag™ showed that oxidative stress, triggered by the application of H_2O_2, caused an appearance of multiple bands in the cytosolic but not in the microsomal fraction when tested for MPK4 and MPK6. In the case of MPK3, multiple bands appeared in both fractions even in unstressed plants. However, in H_2O_2 stressed plants the intensity of bands that appeared in the cytosol was significantly stronger, while there was a reduction of signal in the microsomal fraction in the same experiment. This indicates that H_2O_2 causes the release of MPK3 from microsomal structures into the cytosol in some extend.

Oxidative stress is one of the first responses to pathogens and abiotic stress in plants (for review see Hung *et al.* 2005). It is mainly induced by the production of H_2O_2, which is thought to be a common second messenger in the early response to diverse stress stimuli. Exogenous application of H_2O_2 was shown to activate diverse MAPKs in *Arabidopsis*, including MPK3, MPK4 and MPK6 (Kovtun *et al.* 2000, Nakagami *et al.* 2006). It is known to act as an activator of MPK3, MPK4 and also of MPK6 in the response to osmotic stress. H_2O_2 is also thought to be involved in the activation of the same MAPKs in the course of pathogen response. Moreover, H_2O_2 seems to induce stomatal closure via the activation of MPK3 and is involved in the activation of MPK3 and MPK6 after ozone treatment (reviewed by Colcombet and Hirt 2008). However, each of these stimuli elicits a complex answer, including the activation of the appropriate MAPK cascades (see Introduction). Thus, even if H_2O_2 is legitimately discussed as a general upstream activator of MAPK cascades, it seems to be unlikely that its presence alone provides sufficient and specific information for an appropriate cellular response.

The results presented here support previous studies which showed phosphorylation of all investigated MAPKs upon H_2O_2 treatment. However, the fact that only the cytosolic fraction of MPK4 and MPK6 was phosphorylated might indicate that the application of H_2O_2 alone is not sufficient for targeted activation of microsomal MAPK subpopulations. On the other hand, specific activation of microsomal MAPKs was demonstrated in the case of MPK6, which is activated after application of flagellin and which was previously shown to come along with endocytosis of the flagellin receptor FLS2 (Robatzek *et al.* 2006).

4.4 MPK3, MPK4 and MPK6 behave as peripheral TGN-localized proteins

BFA is commonly used as an inhibitor of membrane recycling by effectively inhibiting secretion. As a consequence of the unidirectional inhibitory effect, BFA causes the formation of so called BFA compartments consisting of accumulated endocytotic and TGN-derived vesicles surrounded by remnants of Golgi-stacks in *Arabidopsis* root cells (see also chapter 1.4.2).

Immunoblot experiments revealed that all three MAPKs redistributed from the microsomal fraction towards the cytosol after application of BFA to root cells. The strongest cytosolic shift was found for MPK3 (32.8%) and MPK6 (27%), while there was only a minor reaction observed for MPK4 (9.8%). Previously, a very similar behavior was shown for proteins of the clathrin coat. Robinson and Kreis (1992) described rapid but reversible dissociation of peripheral TGN-resident coat proteins like γ-adaptin and clathrin after incubation with BFA in kidney epithelial cells from monkey. In contrast, membrane-integral TGN resident proteins like SYP41 and the small GTPases, Rab-A2 and Rab-A3, were described to accumulate within BFA induced compartments (Uemura *et al.* 2004; Chow *et al.* 2008). From animal cells it is known that MAPKs indirectly associate with the surface of endosomes via scaffold and appropriate adaptor proteins like the p14/MP1 complex (reviewed by Dhanasekaran *et al.* 2007). Thus, the BFA-induced shift of MPK3, MPK4 and MPK6 into the cytosol might resemble the behavior of other peripheral TGN-associated proteins and further supports the assumption that the investigated MAPKs are associated with early endocytotic/secretory TGN compartments.

However, it still remained an open question, as to whether the observed redistribution was a primary effect constituting a BFA-triggered response, or whether this was a secondary effect of TGN fusion, which could cause a loss of MAPKs peripheral attachment. Since BFA-induced redistribution might be accompanied by a change in the activation and phosphorylation status of the MAPKs, the phosphorylation status of microsomal and cytosolic MAPKs in BFA-treated versus control plants was compared by immunoblot analysis using Phos-tag^{TM} gels. However, no significant additional bands could be detected upon BFA treatment. This indeed suggests that the cytosolic MAPK shift was an indirect effect of the morphological subcellular changes, which is not dependent on MAPK phosphorylation status.

4.5 Microsomal MPK6 participates in flagellin signalling

Previous studies described that MPK6 participates in signalling events triggered by the bacterial elicitor flagellin or the flagellin peptide flg22 (Nühse *et al.*, 2000). The analysis of MPK6 activity by the use of Phos-tag™ gels revealed that both microsomal and cytosolic MPK6 subpopulations are activated by flg22. The fact that two variants were identified in the cytosol, whereas only one of the variants was found to be associated with microsomes, might suggest that different phosphorylated forms are preferentially associated with one and not the other compartment. However, because of the previous discussed restriction with regard to the use of Phos-tag™, interpretation of this particular detail has to be made with caution.

Robatzek *et al.* (2006) showed that the *Arabidopsis* LRR (leucin rich repeat) receptor FLS2 (Flagellin sensitive 2) gets internalized from the PM into yet non identified endosomal compartments upon binding of its ligand, flagellin (see chapter 1.3). As a conclusion, they proposed that endocytosis and signalling are coupled to each other. Thus, the phosphorylated microsomal subpopulation of MPK6 might be specifically involved in this signalling event.

Interestingly, it was previously shown that the constitutive active (CA) form of the MAP3K ANP1, which is known to mimic the H_2O_2 signal (Kovtun *et al.* 2000) is not able to activate MKK5, which in turn was predicted to act as an upstream activator of MPK6 in the flagellin pathway (Asai *et al.* 2002). Therefore, the authors suggested that flagellin and H_2O_2 activate different MAPK pathways, both resulting in the activation of MPK6. The experiments presented in this thesis revealed that phosphorylated microsomal MPK6 was exclusively found in flagellin- but not in H_2O_2-treated roots. Thus, they strengthen the assumption that the microsomal subpopulation is specifically associated with a signalling module that is connected to the flagellin response.

Another evidence for this assumption came from experiments performed by Karin Zwerger (University of Vienna, Austria, personal communication). She tested, whether the disturbance of vesicular trafficking affects flg22-triggered MPK6 activation by performing immunokinase assays on transiently transformed protoplasts isolated from *Arabidopsis* suspension cells after flagellin treatment. Additionally, the protoplasts were pre-incubated with Wortmannin or BFA prior to flagellin treatment. Wortmannin is known to inhibit endocytotic and vacuolar trafficking by targeting phosphoinositol-3-kinase (Matsuoka *et al.*, 1995; Ui *et al.* 1995; Emans *et al.* 2002). Importantly, wortmannin was shown to inhibit the flg22 triggered internalization of FLS2-GFP in leaves (Robatzek *et al.* 2006) and endocytotic uptake of FM4-64 (Emans *et al.* 2002, Reichardt *et al.* 2007). Because BFA is able to enhance

endocytosis (Emans *et al.* 2002; Wang *et al.* 2005) it is acting opposite to Wortmannin in this respect. As expected, the experiment showed that flagellin treatment resulted in the activation of MPK6, while Wortmannin and BFA alone caused none or only very slight activation, respectively. These data are consistent with the experiments presented in this thesis showing that BFA treatment alone did not activate MPK6. However, pre-incubation with Wortmannin completely inhibited the flg22-triggered MPK6 activation, while pre-treatment with BFA significantly amplified flg22-triggered MPK6 activity. Thus, the results from Karin Zwerger showed that the disturbance of vesicular trafficking has a strong impact on subsequent MPK6 activation by flagellin. Future work should focus on the putatively specific role of endosomal MPK6 during flagellin signalling.

4.6 Internalized FLS2 partially localizes to early endosomal compartments

The subcellular fractionation analysis showed that FLS2 mainly localizes in fractions that are also enriched with the late endosomal marker PEP12. Interestingly, after 15 minutes of flagellin treatment FLS2 was additionally found in fractions enriched with MPK3, MPK4, MPK6 and clathrin as well as PM and TGN markers. This result suggests that internalized FLS2, triggered by flagellin, is targeted towards early endosomal compartments in a first step. At variance with this conclusion, Robatzek *et al.* (2006) described that an FLS2-GFP fusion protein was predominantly localized to the PM in untreated leaf epidermal cells. However, it can not be excluded that the pronounced PM localization of the FLS2-GFP fusion protein is an artefact of the GFP-tag, probably blocking some functional domains on the FLS2 protein. Moreover, Robatzek *et al.* (2006) also put forward some evidence that flagellin triggered internalization of FLS2 is followed by subsequent degradation and therefore, they additionally proposed a slow constitutive turnover of the receptor. This would again be consistent with the results obtained here by subcellular fractionation analysis, which might suggest that the major part of FLS2 resides at late endosomes. The redistribution of FLS2 towards the fractions containing MAPKs further supports the idea that flagellin-triggered MAPK signalling is at least partially located at endosomal compartments such as the TGN.

The co-localization experiments using the endocytotic marker dye FM4-64 on stably transformed plants expressing an *FLS2prom::FLS2:GFP* fusion construct support the previous study of Robatzek *et al.* (2006) and reveal that FLS2-GFP localizes to the PM and to cytosolic spot-like organelles also in roots. However, since these organelles did not co-

localize with FM4-64 in untreated roots epidermal cells, this result might suggest an association with organelles that are not involved in endocytosis. Nevertheless, the fact that in BFA-treated plants FLS2-GFP accumulated in BFA induced compartments and partially co-localized with FM4-64 positive cytosolic spots indicates that part of the FLS2 is recycled from the PM. This observation might suggest that a small portion of FLS2-GFP is likely constitutively retrieved from the PM in root cells.

4.7 MPK6 localizes to microtubules and participates in control of cell division

The whole-mount co-immunolabelling experiments revealed that MPK6 associates with cortical MTs. Sometimes MPK6 labelling appeared distinct, however, in most cases spot-like structures could be described, which aligned along MTs, especially in non dividing meristematic and postmeristematic cells. Moreover, co-localization was found on subcortical cytosolic spots primarily in elongating cells. These results are generally consistent with the previous experiments, which revealed similar distribution of MPK6 at clathrin-coated PM and TGN in these cell types. Thus, it might indicate that these spots represent a population of TGN, which are associated with the microtubular cytoskeleton. Indeed, an association of endomembraneous structures with MTs in plants was already suggested before (Mathur *et al.* 2003). Most recently, Crowell *et al.* (2009) provided evidence that Golgi stacks and TGN reside on cortical MTs in order to regulate the precise insertion of cellulose synthase complexes (CSC) into the PM.

Nevertheless, the identity of these spots as well as the putative function of MPK6 on cortical MTs still remains to be elucidated. First experiments presented in this thesis indicate that a general inhibition of MAPK activity, by the use of the MAPK inhibitor PD98059 causes bundling of cortical MTs without inhibiting their potential for dynamic rearrangements. However, this might be an effect of general inhibition of other MAPKs.

In contrast, MPK6 only weakly associated with the dense actin network. Consistent with this result, biochemical fractionation experiments showed that tubulin but not actin resemble the behavior of MAPKs after BFA treatment, i.e. MAPKs shift from microsomal to the cytosolic fraction, just like MTs do. The finding that there was a slight reduction of the number of MPK6 and α-tubulin labelled spots that could be observed in immunofluorescently labelled BFA treated roots confirmed this result. In general, no significant changes were observed with respect to the overall arrangement of MPK6 and MTs in BFA treated root epidermal cells.

On the other hand, BFA treatment caused massive rearrangements of the actin cytoskeleton resulting in bundling and accumulation of actin around the newly formed BFA compartments. The fact that BFA compartments were found to be highly mobile and moved along actin bundles implicates that these changes were not accompanied by a general disturbance of actin-depend movements. Eventually, such changes may represent a regulated adaptation of the actin cytoskeleton in order to maintain the mobility of those thick BFA-induced aggregates. Indeed, preliminary results, not presented in this thesis indicate that the actin cytoskeleton completely recovers after removal of BFA. Moreover, Dhonukshe *et al.* (2006) provided evidence that the formation of BFA compartments does not generally inhibit the functionality of aggregated endosomes because it was shown that during cytokinesis these aggregates are directed towards the growing cell plate in order to fuse with their edges. Thus, they actively contribute to the development of the newly formed PM.

The experiments conducted in this thesis work provide evidence that MPK6 localizes to cytokinetic MTs such as the PPB and the phragmoplast. Localization generally appeared as a diffuse labelling with partially embedded spot like structures. This result is consistent with previous studies describing phragmoplast localization for SIMK, the MPK6 homolog in Medicago (Baluška *et al.* 2000, Šamaj *et al.* 2004b). In the recent years, a number of studies provided evidence that a tobacco MAPK module, consiting of NRK1 (MAPK), NQK1 (MAPKK) and NPK1 (MAPKKK) is involved in the lateral expansion of the phragmoplast in order to regulate cell plate formation (for review see Sasabe *et al.* 2006a). Sasabe *et al.* (2006b) reported that in tobacco BY-2 cells MAPK phosphorylation of NtMAP65-1, a MT bundling protein, stimulates progression of cytokinesis by deactivation of its bundling activity. Interestingly, Smertenko *et al.* (2006) showed that the *Arabidopsis* MAP65-1 is also regulated by MPK4 and MPK6. However, data presented here reveal that the *mpk6-2* knock-out mutant has no cytokinetic defects, but rather shows serious defects in the determination of cell division planes.

MPK6 was not found at the initiating cell plate or its growing edges in the midzone of the phragmoplast. On the other hand, MPK6 was found to localize to the expanded cell plate in a spot-like pattern resembling PM localization in non dividing cells. Interestingly, recent studies showed that several endosomal markers, including the TGN marker SCAMP1, localize to the cell plate (Dhonukshe *et al.* 2006; Lam *et al.* 2007a and 2008). The whole-mount co-immunolabelling experiments performed here reveal that MPK6 co-localizes with

SCAMP1 at the TGN. However, unlike MPK6, SCAMP1 was localized to all stages of cell plate formation and distinctly along its complete surface in Tobacco BY2 cells (Lam *et al.* 2008). Thus, MPK6 localization to the cell plate might be temporally and developmentally regulated. Due to the fact that MPK6 is known to participate in several signalling modules (see chapter 1.3), these data indicate a dual role for MPK6 on mitotic MTs and later on the cell plate. Indeed, analysis of the *mpk6-2* knock-out mutant nicely demonstrates that MPK6 is involved in the determination of cell division planes as well as in temporal and spatial control of cell division in *Arabidopsis* roots. Microscopical analysis of *mpk6-2* mutant roots reveals serious defects in the alignment of PPBs, spindles and phragmoplasts within clusters of dividing cells at the root transition zone as well as irregular, disoriented divisions within the QC in the stem cell niche at the root tip. Interestingly, these positions of aberrantly and redundant division in the root nicely correlate with the expression pattern of MPK6 as shown in the *MPK6prom::GUS* expression experiment. Both, cells of the QC as well as cells from the transition zone are known to be mitotically inactive but competent cells (for example Jiang and Feldmann 2005; Verbelen *et al.* 2006). The finding that these cells are dividing in the *mpk6-2* mutant suggests a role of MPK6 in the regulation of mitotic activity.

So far, a multitude of genes were described to have impact on the determination and maintenance of the cortical division site (CDS) in mitotic cells and some of these candidates, including MAP65-1 are known to be regulated by phosphorylation (for review see Müller *et al.* 2009). Future work should address the putative role of these proteins in the determination of cell division planes.

4.8 MPK6 participates in early root development

Further observations reveal a disturbance of root development, which was correlated with the degree of redundant and missoriented cell divisions. Quantitative analysis on mutant seedlings demonstrated a general growth inhibition with the strongest effect in roots. Moreover, one portion of mutant seedlings completely lacked primary roots during the early phase of postembryonic development while older seedlings with a less pronounced disturbance in root development showed increased production of adventitious roots. Diverse genetic, biochemical and cell-biological studies described the role of a set of genes, phytohormones and environmental factors in regulation of embryonic and postembryonic root development. In the recent years several review articles summarized the most important findings (for example Jiang and Feldmann 2005; Verbelen *et al.* 2006; Petricka and Benfey

2008; Iyer-Pascuzzi *et al.* 2009; Iyer-Pascuzzi and Benfey 2009). Perhaps, the most interesting in the context of the *mpk6-2* root phenotype is the role of the phytohormones auxin and ethylene. Auxin was shown to regulate meristematic patterning and root development during embryogenesis and in growing seedlings. Recently, it was shown that specifically cells of the transition zone and the stem cell niche are extremely sensitive to auxin (see also Jiang and Feldmann 2005; Verbelen *et al.* 2006; Petricka and Benfey 2008). Moreover, it was shown most recently that *Arabidopsis* MPK12 negatively regulates the auxin response and that exogenous application of auxin on *MPK12RNAi* suppressor lines caused reduced root growth (Lee *et al.* 2009). On the other hand, ethylene was discovered as a regulator of mitotic activity (for example Heidstra *et al.* 1997; Kazama *et al.* 2004; Ortega-Martinez *et al.* 2007; Love *et al.* 2009). Additionally, several ethylene sensitive and insensitve mutants were identified that partially exhibited typical disturbances in the development of roots (for review see Guzmán and Ecker 1990; Guo and Ecker 2004). Most interesting, *ethylene overproducer1* (*eto1)* and constitutive triple response1 (*ctr1)* mutants were shown to resemble the *mpk6-2* phenotype, all showing redundant and irregular cell division of QC root cells (Ortega-Martinez *et al.* 2007). Both, *eto1* and *ctr1* mutants are characterized by enhanced ethylene response and it was shown that division of QC cells can be induced by exogenous application of ethylene. So far, several studies provided evidence that MPK6 is involved in both biosynthesis and response to ethylene. As mentioned in chapter 1.3, MPK6 was found to promote ethylene synthesis by activation of ACS6 in the course of the flagellin response. Simultaneously, MPK6 was shown to become activated by ethylene and counteracts CTR1, which is involved in the negative regulation of the ethylene response (see also Hahn and Harter 2009). Thus, MPK6 seems to be a positive regulator both upstream and downstream of ethylene. Surprisingly, the characterization of the *mpk6-2* mutant revealed that the absence of MPK6 causes a phenotype that implicates increased ethylene response. A most recent work by Bethke *et al.* (2009) may shed light on these contrary observations. Using fluorescence resonance energy transfer (FRET) analysis, the authors showed that MPK6 forms complexes with ethylene response factor 104 (ERF104) and therefore inhibits its activity. ERF104 is a nuclear transcription factor and it was shown that it is involved in upregulation of various stress-related genes. Most interestingly, ERF104 was shown to be phosphorylated by and released from MPK6 upon ethylene and flagellin treatment. Moreover, the authors showed that a non-phosphorylatable form of ERF104 is still functional. Thus, these results implicated that MPK6 might be a positive regulator of the ethylene response by negative regulation of ERF104 in the absence of ethylene. It further suggests that the release but not phosphorylation

of ERF104 is essential for its activity. Future work should address the question, as to whether the *mpk6-2* mutant phenotype might be a result of increased activity of ERF104.

4.9 Disruption and recovery of actin and microtubules after heat shock stress

Previously, the actin and MT cytoskeletons were proposed to have a function in cold and heat sensing with reference to the plasma membrane fluidity (Orvar *et al.* 2000, Sangwan *et al.* 2002), but the underlying mechanism is largely unknown. Moreover, transient disruption of the MT cytoskeleton upon abiotic stress such as cold or heavy metals was reported previously (Sivaguru *et al.* 1999, 2003; Abdrakhamanova *et al.* 2003). Based on these studies, Wasteneys *et al.* (2003 and 2004) put forward the hypothesis that stress-related and transient depolymerization of the cytoskeleton might lead to the release of formerly bound signalling molecules or complexes, which would be leading to specific cellular responses. More recently, Thomas *et al.* (2006) reported that rapid transient depolymerization of filamentous actin (within 1 min) induces self-incompatibility (SI) related programmed cell death (PCD) in pollen of *Papaver rhoeas*. Interestingly, it was shown that this SI reaction is mediated by subsequent MAPK signalling within 10 min (Rudd *et al.* 2003; Li *et al.* 2007; Bosch and Franklin-Tong 2008).

The experiments in this thesis revealed that both actin and microtubules undergo dramatic changes upon heat stress. These encompassed partial or full depolymerization as well as the eventual reorganization of the cytoskeletons. During recovery from heat shock epidermal cells re-established both MT and actin filament cytoskeletons similar to those in controls in a time-dependent manner. Interestingly, cytoskeletal changes triggered by heat shock were dependent both on cell type and developmental stage of epidermal cells. Thus, MTs were more stable against heat in older cells and in non root hair cells, while actin was equally disrupted in all cell-types regardless of the developmental stage. This might point to differential roles of actin in MTs to heat stress in a cell type specific manner.

Targets for cytoskeletal disruption might be the actin and tubulin subunits or rather specific associated proteins. In the case of MTs, their disassembly is likely due to a chemical reaction of tubulin subunits which start to dissociate in response to temperatures over 40°C. On the other hand, the F-actin bundling under heat conditions (35-42°C) is probably a physiological response of cells because thick F-actin bundles were formed in cases, when F-actin was depolymerized first (at higher temperature, 40-42°C) but also without previous

depolymerization (at lower temperature, 35°C). Additionally, the MT-bundling MAP65-proteins might be considered as possible cytoskeletal targets of the heat shock since it was reported that the carrot MAP65 protein is heat-labile (Chan *et al.* 1999). For actin, a temperature sensitivity of binding proteins has not been reported so far.

When comparing the reactions of both cytoskeletons to heat shock, it is becoming obvious that actin filaments are more sensitive and take longer to recover than MTs. Nevertheless, as soon as the actin cytoskeleton also begins to recover, a synergetic effect between the two systems may help to speed up the recovery process. Extensive interactions of MTs with actin filaments are known in many cell types (Yoneda *et al.* 2004, Justus *et al.* 2004, Saedler *et al.* 2004), and it has been proposed that cross talk between both cytoskeletons is achieved via motor molecules such as myosins (Šamaj *et al.* 2000) and kinesins (Preuss *et al.* 2004b).

The experiments also reveal that some oblique and especially longitudinally oriented MTs are more resistant to heat stress in young growing cells. This is consistent with previous studies, which showed that the stability of cortical MTs depends on their orientation (Wiesler *et al.* 2002). Recovery experiments presented in this thesis indicate that MTs which survived heat shock might serve as a template for the orientation of new MTs. Only those newly forming MTs, which are growing in a parallel direction to the existing ones were subsequently stabilized or escaped destruction. However, the mechanism of stabilization remains unknown at the moment and future work should focus on the potential role of microtubule-associated proteins (MAPs). Moreover, although this would explain, how reconstitution of a regular MT pattern works in mature non root hair cells, it remains obscure, how a preferred direction of alignment is achieved in cells, which have lost the major part of their MTs by heat stress. In these cells (e.g. root hair cells) new MTs must be formed and oriented without a pre-existing template.

Recovery experiments revealed either transient or long-term formation of long and thick actin bundles in young epidermal cells, all non root hair cells and nearly full-grown root hair cells but not in young, fast growing root hair cells. These young root hair cells showed cell-death in a great extent of 71%. Furthermore, with the exception of undifferentiated epidermal cells and young non root hair cells from the early root hair zone, all other cell types disassemble these thick bundles into a fine F-actin network after several hours of recovery. These data indicate that the early root hair zone is extremely sensitive to heat. One possible explanation for the appearance of these bundles would be that they stabilize structurally

recovering cells similarly to the situation of osmotic stress, where thick bundles stabilize the contracting protoplasts (Komis *et al.* 2002). The finding that non root hair cells as well as full-grown cells survived much better after heat stress indicate that transient formation of thick bundles is needed for the maintenance of cell integrity and for cell survival. This is consistent with previous work in our laboratory showing thick actin bundles in lateral root cap cells (Voigt *et al.* 2005), which are known to survive for several days after they are detached from the root. Another possibility could be, that the long-term maintenance of rigid thick bundles is related to the programmed cell death (PCD), a phenomenon, which has been described in apoptotic suspensor cells in embryonic cultures (Smertenko *et al.* 2003). Future detailed studies should reveal the connection between immobile thick actin bundles and PCD in cells recovering from heat-shock stress.

5. SUMMARY

In plants, development and morphogenesis as well as adaptation to a constantly changing environment strongly depend on regulated perception and transmission of stimuli leading to highly specific cellular responses. Among others, mitogen activated protein kinases (MAPKs) are main players, known to be responsible for proper signal transduction and regulation of subcellular changes in all eukaryotes. In this context, cytoskeletal rearrangements are commonly described as a result of MAPK activation, although the status of the cytoskeleton may also constitute a predisposition for MAPK activation. Since MAPKs seem to be able to mediate the responses to a large variety of stimuli, specificity may not only reside in the molecular diversity of the MAPKs but also in the spatial and temporal organization of MAPK-modules.

This doctoral thesis addresses the dynamic changes of the cytoskeleton during heat stress, the subcellular localization of *Arabidopsis* MPK3, MPK4 and MPK6 and it investigates putative functions of MPK6 subpopulations. New insights are provided with respect to the following points:

1) Biochemical fractionation and immunofluorescence localization studies provide evidence that all three investigated MAPKs, namely MPK3, MPK4 and MPK6 are associated not only within the cytosol and nucleus but also with the microsomal fraction in *Arabidopsis* roots. These microsomes comprise the PM and a population of clathrin positive organelles. In the

case of MPK6 it is shown to be localized to the early endosomal/secretory trans-golgi network (TGN). Subcellular fractionation and inhibitor studies suggest a similar localization also for MPK3 and MPK4. Except for a few studies that described MAPK localization at the phragmoplast during cytokinesis, this is the first detailed study that characterizes the subcellular localization of MAPKs in *Arabidopsis* roots.

2) Phosphorylation analysis revealed that the activation of a particular MAPK subpopulation depends on the respective stimulus. Microsomal-associated MPK6 was shown to participate in the response to the elicitor peptide flg22, which is likely accompanied by endocytosis. The experimental results of this thesis suggest that microsomal MPK6 and the flagellin-triggered, subsequently internalized FLS2 receptor might reside on the same endosomal compartment. In contrast, the general MAPK upstream activator H_2O_2 causes phosphorylation of only the cytosolic but not the microsomal fraction of MAPKs.

3) Whole mount immunolabelling studies provide evidence that MPK6 also localizes to cortical and cytokinetic MTs, especially to the PPB and phragmoplast. The labelling pattern supports the idea that TGN-associated MPK6 participates in the organization and/or function of the MT cytoskeleton. Indeed, the characterization of the *Arabidopsis mpk6-2* knock-out mutant line reveals serious defects in cell division patterns during root development and growth. Moreover, expression of MPK6 in roots correlates well with defects in cytokinesis observed in the *mpk6-2* mutant. Irregular clusters of dividing cells and appearance of skewed division planes is caused by crookedly shifted PPBs, spindles and phragmoplasts. Thus, the experiments indicate that MPK6 plays an important role in root development, especially in the control of cytokinesis and cell division planes, which strongly depend on the MT cytoskeleton.

4) Both actin and microtubules are transiently disrupted but subsequently recover during short term heat shock stress. It is shown that the process of disintegration and reconstitution strongly depends on the cell type. Thus, the experiments provide a depper insight into the cytoskeletal behaviour upon heat stress.

6. REFERENCES

Abdrakhamanova A, Wang QY, Khokhlova L, Nick P (2003) Is microtubule disassembly a trigger for cold acclimation? Plant Cell Physiol. **44:** 676–686.

Ahlfors R, Macioszek V, Rudd J, Brosché M, Schlichting R, Scheel D, Kangasjärvi J (2004) Stress hormone-independent activation and nuclear translocation of mitogen-activated protein kinases in *Arabidopsis* thaliana during ozone exposure. Plant J. **40:** 512-22.

Alessi DR, Cuenda A, Cohen P, Dudley DT, Saltiel AR (1995) PD 098059 is a specific inhibitor of the activation of mitogen-activated protein kinase kinase in vitro and in vivo. J. Biol. Chem. **270:** 27489-94.

Andreasson E, Jenkins T, Brodersen P, Thorgrimsen S, Petersen NH, Zhu S, Qiu JL, Micheelsen P, Rocher A, Petersen M, Newman MA, Bjørn Nielsen H, Hirt H, Somssich I, Mattsson O, Mundy J (2005) The MAP kinase substrate MKS1 is a regulator of plant defense responses. EMBO J. **24**: 2579–2589.

Asai T, Tena G, Plotnikova J, Willmann MR, Chiu WL, Gomez-Gomez L, Boller T, Ausubel FM, Sheen J (2002) MAP kinase signalling cascade in *Arabidopsis* innate immunity. Nature **415:** 977-983.

Baluška F, Ovecka M, Hirt H (2000) Salt stress- and cell cycle phase-dependent changes in expression and subcellular localization of the alfalfa mitogen-activated protein kinase SIMK. Protoplasma **212**: 262-267.

Baluška F, Hlavacka A, Šamaj J, Palme K, Robinson DG, Matoh T, McCurdy DW, Menzel D, and Volkmann D (2002) F-actin-dependent endocytosis of cell wall pectins in meristematic root cells. Insights from brefeldin A-induced compartments. Plant Physiol. **130:** 422–431.

Bar-Peled M, Raikhel NV (1997) Characterization of AtSEC12 and AtSAR1. Proteins likely involved in endoplasmic reticulum and Golgi transport. Plant Physiol. **114:** 315-324.

Barth M, Holstein SE (2004) Identification and functional characterization of *Arabidopsis* AP180, a binding partner of plant alphaC-adaptin. J. Cell Sci. **117:** 2051-2062.

Bayer M, Nawy T, Giglione C, Galli M, Meinnel T, Lukowitz W (2009) Paternal control of embryonic patterning in *Arabidopsis thaliana*. Science **323:** 1485-8.

Bethke G, Unhan T, Uhrig JF, Pöschl Y, Gust AA, Scheel D, Lee J (2009) Flg22 regulates the release of an ethylene response factor substrate from MAP kinase 6 in *Arabidopsis thaliana* via ethylene signaling. Proc. Natl. Acad. Sci. U S A. **106:** 8067-72.

Block MD and Debrouwer D (1992) In-situ enzyme histochemistry on plastic-embedded plant material. The development of an artefact-free ß-glucuronidase assay. Plant J. **2:** 261-266.

Bögre L, Calderini O, Binarova P, Mattauch M, Till S, Kiegerl S, Jonak C, Pollaschek C, Barker P, Huskisson NS, Hirt H, Heberle-Bors E (1999) A MAP kinase is activated late in plant mitosis and becomes localized to the plane of cell division. Plant Cell **11:** 101-113.

Bolte S, Talbot C, Boutte Y, Catrice O, Read ND, Satiat-Jeunemaitre B (2004) FM- dyes as experimental probes for dissecting vesicle trafficking in living plant cells. J Microsc. **214:** 159–173.

Bosch M, Franklin-Tong VE (2008) Self-incompatibility in Papaver: signalling to trigger PCD in incompatible pollen. J. Exp. Bot. **59:** 481-90.

Boutté Y, Vernhettes S, Satiat-Jeunemaitre B (2007) Involvement of the cytoskeleton in the secretory pathway and plasma membrane organisation of higher plant cells. Cell Biol. Int. **31:** 649-54.

Bright NA, Lindsay MR, Stewart A, Luzio JP (2001) The relationship between lumenal and limiting membranes in swollen late endocytic compartments formed after wortmannin treatment or sucrose accumulation. Traffic **2:** 631–642.

Bush SM, Krysan PJ (2007) Mutational evidence that the *Arabidopsis* MAP kinase MPK6 is involved in anther, inflorescence, and embryo development. J. Exp. Bot. **58:** 2181-91.

Calderini O, Bögre L, Vicente O, Binarova P, Heberle-Bors E, Wilson C (1998) A cell cycle regulated MAP kinase with a possible role in cytokinesis in tobacco cells. J. Cell Sci. **111:** 3091-3100.

Chan J, Jensen CG, Jensen LC, Bush M, Lloyd CW (1999) The 65-kDa carrot microtubule-associated protein forms regularly arranged filamentous cross-bridges between microtubules. Proc. Natl. Acad. Sci. USA **96:** 14931-14936.

Chinchilla D, Zipfel C, Robatzek S, Kemmerling B, Nürnberger T, Jones JD, Felix G, Boller T (2007) A flagellin-induced complex of the receptor FLS2 and BAK1 initiates plant defence. Nature **448**: 497-500.

Chow CM, Neto H, Foucart C, Moore I (2008) Rab-A2 and Rab-A3 GTPases define a trans-golgi endosomal membrane domain in *Arabidopsis* that contributes substantially to the cell plate. Plant Cell, **20:** 101-123.

Colcombet J, Hirt H (2008) *Arabidopsis* MAPKs: a complex signalling network involved in multiple biological processes. Biochem. J. **413:** 217-226.

Coronado MJ, González-Melendi P, Seguí JM, Ramírez C, Bárány I, Testillano PS, Risueño MC (2002) MAPKs entry into the nucleus at specific interchromatin domains in plant differentiation and proliferation processes. J. Struct. Biol. **140:** 200-13.

Coronado MJ, Testillano PS, Wilson C, Vicente O, Heberle-Bors E, Risueño MC (2007) In situ molecular identification of the Ntf4 MAPK expression sites in maturing and germinating pollen. Biol. Cell **99:** 209-21.

Crowell EF, Bischoff V, Desprez T, Rolland A, Stierhof YD, Schumacher K, Gonneau M, Höfte H, Vernhettes S (2009) Pausing of Golgi bodies on microtubules regulates secretion of cellulose synthase complexes in *Arabidopsis*. Plant Cell **21:** 1141-54.

da Silva Conceição A, Marty-Mazars D, Bassham DC, Sanderfoot AA, Marty F, Raikhel NV (1997) The syntaxin homolog AtPEP12p resides on a late post-Golgi compartment in plants. Plant Cell **9:** 571-582.

Dardick C, Chen J, Richter T, Ouyang S, Ronald P (2007) The rice kinase database. A phylogenomic database for the rice kinome. Plant Physiol. **143:** 579–586.

Desikan R, Clarke A, Atherfold P, Hancock JT, Neill SJ (1999) Harpin induces mitogen-activated protein kinase activity during defence responses in *Arabidopsis thaliana* suspension cultures. Planta **210**: 97–103.

Desikan R, Hancock J, Ichimura K, Shinozaki K, Neill SJ (2001) Harpin induces activation of the *Arabidopsis* mitogen-activated protein kinases AtMPK4 and AtMPK6. Plant Physiol. **126**: 1579–1587.

Dettmer J, Hong-Hermesdorf A, Stierhof YD, Schumacher K (2006) Vacuolar H1 ATPase activity is required for endocytic and secretory trafficking in *Arabidopsis*. Plant Cell **18:** 715–730.

Dhanasekaran DN, Kashef K, Lee CM, Xu H, Reddy EP (2007) Scaffold proteins of MAP-kinase modules. Oncogene **26:** 3185-202.

Dhonukshe P, Laxalt AM, Goedhart J, Gadella TW, Munnik T (2003) Phospholipase D activation correlates with microtubule reorganization in living plant cells. Plant Cell **15:** 2666–2679.

Dhonukshe P, Baluska F, Schlicht M, Hlavacka A, Samaj J, Friml J, Gadella TW Jr (2006) Endocytosis of cell surface material mediates cell plate formation during plant cytokinesis. Dev. Cell **10:** 137-50.

Dhonukshe P, Aniento F, Hwang I, Robinson DG, Mravec J, Stierhof YD, Friml J (2007) Clathrin-mediated constitutive endocytosis of PIN auxin efflux carriers in *Arabidopsis*. Curr. Biol., **17:** 520-527.

Djamei A, Pitzschke A, Nakagami H, Rajh I, Hirt H (2007) Trojan horse strategy in Agrobacterium transformation: abusing MAPK defense signaling. Science **318**: 453–456.

Doerner P (1998) Root development: quiescent center not so mute after all. Curr. Biol. **8:** 42-4.

Dudley DT, Pang L, Decker SJ, Bridges AJ, Saltiel AR (1995) A synthetic inhibitor of mitogen-activated protein kinase cascade. Proc. Natl. Acad. Sci. USA **92:** 7686-9.

Emans N, Zimmermann S, Fischer, R (2002) Uptake of a fluorescent marker in plant cells is sensitive to brefeldin A and wortmannin. Plant Cell **14:** 71-86.

Faure R, Gaulin JF, Bourgoin S, Fortier S (1999) Compartmentalization of the mitogen-activated protein kinase (MAPK) in hepatic endosomes: association with the internalized epidermal growth factor (EGF) receptor. Mol. Cell. Biol. Res. Commun. **1:** 132-9.

Feilner T, Hultschig C, Lee J, Meyer S, Immink RG, Koenig A, Possling A, Seitz H, Beveridge A, Scheel D, Cahill DJ, Lehrach H, Kreutzberger J, Kersten B (2005) High Throughput Identification of Potential *Arabidopsis* Mitogen-activated Protein Kinases Substrates. Mol. Cell Proteomics **4:** 1558-1568.

Galway ME, Rennie PJ, Fowke LC (1993) Ultrastructure of the endocytotic pathway in glutaraldehyde-fixed and high-pressure frozen/freezesubstituted protoplasts of white spruce (Picea glauca). J Cell Sci **106:** 847–858.

Gao Z, Chen YF, Randlett MD, Zhao XC, Findell JL, Kieber JJ, Schaller GE (2003) Localization of the Raf-like kinase CTR1 to the endoplasmic reticulum of *Arabidopsis* through participation in ethylene receptor signaling complexes. J. Biol. Chem. **278:** 34725-32.

Geldner N, Anders N, Wolters H, Keicher J, Kornberger W, Müller P, Delbarre A, Ueda T, Nakano A, Jürgens G (2003) The *Arabidopsis* GNOM ARF-GEF mediates endosomal recycling, auxin transport, and auxin-dependent plant growth. Cell **112:** 219–230.

Geldner N, Jürgens G (2006) Endocytosis in signalling and development. Curr. Opin. Plant Biol. **9:** 589–594.

Gerthoffer WT (2008) Migration of airway smooth muscle cells. Proc Am Thorac Soc. **5:** 97-105.

Gomez-Gomez L, Bauer Z, Boller T (2001) Both the extracellular leucine-rich repeat domain and the kinase activity of FSL2 are required for flagellin binding and signaling in *Arabidopsis*. Plant Cell **13:** 1155–1163.

Gomez-Gomez L, Boller T (2002) Flagellin perception: a paradigm for innate immunity. Trends Plant Sci. **7:** 251–256.

Grebe M, Xu J, Möbius W, Ueda T, Nakano A, Geuze HJ, Rook MB, Scheres B (2003) *Arabidopsis* sterol endocytosis involves actin-mediated trafficking via ARA6-positive early endosomes. Curr. Biol. **13:** 1378-1387.

Gruenberg, J (2001) The endocytic pathway: a mosaic of domains. Nat. Rev. Mol. Cell Biol. **2:** 721–730.

Guo H, Ecker JR (2004) The ethylene signaling pathway: new insights. Curr. Opin. Plant Biol. **7:** 40-9.

Guzmán P, Ecker JR (1990) Exploiting the triple response of *Arabidopsis* to identify ethylene-related mutants. Plant Cell. **2:** 513-23.

Hahn A, Harter K (2009) Mitogen-activated protein kinase cascades and ethylene: signaling, biosynthesis, or both? Plant Physiol. **149:** 1207-10.

Hai CM, Gu Z (2006) Caldesmon phosphorylation in actin cytoskeletal remodeling. Eur. J. Cell Biol. **85:** 305-9.

Hamada T (2007) Microtubule-associated proteins in higher plants. J Plant Res. **120:** 79-98.

Hamel LP, Nicole MC, Sritubtim S, Morency MJ, Ellis M, Ehlting J, Beaudoin N, Barbazuk B, Klessig D, Lee J, Martin G, Mundy J, Ohashi Y, Scheel D, Sheen J, Xing T, Zhang S, Seguin A, Ellis BE (2006) Ancient signals: comparative genomics of plant MAPK and MAPKK gene families. Trends Plant Sci. **11:** 192-198

Hause G, Samaj J, Menzel D, Baluska F (2006) Fine structural analysis of brefeldin A induced compartment formation after high-pressure freeze fixation of maize root epidermis: compound exocytosis resembling cell plate formation during cytokinesis. Plant Sign. Behav. **1:** 134–139.

Heese A, Hann DR, Gimenez-Ibanez S, Jones AM, He K, Li J, Schroeder JI, Peck SC, Rathjen JP (2007) The receptor-like kinase SERK3/BAK1 is a central regulator of innate immunity in plants. Proc Natl Acad Sci U S A. **104:** 12217-22.

Heidstra R, Yang WC, Yalcin Y, Peck S, Emons AM, van Kammen A, Bisseling T (1997) Ethylene provides positional information on cortical cell division but is not involved in Nod factor-induced root hair tip growth in Rhizobium-legume interaction. Development. **124:** 1781-7.

Higaki T, Sano T, Hasezawa S (2007) Actin microfilament dynamics and actin side-binding proteins in plants. Curr. Opin. Plant Biol. **10:** 549-56.

Hillmer S, Depta H, Robinson DG (1986) Confirmation of endocytosis in higher plant protoplasts using lectin-gold conjugates. Eur. J. Cell Biol. **41:** 142–149.

Hillmer S, Freundt H, Robinson DG (1988) The partially coated reticulum and its relationship to the Golgi apparatus in higher plant cells. Eur. J. Cell Biol. **47:** 206–212.

Horn MA, Heinstein PF, Low PS (1990) Biotin-mediated delivery of exogenous macromolecules into soybean cells. Plant Physiol. **93:** 1492–1496.

Howe CL, Valletta JS, Rusnak AS, Mobley WC (2001) NGF signaling from clathrin-coated vesicles: evidence that signaling endosomes serve as a platform for the Ras-MAPK pathway. Neuron **32:** 801-14.

Hung SH, YU CW, Lin CH (2005) Hydrogen peroxide functions as a stress signal in plants. Bot. Bull. Acad. Sin. **46:** 1-10

Ichimura K, Mizoguchi T, Irie K, Morris P, Giraudat J, Matsumoto K, Shinozaki K (1998) Isolation of ATMEKK1 (a MAP kinase kinase kinase)-interacting proteins and analysis of a MAP kinase cascade in *Arabidopsis*. Biochem. Biophys. Res. Commun. **253**: 532–543.

Iyer-Pascuzzi A, Simpson J, Herrera-Estrella L, Benfey PN (2009) Functional genomics of root growth and development in *Arabidopsis*. Curr. Opin. Plant Biol. **12:** 165-71.

Iyer-Pascuzzi AS, Benfey PN (2009) Transcriptional networks in root cell fate specification. Biochim. Biophys. Acta. **1789:** 315-25.

lm R, Ichimura K, Mizoguchi T, Peck SC, Zhu T, Wang X, Shinozaki K, Paszkowski J (2002) Distinct regulation of salinity and genotoxic stress responses by *Arabidopsis* MAP kinase phosphatase 1. EMBO J. **21:** 6483-93.

Ishikawa M, Soyano T, Nishihama R, Machida Y (2002) The NPK1 mitogen-activated protein kinase kinase kinase contains a functional nuclear localization signal at the binding site for the NACK1 kinesin-like protein. The Plant Journal **32:** 789-798.

Jackson CL, Casanova JE (2000) Turning on ARF: the Sec7 family of guanine Nucleotide exchange factors. Trends Cell Biol. **10:** 60–67.

Jaillais Y, Fobis-Loisy I, Miege C, Rollin C, Gaude T (2006) AtSNX1 defines an endosome for auxin-carrier trafficking in *Arabidopsis*. Nature **443:** 106–109.

Jaillais Y, Santambrogio M, Rozier F, Fobis-Loisy I, Miege C, Gaude T (2007) The retromer protein VPS29 links cell polarity and organ initiation in plants. Cell **130:** 1057–1070.

Jaillais Y, Fobis-Loisy I, Miege C, Gaude T (2008) Evidence for a sorting endosome in *Arabidopsis* root cells. Plant J. **53:** 237–247.

Jiang K, Feldman LJ (2005) Regulation of root apical meristem development. Annu. Rev. Cell Dev. Biol. **21:** 485-509.

Jones JD, Dangl JL (2006) The plant immune system. Nature **444:** 323-9.

Joo S, Liu Y, Lueth A, Zhang S (2008) MAPK phosphorylation-induced stabilization of ACS6 protein is mediated by the non-catalytic C-terminal domain, which also contains the cis-determinant for rapid degradation by the 26 S proteasome pathway. Plant J. **54**: 129–140.

Junttila MR, Li SP, Westermarck J (2008) Phosphatase-mediated crosstalk between MAPK signaling pathways in the regulation of cell survival. FASEB J. **22:** 954-965.

Justus CD, Anderhag P, Goins JL, Lazzaro MD (2004) Microtubules and microfilaments coordinate to direct a fountain streaming pattern in elongating conifer pollen tube tips. Planta **219:** 103-109.

Kazama H, Dan H, Imaseki H, Wasteneys GO (2004) Transient exposure to ethylene stimulates cell division and alters the fate and polarity of hypocotyl epidermal cells. Plant Physiol. **134:** 1614-23.

Kerk D, Bulgrien J, Smith DW, Barsam B, Veretnik S, Gribskov M (2002) The complement of protein phosphatase catalytic subunits encoded in the genome of *Arabidopsis*. Plant Physiol **129:** 908-925.

Kinoshita E, Kinoshita-Kikuta E, Takiyama K, Koike T (2006) Phosphate-binding tag, a new tool to visualize phosphorylated proteins. Mol. Cell Proteomics. **5:** 749-57.

Komis G, Apostolakos P, Galatis B (2002) Hyperosmotic stress-induced actin filament reorganization in leaf cells of Chlorophyton comosum. J Exp Bot **53:** 1699-1710

Konopka CA, Backues SK, Bednarek SY (2008) Dynamics of *Arabidopsis* dynamin-related protein 1C and a clathrin light chain at the plasma membrane. Plant Cell **20:** 1363-1380.

Kotzer AM, Brandizzi F, Neumann U, Paris N, Moore I, Hawes C (2004) AtRabF2b (Ara7) acts on the vacuolar trafficking pathway in tobacco leaf epidermal cells. J Cell Sci **117:** 6377–6389.

Kovtun Y, Chiu WL, Tena G, Sheen J (2000) Functional analysis of oxidative stress-activated mitogen-activated protein kinase cascade in plants. Proc. Natl. Acad. Sci. U.S.A. **97**: 2940–2945.

Laemmli UK (1970) Cleavage of structural proteins during the assembly of the head of bacteriophage T4. Nature **227:** 680-685.

Lam SK, Siu CL, Hillmer S, Jang S, An G, Robinson DG, Jiang L (2007a) Rice SCAMP1 defines clathrin-coated, trans-golgi-located tubular-vesicular structures as an early endosome in tobacco BY-2 cells. Plant Cell **19:** 296-319.

Lam SK, Tse YC, Robinson DG, Jiang L (2007b) Tracking down the elusive early endosome. Trends Plant Sci. **12:** 497-505.

Lam SK, Cai Y, Hillmer S, Robinson DG, Jiang L (2008) SCAMPs highlight the developing cell plate during cytokinesis in tobacco BY-2 cells. Plant Physiol. **147:** 1637-45.

Lampard GR, Macalister CA, Bergmann DC (2008) *Arabidopsis* stomatal initiation is controlled by MAPK-mediated regulation of the bHLH SPEECHLESS. Science **322:** 1113-6.

Lee GJ, Sohn EJ, Lee MH, Hwang I (2004) The *Arabidopsis* rab5 homologs rha1 and ara7 localize to the prevacuolar compartment. Plant Cell Physiol. **45:** 1211–1220.

Lee JS, Wang S, Sritubtim S, Chen JG, Ellis BE (2009) *Arabidopsis* mitogen-activated protein kinase MPK12 interacts with the MAPK phosphatase IBR5 and regulates auxin signaling. Plant J. **57:** 975-85.

Li Y, Yan L (2000) Golgi 58K-like protein in pollens and pollen tubes of Lilium davidii. Sci China C Life Sci. **43:** 402-408.

Li YB, Rogers SW, Tse YC, Lo SW, Sun SS, Jauh GY, Jiang L (2002) BP-80 and homologs are concentrated on post-Golgi, probable lytic prevacuo-lar compartments. Plant Cell Physiol. **43:** 726–742.

Li S, Samaj J, Franklin-Tong VE (2007) A mitogen-activated protein kinase signals to programmed cell death induced by self-incompatibility in Papaver pollen. Plant Physiol. **145:** 236-45.

Ligterink W, Kroj T, zur Nieden U, Hirt H, Scheel D (1997) Receptor-mediated activation of a MAP kinase in pathogen defense of plants. Science **276:** 2054-7.

Limmongkon A, Giuliani C, Valenta R, Mittermann I, Heberle-Bors E, Wilson C (2004) MAP kinase phosphorylation of plant profilin. Biochem Biophys Res Commun. **324:** 382-6.

Link V, Sinha AK, Vashista P, Hofmann MG, Proels RK, Ehness R, Roitsch T (2002) A heat-activated MAP kinase in tomato: a possible regulator of the heat stress response. FEBS Lett. **531:** 179-183.

Liu Y, Zhang S (2004) Phosphorylation of 1-aminocyclopropane-1-carboxylic acid synthase by MPK6, a stress-responsive mitogen-activated protein kinase, induces ET biosynthesis in *Arabidopsis*. Plant Cell **16**: 3386–3399.

Love J, Björklund S, Vahala J, Hertzberg M, Kangasjärvi J, Sundberg B (2009) Ethylene is an endogenous stimulator of cell division in the cambial meristem of Populus. Proc. Natl. Acad. Sci. U S A. **106:** 5984-9.

Luan S (2003) Protein phosphatases in plants. Annu. Rev. Plant Biol. **54:** 63-92.

MAPK group (2002) Mitogen-activated protein kinase cascades in plants: a new nomenclature. Trends Plant Sci. **7**: 301–308.

Marc J, Granger CL, Brincat J, Fisher DD, Kao TH, McCubbin AG, Cyr RJ (1998) Use of a GFP-MAP4 reporter gene for visualizing cortical microtubule rearrangements in living epidermal cells. Plant Cell **11:** 1927-1939.

Mathur J, Mathur N, Kernebeck B, Srinivas BP, Hulskamp M (2003) A novel localization pattern for an EB1-like protein links microtubule dynamics to endomembrane organization. Curr. Biol. **13:** 1991-1997.

Matsuoka K, Bassham DC, Raikhel NV, Nakamura K (1995) Different sensitivity to wortmannin of two vacuolar sorting signals indicates the presence of distinct sorting machineries in tobacco cells. J. Cell Biol. **130:** 1307-1318.

Meskiene I, Bögre L, Glaser W, Balog J, Brandstötter M, Zwerger K, Ammerer G, Hirt H (1998) MP2C, a plant protein phosphatase 2C, functions as a negative regulator of mitogen-activated protein kinase pathways in yeast and plants. Proc Natl Acad Sci U S A **95:** 1938-43.

Meskiene I, Hirt H (2000) MAP kinase pathways: molecular plug-and-play chips for the cell. Plant Mol. Biol. **42:** 791-806.

Meskiene I, Baudouin E, Schweighofer A, Liwosz A, Jonak C, Rodriguez PL, Jelinek H, Hirt H (2003) Stress-induced protein phosphatase 2C is a negative regulator of a mitogen-activated protein kinase. J. Biol. Chem. **278:** 18945-52.

Meszaros T, Helfer A, Hatzimasoura E, Magyar Z, Serazetdinova L, Rios G, Bardoczy V, Teige M, Koncz C, Peck S, Bogre L (2006) The *Arabidopsis* MAP kinase kinase MKK1 participates in defence responses to the bacterial elicitor flagellin. Plant J. **48**: 485–498.

Mishra NS, Tuteja R, Tuteja N (2006) Signaling through MAP kinase networks in plants. Arch. Biochem. Biophys. **452:** 55-68.

Miya A, Albert P, Shinya T, Desaki Y, Ichimura K, Shirasu K, Narusaka Y, Kawakami N, Kaku H, Shibuya N (2007) CERK1, a LysM receptor kinase, is essential for chitin elicitor signaling in *Arabidopsis*. Proc. Natl. Acad. Sci. U.S.A. **104**: 19613–19618.

Mo B, Tse YC, Jiang L (2006) Plant prevacuolar/endosomal compartments. Int. Rev. Cytol. **253:** 95-129.

Mohrmann K, van der Sluijs P (1999) Regulation of membrane transport through the endocytic pathway by rabGTPases. Mol. Membr. Biol. **16:** 81–87.

Müller J, Menzel D, Samaj J (2007a) Cell-type-specific disruption and recovery of the cytoskeleton in *Arabidopsis thaliana* epidermal root cells upon heat shock stress. Protoplasma. **230:** 231-42.

Müller J, Mettbach U, Menzel D, Samaj J (2007b) Molecular dissection of endosomal compartments in plants. Plant Physiol. **145:** 293-304.

Müller S, Wright AJ, Smith LG (2009) Division plane control in plants: new players in the band. Trends Cell Biol. **19:** 180-8.

Nada S, Hondo A, Kasai A, Koike M, Saito K, Uchiyama Y, Okada M (2009) The novel lipid raft adaptor p18 controls endosome dynamics by anchoring the MEK-ERK pathway to late endosomes. EMBO J. **28:** 477-89.

Nagatani A (1998) Regulated nuclear targeting. Curr. Opin. Plant Biol. **1:** 470-4.

Nakagami H, **Kiegerl S**, **Hirt H** (2004) OMTK1, a novel MAPKKK, channels oxidative stress signalling through direct MAPK interaction. J. Biol. Chem. **279:** 26959-26966.

Nakagami H, Pitzschke A, Hirt H (2005) Emerging MAP kinase pathways in plant stress signalling. Trends Plant Sci. **10:** 339-346.

Nakagami H, **Soukupová H**, **Schikora A**, **Zárský V**, **Hirt H** (2006) A mitogen-activated protein kinase kinase kinase mediates reactive oxygen species homeostasis in *Arabidopsis*. J. Biol. Chem. **281:** 38697-38704.

Naoi K, Hashimoto T (2004) A semidominant mutation in an *Arabidopsis* mitogen-activated protein kinase phosphatase-like gene compromises cortical microtubule organization. Plant Cell **16:** 1841-53.

Nebenfuhr A, Ritzenthaler C, Robinson DG (2002) Brefeldin A: deciphering an enigmatic inhibitor of secretion. Plant Physiol. **130:** 1102–1108.

Nishihama R, Ishikawa M, Araki S, Soyano T, Asada T, Machida Y (2001) The NPK1 mitogen-activated protein kinase kinase kinase is a regulator of cell-plate formation in plant cytokinesis. Genes Dev. **15:** 352-363.

Nishihama R, Soyano T, Ishikawa M, Araki S, Tanaka H, Asada T, Irie K, Ito M, Terada M, Banno H, Yamazaki Y, Machida Y (2002) Expansion of the cell plate in plant cytokinesis requires a kinesin-like protein/MAPKKK complex. Cell **109:** 87-99.

Noriega A, Tocino A, Cervantes E (2009) Hydrogen peroxide treatment results in reduced curvature values in the *Arabidopsis* root apex. J. Plant Physiol. **166:** 554-8.

Novikova GV, Moshkov IE, Smith AR, Hall MA (2000) The effect of ET on MAPKinase-like activity in *Arabidopsis thaliana*. FEBS Lett. **474**: 29–32.

Nühse TS, Peck SC, Hirt H, Boller T (2000) Microbial elicitors induce activation and dual phosphorylation of the *Arabidopsis thaliana* MAPK 6. J. Biol. Chem. **275:** 7521-7526.

Oliviusson P, Heinzerling O, Hillmer S, Hinz G, Tse YC, Jiang L, Robinson DG (2006) Plant retromer, localized to the prevacuolar compartment and microvesicles in *Arabidopsis*, may interact with vacuolar sorting receptors. Plant Cell **18:** 1239–1252.

Ortega-Martínez O, Pernas M, Carol RJ, Dolan L (2007) Ethylene modulates stem cell division in the *Arabidopsis thaliana* root. Science. **317:** 507-10.

Ortiz-Zapater E, Soriano-Ortega E, Marcote MJ, Ortiz-Masia D, Aniento F (2006) Trafficking of the human transferrin receptor in plant cells: effects of tyrphostin A23 and brefeldin A. Plant J. **48:** 757–770.

Orvar BL, Sangwan V, Omann F, Dhindsa RS (2000) Early steps in cold sensing by plant cells: the role of actin cytoskeleton and membrane fluidity. Plant J. **23:** 785-794.

Ory S, Zhou M, Conrads TP, Veenstra TD, Morrison DK (2003) Protein phosphatase 2A positively regulates Ras signaling by dephosphorylating KSR1 and Raf-1 on critical 14-3-3 binding sites. Curr. Biol. **13:** 1356–1364.

Ouaked F, Rozhon W, Lecourieux D, Hirt H (2003) A MAPK pathway mediates ET signaling in plants. EMBO J. **22**: 1282–1288.

Owens DM, Keyse SM (2007) Differential regulation of MAP kinase signalling by dual-specificity protein phosphatases. Oncogene **26:** 3203-13.

Panteris E (2008) Cortical actin filaments at the division site of mitotic plant cells: a reconsideration of the 'actin-depleted zone'. New Phytol. **179:** 334-41.

Petersen M, Brodersen P, Naested H, Andreasson E, Lindhart U, Johansen B, Nielsen HB, Lacy M, Austin MJ, Parker JE, Sharma SB, Klessig DF, Martienssen R, Mattsson O, Jensen AB, Mundy J (2000) *Arabidopsis* map kinase 4 negatively regulates systemic acquired resistance. Cell **103**: 1111–1120.

Petricka JJ, Benfey PN (2008) Root layers: complex regulation of developmental patterning. Curr. Opin. Genet. Dev. **18:** 354-61.

Pollard TD, Borisy GG (2003) Cellular motility driven by assembly and disassembly of actin filaments. Cell. **112:** 453-65.

Popescu SC, Popescu GV, Bachan S, Zhang Z, Gerstein M, Snyder M, Dinesh-Kumar SP (2009) MAPK target networks in *Arabidopsis thaliana* revealed using functional protein microarrays. Genes Dev. **23:** 80-92.

Preuss ML, Serna J, Falbel TG, Bednarek SY, Nielsen E (2004) The *Arabidopsis* Rab GTPase RabA4b localizes to the tips of growing root hair cells. Plant Cell **16:** 1589-1603.

Preuss ML, Kovar DR, Lee YR, Staiger CJ, Delmer DP, Liu B (2004b) A plant-specific kinesin binds to actin microfilaments and interacts with cortical microtubules in cotton fibers. Plant Physiol. **136:** 3945-3955.

Preuss ML, Schmitz AJ, Thole JM, BonnerHK, Otegui MS, Nielsen E (2006) A role for the RabA4b effector protein PI-4Kbeta1 in polarized expansion of root hair cells in *Arabidopsis thaliana*. J Cell Biol **172:** 991–998.

Pullikuth AK, Catling AD (2007) Scaffold mediated regulation of MAPK signaling and cytoskeletal dynamics: a perspective. Cell Signal. **19:** 1621-32

Qiu JL, Fiil BK, Petersen K, Nielsen HB, Botanga CJ, Thorgrimsen S, Palma K, Suarez-Rodriguez MC, Sandbech-Clausen S, Lichota J, Brodersen P, Grasser KD, Mattsson O, Glazebrook J, Mundy J, Petersen M (2008) *Arabidopsis* MAP kinase 4 regulates gene expression through transcription factor release in the nucleus. EMBO J. **27:** 2214-21.

Reichardt I, Stierhof YD, Mayer U, Richter S, Schwarz H, Schumacher K, Jürgens G (2007) Plant cytokinesis requires de novo secretory trafficking but not endocytosis. Curr. Biol., **17:** 2047-2053.

Ridge RW, Uozumi Y, Plazinski J, Hurley UA, Williamson RE (1999) Developmental transitions and dynamics of the cortical ER of *Arabidopsis* cells seen with green fluorescent protein. Plant Cell Physiol. **40:** 1253-61.

Robatzek S, Chinchilla D, Boller T (2006) Ligand-induced endocytosis of the pattern recognition receptor FLS2 in *Arabidopsis*. Genes Dev. **20:** 537-542.

Robatzek S (2007) Vesicle trafficking in plant immune responses. Cell Microbiol. 9: 1–8.

Robinson DG, Hillmer S (1990) Endocytosis in plants. Physiol. Plant **79:** 96–104.

Robinson MS, Kreis TE (1992) Recruitment of coat proteins onto Golgi membranes in intact and permeabilized cells: effects of brefeldin A and G protein activators. Cell **69:** 129-138.

Robinson DG, Jiang L, Schumacher K (2008) The endosomal system of plants: charting new and familiar territories. Plant Physiol. **147:** 1482-92.

Rudd JJ, Osman K, Franklin FC, Franklin-Tong VE (2003) Activation of a putative MAP kinase in pollen is stimulated by the self-incompatibility (SI) response. FEBS Lett. **547:** 223-7.

Saedler R, Mathur N, Srinivas BP, Kernebeck B, Hulskamp M, Mathur J (2004) Actin control over microtubules suggested by DISTORTED2 encoding the *Arabidopsis* ARPC2 subunit homolog. Plant Cell Physiol. **45:** 813-822.

Sangwan V, Orvar BL, Beyerly J, Hirt H, Dhindsa RS (2002) Opposite changes in membrane fluidity mimic cold and heat stress activation of distinct plant MAP kinase pathways. Plant J. **31:** 629-638.

Šamaj J, Peters M, Volkmann D, Baluška F (2000) Effects of myosin ATPase inhibitor 2,3-butanedione 2-monoxime on distributions of myosins, F-actin, microtubules, and cortical endoplasmic reticulum in maize root apices. Plant Cell Physiol. **41:** 571-582.

Šamaj J, Ovecka M, Hlavacka A, Lecourieux F, Meskiene I, Lichtscheidl I, Lenart P, Salaj J, Volkmann D, Bögre L, Baluška F, Hirt H (2002) Involvement of the mitogen-activated protein kinase SIMK in regulation of root hair tip growth. EMBO J. **21:** 3296-3306.

Šamaj J, Baluška F, Voigt B, Schlicht M, Volkmann D, Menzel D (2004a) Endocytosis, actin cytoskeleton, and signaling. Plant Physiol. **135:** 1150-1161.

Šamaj J, Baluška F, Hirt H (2004b) From signal to cell polarity: mitogen-activated protein kinases as sensors and effectors of cytoskeleton dynamicity. J. Exp. Bot. **55:** 189-98.

Šamaj J, Müller J, Beck M, Bohm N, Menzel D (2006) Vesicular trafficking, cytoskeleton and signalling in root hairs and pollen tubes. Trends Plant Sci. **11:** 594–600.

Sasabe M and Machida Y (2006a) MAP65: a bridge linking a MAP kinase to microtubule turnover. Curr. Opin. Plant Biol. **9:** 563-570.

Sasabe M, Soyano T, Takahashi Y, Sonobe S, Igarashi H, Itoh TJ, Hidaka M, Machida Y (2006b) Phosphorylation of NtMAP65-1 by a MAP kinase down-regulates its activity of

microtubule bundling and stimulates progression of cytokinesis of tobacco cells. Genes Dev. **20:** 1004-1014.

Scheele U, Holstein SE (2002) Functional evidence for the identification of an *Arabidopsis* clathrin light chain polypeptide. FEBS Lett. **514:** 355-360.

Schweighofer A, Kazanaviciute V, Scheikl E, Teige M, Doczi R, Hirt H, Schwanninger M, Kant M, Schuurink R, Mauch F, Buchala A, Cardinale F, Meskiene I (2007) The PP2C-type phosphatase AP2C1, which negatively regulates MPK4 and MPK6, modulates innate immunity, jasmonic acid, and ethylene levels in *Arabidopsis*. Plant Cell **19:** 2213-24.

Shaw SL, Kamyar R, Ehrhardt DW (2003) Sustained microtubule treadmilling in *Arabidopsis* cortical arrays. Science **300:** 1715-1718.

Sheahan MB, Staiger CJ, Rose RJ, McCurdy DW (2004). A green fluorescent protein fusion to actin-binding domain 2 of *Arabidopsis* fimbrin highlights new features of a dynamic actin cytoskeleton in live plant cells. Plant Physiol. **136:** 3968-3978.

Shimada T, Koumoto Y, Li LX, Yamazaki M, Kondo M, Nishimura M, Hara-Nishimura I (2006) AtVPS29, a putative component of a retromer complex, is required for the efficient sorting of seed storage proteins. Plant Cell Physiol. **47:** 1187–1194.

Sivaguru M, Baluška F, Volkmann D, Felle HH, Horst WJ (1999) Impacts of aluminum on the cytoskeleton of the maize root apex. short-term effects on the distal part of the transition zone. Plant Physiol. **119:** 1073-1082.

Sivaguru M, Pike S, Gassmann W, Baskin TI (2003) Aluminum rapidly depolymerizes cortical microtubules and depolarizes the plasma membrane: evidence that these responses are mediated by a glutamate receptor. Plant Cell Physiol. **44:** 667–675.

Smertenko A, Draber P, Viklicky V, Opatrny Z (1997) Heat stress affects the organization of microtubules and cell division in Nicotinia tabacum cells. Plant, Cells and Enviroment **20:** 1534-1542.

Smertenko AP, Bozhkov PV, Filonova LH, von Arnold S, Hussey PJ (2003) Re-organisation of the cytoskeleton during developmental programmed cell death in Picea abies embryos. Plant J. **33:** 813-824.

Smertenko AP, Chang HY, Sonobe S, Fenyk SI, Weingartner M, Bögre L, Hussey PJ (2006) Control of the AtMAP65-1 interaction with microtubules through the cell cycle. J Cell Sci. **119:** 3227-37.

Sohn EJ, Kim ES, Zhao M, Kim SJ, Kim H, Kim YW, Lee YJ, Hillmer S, Sohn U, Jiang L, Hwang I (2003) Rha1, an *Arabidopsis* Rab5 homolog, plays a critical role in the vacuolar trafficking of soluble cargo proteins. Plant Cell. **15:** 1057-70.

Sönnichsen B, De Renzis S, Nielsen E, Rietdorf J, Zerial M (2000) Distinct membrane domains on endosomes in the recycling pathway visualized by multicolor imaging of Rab4, Rab5, and Rab11. J. Cell Biol. **149:** 901-14.

Staehelin LA and Moore I (1995) The plant Golgi apparatus. Annu. Rev. Plant Physiol. Plant Mol. Biol. **46:** 261–288.

Staehelin LA, Kang BH (2008) Nanoscale architecture of endoplasmic reticulum export sites and of Golgi membranes as determined by electron tomography. Plant Physiol. **147:** 1454-1468.

Suarez-Rodriguez MC, Adams-Phillips L, Liu Y, Wang H, Su SH, Jester PJ, Zhang S, Bent AF, Krysan PJ (2007) MEKK1 is required for flg22-induced MPK4 activation in *Arabidopsis* plants. Plant Physiol. **143**: 661–669.

Tahara H, Yokota E, Igarashi H, Orii H, Yao M, Sonobe S, Hashimoto T, Hussey PJ, Shimmen T (2007) Clathrin is involved in organization of mitotic spindle and phragmoplast as well as in endocytosis in tobacco cell cultures. Protoplasma, **230:** 1-11.

Takahashi F, Yoshida R, Ichimura K, Mizoguchi T, Seo S, Yonezawa M, Maruyama K, Yamaguchi-Shinozaki K, Shinozaki K (2007) The mitogen-activated protein kinase cascade

MKK3-MPK6 is an important part of the jasmonate signal transduction pathway in *Arabidopsis*. Plant Cell **19:** 805-18.

Tanchak MA, Fowke LC (1987) The morphology of multivesicular bodies in soybean protoplasts and their role in endocytosis. Protoplasma **138:** 173–182.

Taub N, Teis D, Ebner HL, Hess MW, Huber LA (2007) Late endosomal traffic of the epidermal growth factor receptor ensures spatial and temporal fidelity of mitogen-activated protein kinase signaling. Mol Biol Cell1**8:** 4698-710.

Teige M, Scheikl E, Eulgem T, Dóczi R, Ichimura K, Shinozaki K, Dangl JL, Hirt H (2004) The MKK2 pathway mediates cold and salt stress signaling in *Arabidopsis*. Mol Cell. **15:**141-52.

Teis D, Wunderlich W, Huber LA (2002) Localization of the MP1-MAPK scaffold complex to endosomes is mediated by p14 and required for signal transduction. Dev. Cell. **3:** 803-14.

Teis D, Taub N, Kurzbauer R, Hilber D, de Araujo ME, Erlacher M, Offterdinger M, Villunger A, Geley S, Bohn G, Klein C, Hess MW, Huber LA (2006) p14-MP1-MEK1 signaling regulates endosomal traffic and cellular proliferation during tissue homeostasis. J Cell Biol. **175:** 861-8.

Thomas SG, Huang S, Li S, Staiger CJ, Franklin-Tong VE (2006) Actin depolymerization is sufficient to induce programmed cell death in selfincompatible pollen. J. Cell Biol. **174:** 221–229.

Towbin H, Staehelin T, Gordon J (1979) Electrophoretic transfer of proteins from polyacrylamide gels to nitrocellulose sheets: procedure and some applications. Proc. Natl. Acad. Sci. USA **76:** 4350-4354.

Tse YC, Mo B, Hillmer S, Zhao M, Lo SW, Robinson DG, and Jiang L (2004) Identification of multivesicular bodies as prevacuolar compartments in Nicotiana tabacum BY-2 cells. Plant Cell **16:** 672-693.

Turjanski AG, Vaqué JP, Gutkind JS (2007) MAP kinases and the control of nuclear events. Oncogene **26:** 3240-53.

Ueda T, Yamaguchi M, Uchimiya H, Nakano A (2001) Ara6, a plant unique novel type Rab GTPase, functions in the endocytic pathway of *Arabidopsis thaliana*. EMBO J. **20:** 4730–474.

Ueda T, Uemura T, Sato MH, Nakano A (2004) Functional differentiation of endosomes in *Arabidopsis* cells. Plant J. **40:** 783–789.

Uemura T, Ueda T, Ohniwa RL, Nakano A, Takeyasu K, Sato MH (2004) Systematic analysis of SNARE molecules in *Arabidopsis*: dissection of the post-Golgi network in plant cells. Cell Struct. Funct. **29:** 49–65.

Ui M, Okada T, Hazeki K, Hazeki O (1995) Wortmannin as a unique probe for an intracellular signalling protein, phosphoinositide 3-kinase. Trends Biochem. Sci. **20:** 303–307.

Ullrich O, Reinsch S, Urbe S, Zerial M, Parton RG (1996) Rab11 regulates recycling through the pericentriolar recycling endosome. J Cell Biol **135:** 913–924.

Ulm R, Ichimura K, Mizoguchi T, Peck SC, Zhu T, Wang X, Shinozaki K, Paszkowski J (2002) Distinct regulation of salinity and genotoxic stress responses by *Arabidopsis* MAP kinase phosphatase 1. EMBO J. **21:** 6483-93.

Van Bruaene N, Joss G, Van Oostveldt P (2004) Reorganization and in vivo dynamics of microtubules during *Arabidopsis* root hair development. Plant Physiol **136:** 3905-3919.

van den Berg C, Weisbeek P, Scheres B (1998) Cell fate and cell differentiation status in the *Arabidopsis* root. Planta **205:** 483-91.

van der Geer P, Hunter T, Lindberg RA (1994) Receptor protein-tyrosine kinases and their signal transduction pathways. Annu. Rev. Cell. Biol. **10:** 251-337.

Verbelen JP, De Cnodder T, Le J, Vissenberg K, Baluška F (2006) The root apex of *Arabidopsis thaliana* consists of four distinct zones of cellular activities: meristematic zone, transition zone, fast elongation zone, and growth terminating zone. Plant Signal. Behav. **1:** 296-304.

Vida TA, Emr SD (1995) A new vital stain for visualizing vacuolar membrane dynamics and endocytosis in yeast. J. Cell Biol. **128:** 779–792.

Voigt B, Timmers AC, Samaj J, Müller J, Baluska F, Menzel D (2005) GFP-FABD2 fusion construct allows in vivo visualization of the dynamic actin cytoskeleton in all cells of *Arabidopsis* seedlings. Eur. J. Cell Biol. **84:** 595-608.

Wang D, Harper JF, Gribskov M (2003) Systematic transgenomic comparison of protein kinases between *Arabidopsis* and nSaccharomyces cerevisiae. Plant Physiol. **132:** 2152–2165.

Wang YS, Motes CM, Mohamalawari DR, Blancaflor EB (2004) Green fluorescent protein fusions to *Arabidopsis* fimbrin 1 for spatio-temporal imaging of F-actin dynamics in roots. Cell Motil. Cytoskelet. **59:** 79-93.

Wang Q, Kong L, Hao H, Wang X, Lin J, Samaj J, Baluska F (2005) Effects of brefeldin A on pollen germination and tube growth. Antagonistic effects on endocytosis and secretion. Plant Physiol. **139:** 1692-1703.

Wang H, Ngwenyama N, Liu Y, Walker JC, Zhang S (2007) Stomatal development and patterning are regulated by environmentally responsive mitogen-activated protein kinases in *Arabidopsis*. Plant Cell **19:** 63-73.

Wasteneys GO (2003) Microtubules show their sensitive nature. Plant Cell Physiol. **44:** 653-4.

Wasteneys GO (2004) Progress in understanding the role of microtubules in plant cells. Curr. Opin. Plant Biol. **7:** 651-60.

Wasteneys GO, Ambrose JC (2009) Spatial organization of plant cortical microtubules:

close encounters of the 2D kind. Trends Cell Biol. **19:** 62-71.

Wessel D, Fluegge UI (1984) A method for the quantitative recovery of protein in dilute solution in the presence of detergents and lipids. Anal. Biochem. **138:** 141-143.

Wiesler B, Wang QY, Nick P (2002) The stability of cortical microtubules depends on their orientation. Plant J. **32:** 1023-1032.

Willoughby EA, Perkins GR, Collins MK, Whitmarsh AJ (2003). The JNK-interacting protein-1 scaffold protein targets MAPK phosphatase-7 to dephosphorylate JNK. J. Biol. Chem. **278:** 10731–10736.

Yang Z (2008) Cell polarity signaling in *Arabidopsis*. Annu. Rev. Cell Dev. Biol. **24:** 551-75.

Yoneda A, Akatsuka M, Kumagai F, Hasezawa S (2004) Disruption of actin microfilaments causes cortical microtubule disorganization and extra-phragmoplast formation at M/G1 interface in synchronized tobacco cells. Plant Cell Physiol. **45:** 761-769.

Yoo SD, Cho YH, Tena G, Xiong Y, Sheen J (2008) Dual control of nuclear EIN3 by bifurcate MAPK cascades in C2H4 signalling. Nature **451:** 789-95.

LIST OF TABLES

LIST OF FIGURES

ABBREVIATIONS

ABD2	actin binding domain 2
ABPs	actin binding proteins
BFA	Brefeldin A
CCV	clathrin coated vesicle
CHC	clathrin heavy chain
CLC	clathrin light chain
Col-0	*Arabidopsis* thaliana ecotype Columbia 0
DIC	differential interphase contrast
DMSO	dimethyl sulfoxide
DNA	desoxyribonucleic acid
DsRed	Discosoma spec. red fluorescent protein
ECL	enhanced chemiluminescence
EDTA	ethylenediamine tetraacetic acid
EGF	epidermal growth factor
EGTA	ethylene glycol tetraacetic acid
ER	endoplasmatic reticulum
ERK	extracellular signal-regulated kinases
ET	ethylene
FA	filamenteous actin
FABD2	fimbrin actin-binding domain 2
F-actin	filamentous actin
Fig	Figure
FLS2	FLAGELLIN SENSING2
FM4-64	N-(3-triethylammoniumpropyl)-4-(6-(4-(diethylamino)phenyl)hexatrienyl)pyridinium dibromide
GFP	green fluorescent protein
GUS	ß-Glucoronidase
HR	hypersensitive response
JA	jasmonic acid
kb	kilobases
kDa	kilo Dalton
LRR	leucine rich repeat

MAP	microtubule associated proteins
MAPK; MPK	(mitogen activated protein kinase)
MAPKK; MAP2K	(mitogen activated protein kinase kinase)
MAPKKK; MAP3K	(mitogen activated protein kinase kinase kinase)
MBD	microtubule binding domain
MKP	MAPK phosphatase
MS	Murashige and Skoog
MT	microtubule
MTSB	microtubule stabilizing buffer
MVB	multivesicular body
PAGE	polyacrylamide gel electrophoresis
PAMP	pathogen associated molecular pattern
PBS	phosphate buffered saline
PCD	programmed cell death
PM	plasma membrane
PPB	preprophase band
PRR	pattern-recognition receptor
PSP	protein serine/threonine phosphatase
PSV	protein storage vacuoles
PTP	protein tyrosine phosphatase
PVC	pre-vacuolar compartments
QC	quiescent center
RLK	receptor-like kinase
RME	receptor-mediated endocytosis
RNA	ribonucleic acid
RT-PCR	reverse transcriptase polymerase chain reaction
SA	salicylic acid
SAR	systemic aquired resistance
SCAMP1	secretory carrier membrane protein 1
SDS	sodium dodecyl sulfate
SI	self incompatibility
SIMK	stress induced MAPK
SNARE	soluble N-ethyl-maleimide sensitive factor attachment protein receptor
TBS	tris buffered saline

TF	transcription factor
TGN	trans-Golgi network
VSR	vacuolar sorting receptor
WM	wortmannin
WT	wild type
YFP	yellow fluorescent protein

PUBLICATIONS

Müller J, Beck M, Mettbach U, Komis G, Hause G, Menzel D, Šamaj J (**2009**) Arabidopsis MPK6 is involved in cell division plane control during early root development and localizes to pre-prophase band, phragmoplast, trans-Golgi network and plasma membrane (plant journal; in print)

Zheng M, Beck M, **Müller J**, Chen T, Wang X, Wang F, Wang Q, Wang Y, Baluska F, Logan DC, Samaj J, Lin J (**2009**) Actin turnover is required for myosin-dependent mitochondrial movements in Arabidopsis root hairs. PLoS One. 4: e5961.

Müller J, Menzel D, Samaj J (**2007a**) Cell-type-specific disruption and recovery of the cytoskeleton in Arabidopsis thaliana epidermal root cells upon heat shock stress. Protoplasma 230: 231-42.

Müller J, Mettbach U, Menzel D, Samaj J (**2007b**) Molecular dissection of endosomal compartments in plants. Plant Physiol. 145: 293-304. (review article)

Samaj J, **Müller J**, Beck M, Böhm N, Menzel D (**2006**) Vesicular trafficking, cytoskeleton and signalling in root hairs and pollen tubes. Trends Plant Sci. 11: 594-600.

Voigt B, Timmers AC, Samaj J, **Müller J**, Baluska F, Menzel D (**2005**) GFP-FABD2 fusion construct allows in vivo visualization of the dynamic actin cytoskeleton in all cells of Arabidopsis seedlings. Eur J Cell Biol. 84: 595-608.

ERKLÄRUNG

Ich versichere hiermit, dass ich die vorliegende Arbeit in allen Teilen selbst und ohne jede unerlaubte Hilfe angefertigt habe. Diese oder eine ähnliche Arbeit ist noch keiner anderen Stelle als Dissertation eingereicht worden. Die Arbeit ist an nachstehend aufgeführten Stellen auszugsweise veröffentlicht worden:

Müller J, Menzel D, Samaj J (**2007a**) Cell-type-specific disruption and recovery of the cytoskeleton in Arabidopsis thaliana epidermal root cells upon heat shock stress. Protoplasma 230: 231-42.

Müller J, Mettbach U, Menzel D, Samaj J (**2007b**) Molecular dissection of endosomal compartments in plants. Plant Physiol. 145: 293-304.

Ich habe früher noch keinen Promotionsversuch unternommen.

Bonn, den